Ph. D. DISSERTATION

All Solution-processed Flexible Polymer Light Emitting Diodes under Low-operation Voltage

저전압에서 구동 가능한 전 용액 공정 기반 플렉시블 폴리머 발광다이오드에 관한 연구

BY

JONGJANG PARK

FEBRUARY 2019

DEPARTMENT OF ELECTRICAL ENGINEERING AND
COMPUTER SCIENCE
COLLEGE OF ENGINEERING
SEOUL NATIONAL UNIVERSITY

All Solution-processed Flexible Polymer Light Emitting Diodes under Low-operation Voltage

저전압에서 구동 가능한 전 용액 공정 기반 플렉시블 폴리머 발광다이오드에 관한 연구

지도교수 홍 용 택

이 논문을 공학박사 학위논문으로 제출함
2019 년 2 월

서울대학교 대학원
전기컴퓨터 공학부
박 종 장

박종장의 공학박사 학위논문을 인준함
2019 년 2 월

위 원 장 _____ (인)

부위원장 _____ (인)

위 원 _____ (인)

위 원 _____ (인)

위 원 _____ (인)

Abstract

All Solution-processed Flexible Polymer Light Emitting Diodes under Low-operation Voltage

JONGJANG PARK

DEPARTMENT OF ELECTRICAL ENGINEERING AND COMPUTER SCIENCE

COLLEGE OF ENGINEERING

SEOUL NATIONAL UNIVERSITY

In this Ph.D. dissertation, I fabricated all solution-processed flexible polymer light emitting diodes (PLEDs) under low-operation voltage which are potentially of interest in the application to low-cost and large-area mass production of future display. In recent years, although many groups have reported all solution-processed PLEDs via various manufacturing methods such as spin coating, inkjet printing and transfer printing, there are still remaining rooms for further improvement to realize the commercial products in terms of customizability and power consumption.

First, formation of additional layers via a solution process on a hydrophobic emission layer (EML) is difficult due to an extremely poor wetting property. Among the methods to improve the wetting property of a poly(3,4-ethylenedioxythiophene):poly(styrenesulfonate) (PEDOT:PSS) hole injection layer (HIL) in various optoelectronic devices such as surfactant addition into the original

solution, surface treatment of organic underlying layers and dilution with a low surface tension, the dilution method is the most promising approach because it changes only surface tension of the PEDOT:PSS solution without causing any degradation of the organic layer or device. Using the optimized dilution condition with ethanol, the PEDOT:PSS HIL was coated uniformly on the hydrophobic EML. Based on these results, I fabricated the inverted PLEDs with solution-processed multi-layers, especially the PEDOT:PSS HIL on the EML, sandwiched between the sputtered indium tin oxide (ITO) and evaporated Al electrodes. In particular, the uniformly coated PEDOT:PSS HIL plays an important role for high device performance and light emission uniformity on one substrate.

Second, it is necessary to replace the vacuum-processed electrodes to the solution-processed electrodes in order to achieve all solution-processed PLEDs. In the early works about all solution-processed PLEDs, however, the complicated and high-cost fabrication, especially in forming both electrodes, limits their development of the cost-effective and large-area commercial display products. For simple pixel definition, the electrodes of the PLEDs should be patterned easily with a high degree of freedom, but the previous works have utilized unproductive electrode deposition methods while demonstrating only one or a few devices on one substrate. In addition, when solvent orthogonality is not satisfied, solvents can damage the underlying layers during the solution process, resulting in the degradation of the device performance. To solve these issues, I integrated the inkjet printing and transfer printing in forming a conductive PEDOT:PSS film, which enables a facile pattering of electrodes and minimal solvent damages, simultaneously. For the successful transfer printing of PEDOT:PSS, I modulated the as-purchased PEDOT:PSS solution by adding a D-sorbitol solution to give the

adhesive force to the film and carefully controlled an adhesive force between the film and each substrate such as donor quartz, polydimethylsiloxane (PDMS) stamp and target substrates. Based on these results, I applied the transferred PEDOT:PSS electrodes to top anodes of all solution-processed inverted PLEDs with the well-defined functional layers via the spin coating on the inkjet-printed Ag cathodes. My rigid and flexible devices showed a high device efficiency and operated normally even under a bending state in the case of those on the plastic substrate. Using the maskless patterning for both Ag and PEDOT:PSS electrodes via the inkjet printing, the customized PLEDs and their array were manufactured with various pixel shapes and fine lines. In particular, for the first time, I demonstrated 5×7 passive matrix PLEDs (PMPLEDs) with a 500 μm pixel width using all solution processing, displaying a variety of characters without any crosstalk.

Third, a low conductivity of electrodes in the devices can cause severe voltage drop and high power consumption during the device operation. My devices also have suffered from the low power efficiency which comes from a high sheet resistance of the transferred PEDOT:PSS electrodes. Therefore, I need to fabricate highly transparent and conductive flexible electrodes for the low-voltage driven flexible electronics including all solution-processed PLEDs while avoiding a complicated fabrication process at the same time. I introduced a facile pattering method of high-performance flexible electrodes by integrating the inkjet printing of the PEDOT:PSS transfer medium and selective transfer of silver nanowire (AgNW) networks only onto the region of the transfer medium. First, for the successful AgNW transfer, I formulated the blended PEDOT:PSS ink with the D-sorbitol aqueous solution to strongly attach the PEDOT:PSS and AgNW networks. Afterwards, it was inkjet-printed on arbitrary substrates with a desired pattern,

thereby obtaining the customized PEDOT:PSS transfer medium. Second, I fabricated highly conductive and transparent AgNW networks on the plasma-treated PDMS stamp by the spin coating. Finally, I conducted the heat treatment for the attached sample of the existing substrate with the PEDOT:PSS film and AgNW-coated PDMS stamp, which results in selective transfer of the AgNW networks and thus highly customizable AgNW-transferred PEDOT:PSS film. Based on these principles, my AgNW-transferred PEDOT:PSS electrodes were formed on the various substrates according to the purpose of use, showing not only excellent optoelectronic properties but also fine lines with hundreds of micrometers in width. In addition, their electrical and optical properties were highly tunable by controlling the AgNW coating conditions and the previous issues of the AgNWs such as a high surface roughness and weak adhesion with the substrate were overcome by the partially embedded AgNWs in the PEDOT:PSS matrix. In the plastic substrate, my AgNW-transferred PEDOT:PSS electrodes showed not only more excellent optoelectronic properties but also more outstanding mechanical flexibility compared to ITO. Employing my flexible electrodes, I exhibited several applications of the customized flexible electronics such as light-emitting diode (LED) arrays and all solution-processed PLEDs. In particular, the low-voltage driven PLEDs exhibited a low operating voltage while maintaining the optical performance.

Keyword : polymer light emitting diodes (PLEDs), solution process, inkjet & transfer printing, PEDOT:PSS, AgNW, flexibility
Student Number : 2012-20772

Table of Contents

List of Tables

List of Figures

Chapter 1 Introduction

1.1 Flexible display

Organic light emitting diodes (OLEDs) have been considered as future display such as rollable, transparent and flexible displays **(Figure 1.1)**. In particular, many people think that next-generation display will be developed toward ubiquitous display based on the flexible and transparent display which can be installed anywhere and utilized anytime. Actually, in some reports, it is forecasted that flexible active matrix OLED panel will grow to more than 55% market share and 400 million unit shipments by 2022, exceeding those of rigid panels **(Figure 1.2)** However, current commercial OLED products have been fabricated by a vacuum process and the flexible displays which are demonstrated by several display companies are also manufactured by a vacuum-based evaporation process, which is incompatible with low-cost and large-area mass production. To realize the ubiquitous display, the cost-effective fabrication method as well as the improvement of efficiency and stability in the OLEDs should be established for scalability of large-scale mass production.

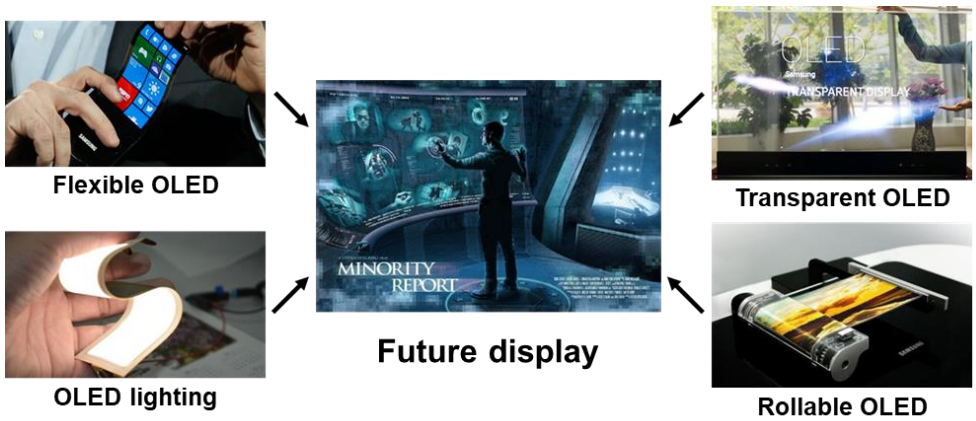

Figure 1.1 Future display (Source: Samsung, LG, Minority report).

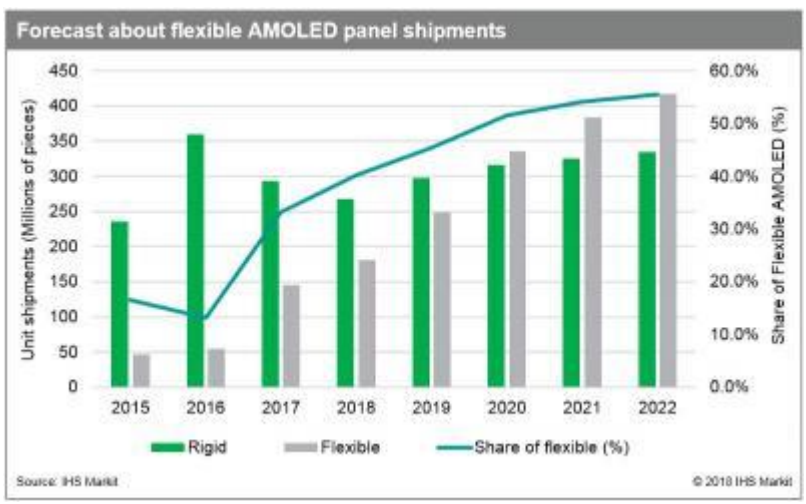

Figure 2.2 Forecast about flexible display panel shipments (Source: IHS Markit).

Recently, all solution-processed polymer light emitting diodes (PLEDs) which are one of the OLEDs by employing soluble polymer emissive materials have been reported in many groups due to the low cost and solution processibility in fabricating the devices [1-8]. However, they used the unproductive fabrication methods, especially in forming top and bottom electrodes which are critical to define pixels precisely. An inkjet printing is a promising candidate to achieve an easy patterning of opaque or transparent conducive electrodes via a drop-on-

demand method. Therefore, all solution-processed PLEDs can be accomplished by combing the inkjet-printed electrodes and multi-stacked functional layers by the spin coating, showing the potential for the manufacturing of cost-effective and large-area products with high throughput.

In addition to the simple fabrication method, the embodiment of high-performance transparent conductive electrodes (TCEs) is also important to realize the flexible display with low power consumption. Indium tin oxide (ITO) has been widely used as the TCEs in rigid optoelectronic devices due to superior electrical and optical properties, but its inherent brittleness by mechanical stress restricts its use in the flexible display. Many alternatives to replace the ITO have been reported such as carbon nanotubes [9, 10], graphene [11, 12], metal nanowires [13-16], oxide-metal-oxide [17, 18], metal girds [19, 20] and conductive polymers [3, 21-23], showing no change of conductivity and no deterioration of surface morphology during the mechanical deformation. Furthermore, the deposition and patterning processes of the high-performance TCEs should be simpler and softer to be compatible with plastic or elastomeric substrates because the complicated conventional method such as wet etching and laser ablation can damage the substrates. Therefore, the facile fabrication of the high-performance TCEs is a key enabling technology to fulfill the high-performance flexible display.

In this Ph.D. dissertation, I studied all solution processing in fabricating the PLEDs and facile patterning of the silver nanowires (AgNWs). By integrating both methods, I demonstrated all solution-processed flexible PLEDs under low-operation voltage.

1.2 Inkjet printing

Inkjet printing is one of thin film deposition methods for various organic/inorganic electronic materials which can be formulated to inks such as electrodes [3, 24-27], dielectrics [25-28], semiconductors [25, 26, 29, 30], optical components [31-33] and so on. Unlike other solution processes, it allows mask-free patterning of thin films because a predesigned digital pattern only need to be input into an equipment, resulting in cost and time effectiveness. In general, it is classified to continuous or drop-on-demand (DOD) mode according to the jetting method **(Figure 1.3)**. Among them, the piezoelectric DOD inkjet printer has been widely used because it is suitable for printing a wide range of electronic materials due to solvent versatility of inks and easy control of printing characteristics. For effective ink jetting and thus well-defined thin films, several printing conditions should be carefully adjusted ranging from ink properties, jetting waveform, annealing time or temperature, substrate temperature to wetting properties. In addition, cartridges with various nozzle diameters which contain to-be-printed inks can be equipped to the equipment, which is appropriate for obtaining the thin films with a variety of pattern widths according to the purpose. Consequently, the high-quality thin films are completed using the inkjet printing technique under the optimized printing conditions.

In this Ph. D. dissertation, I employed DMP-2831 in Dimatix Corp. which is a piezoelectric DOD inkjet printer to create highly customizable transparent poly(3,4-ethylenedioxythiophene):poly(styrenesulfonate) (PEDOT:PSS) electrodes or transfer media and opaque Ag electrodes on various substrates **(Figure 1.4)**.

Especially, I focused on the simple patterning of which the inkjet printing is capable, showing the customized PLED pixels and arrays with a diversity of shapes and widths and applications of easily patternable AgNW electrodes.

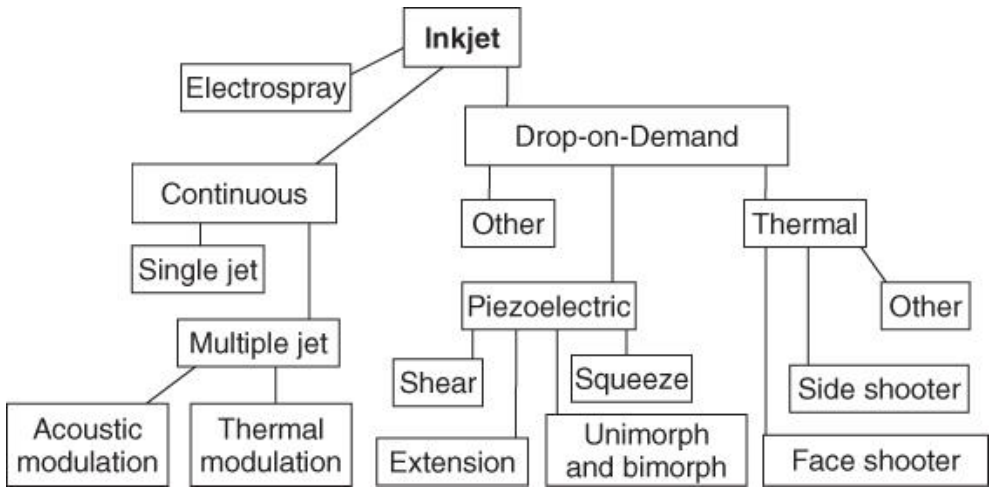

Figure 1.3 Classification of inkjet technologies [34].

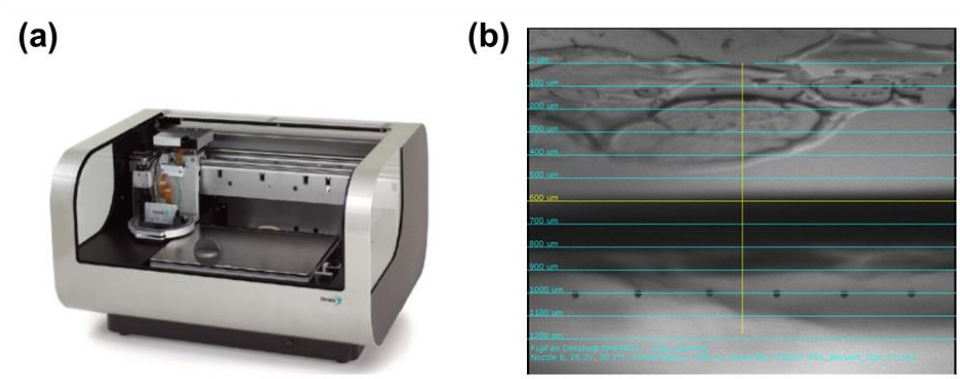

Figure 1.4 (a) A piezoelectric drop-on-demand inkjet printer (DMP-2831, Dimatix Corp.) used in this dissertation, (b) A real-time jetting image of blended PEDOT:PSS ink (Source: Dimatix).

1.3 Transfer printing

Transfer printing is a unique deposition technique for the achievement of micro/nano scale thin films such as metals [35-37], carbon nanocomposites [11, 38-40], nanowires [41-44], organic/inorganic materials [4, 45-48] and quantum dots [49, 50] on a wide range of substrates or systems. In way that it is a solvent-free and dry transfer method, several issues which appear during a solution process can be avoided such as solvent orthogonality which can damage underlying layers if it is not satisfied. In addition, it enables uniform film formation regardless of the surface morphology and wetting property of to-be-deposited substrates.

A. Carlson et al. introduced the recent advance in the transfer printing, reviewing a lot of previously reported papers [51]. In this paper, the author categorized the transfer printing methods into three basic concepts such as additive transfer, subtractive transfer and deterministic assembly **(Figure 1.5)**. The objects are moved from a stamp to a target substrate or from a donor substrate to a stamp and then from a stamp to a target substrate. However, the additive transfer and subtractive transfer need the molded stamp for patterning the film, which is not compatible with the cost-effective fabrication. In the deterministic assembly, on the contrast, if the pre-structured film can be deposited on the donor substrate, the molded stamp is not required. A facile patterning of films on the donor substrate will lead to the simplified manufacturing process.

For the successful transfer printing, adhesion between the film and surface of two substrates should be carefully controlled. In general, detachment of ink from the former substrate and its attachment to the latter substrate are occurred when an

adhesive force between the former and ink is weaker than that between the latter and ink. In order to adjust and alter the adhesion, many approaches have been utilized in the abovementioned reports such as introduction of adhesive or release layers, heat, press, surface treatments and so on.

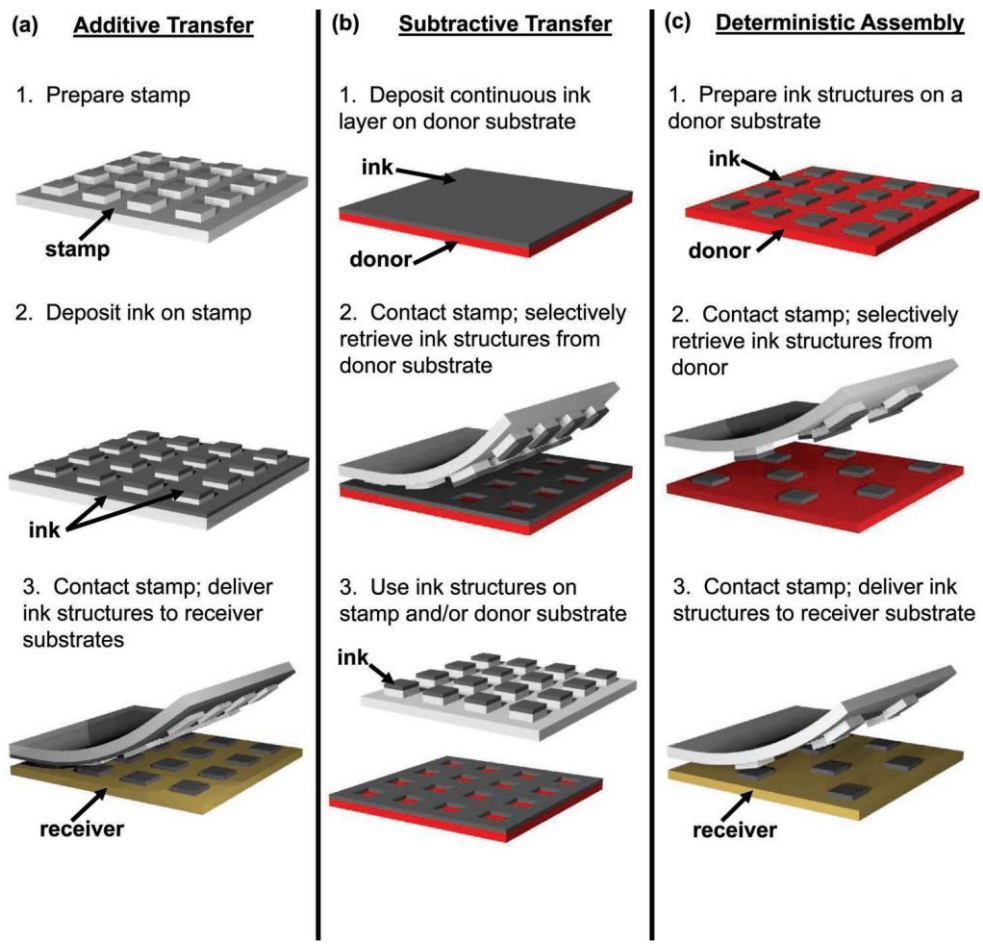

Figure 1.5 Schematic illustrations of three basic concepts for transfer printing. (a) Additive Transfer, (b) Subtractive Transfer, (c) Deterministic Assembly [51].

In this Ph.D. dissertation, I conducted the transfer printing using the blended PEDOT:PSS ink as an electrical glue which is the mixture of the conductive

polymer and D-sorbitol aqueous solution as an adhesive **(Figure 1.6).** Based on this transfer process, I obtained the inkjet-printed PEDOT:PSS electrodes on the PLED devices without top electrodes and easily patternable AgNW-based TCEs on various substrates which are highly customizable**.** Ultimately, I integrated two methods for all solution-processed flexible PLEDs with the AgNW-transferred PEDOT:PSS top anodes which can be driven at low voltage.

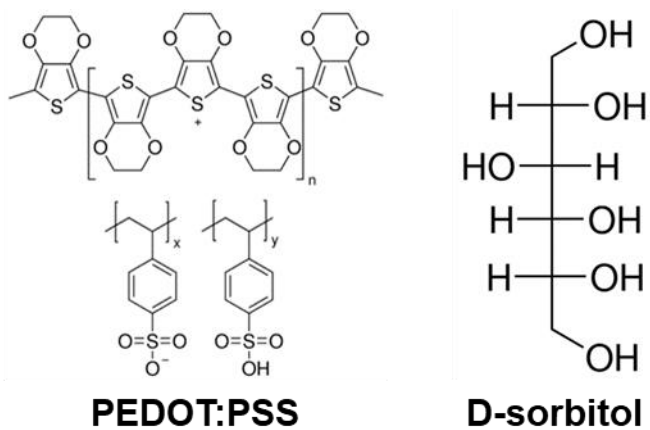

Figure 1.6 Materials for a transfer process used in this dissertation (Source: Sigma Aldrich).

1.4 Organization of this dissertation

In this Ph.D. dissertation, I showed all solution-processed flexible PLEDs under low-operation voltage. To achieve these devices, I studied an additional coating of the PEDOT:PSS HIL on the hydrophobic EML, transfer printing of conductive PEDOT:PSS for top electrodes of devices and facile patterning method of flexible AgNW-based TCEs with superior optoelectronic properties.

This dissertation contains four chapters including **Introduction** and **Conclusion.**

Chapter 1 introduces a need for large-scale flexible display and key enabling technologies to realize it with all solution processing such as inkjet printing and transfer printing of electrodes.

Chapter 2 describes solution-processed inverted PLEDs except for both electrodes. Especially, the PEDOT:PSS HIL on the hydrophobic EML was coated uniformly by improving its wetting property via the ethanol dilution method.

Chapter 3 depicts all solution-processed PLEDs with the transferred PEDOT:PSS top anodes and well-defined functional layers on the inkjet-printed Ag bottom cathodes. Their characteristics including electrical, optical and mechanical properties were investigated and highly customizable PLEDs were also demonstrated including 5×7 passive matrix PLEDs.

Chapter 4 presents the facile patterning method of AgNW networks by combining the inkjet-printed PEDOT:PSS transfer medium and selective transfer of the AgNWs. Using the high-performance flexible electrodes, low-voltage driven flexible electronics are also demonstrated.

Reference

[1] J. Ha, S. Park, D. Kim, J. Ryu, C. Lee, B.H. Hong, Y. Hong, High-performance polymer light emitting diodes with interface-engineered graphene anodes, Org. Electron., 14 (2013) 2324-2330.

[2] H. Zheng, Y. Zheng, N. Liu, N. Ai, Q. Wang, S. Wu, J. Zhou, D. Hu, S. Yu, S. Han, W. Xu, C. Luo, Y. Meng, Z. Jiang, Y. Chen, D. Li, F. Huang, J. Wang, J. Peng, Y. Cao, All-solution processed polymer light-emitting diode displays, Nat. Commun., 4 (2013) 1971.

[3] J. Ha, J. Park, J. Ha, D. Kim, S. Chung, C. Lee, Y. Hong, Selectively modulated inkjet printing of highly conductive and transparent foldable polymer electrodes for flexible polymer light-emitting diode applications, Org. Electron., 19 (2015) 147-156.

[4] N. Kim, H. Kang, J.H. Lee, S. Kee, S.H. Lee, K. Lee, Highly conductive all-plastic electrodes fabricated using a novel chemically controlled transfer-printing method, Adv. Mater., 27 (2015) 2317-2323.

[5] M. Zhang, S. Hofle, J. Czolk, A. Mertens, A. Colsmann, All-solution processed transparent organic light emitting diodes, Nanoscale, 7 (2015) 20009-20014.

[6] Z. Shu, E. Beckert, R. Eberhardt, A. Tünnermann, ITO-free, inkjet-printed transparent organic light-emitting diodes with a single inkjet-printed Al:ZnO:PEI interlayer for sensing applications, J. Mater. Chem. C, 5 (2017) 11590-11597.

[7] H. Zhen, Y. Chen, C. Zhang, Z. Zhou, K. Li, Y. Zhao, X. Mei, Q. Ling, Full-solution processed, flexible, top-emitting polymer light-emitting diodes based on printed Ag electrodes, J. Mater. Chem. C, 5 (2017) 6400-6405.

[8] S. Kee, N. Kim, B. Park, B.S. Kim, S. Hong, J.H. Lee, S. Jeong, A. Kim, S.Y. Jang, K. Lee, Highly Deformable and See-Through Polymer Light-Emitting Diodes with All-Conducting-Polymer Electrodes, Adv. Mater., 30 (2018) 1703437.

[9] C. Feng, K. Liu, J.-S. Wu, L. Liu, J.-S. Cheng, Y. Zhang, Y. Sun, Q. Li, S. Fan, K. Jiang, Flexible, Stretchable, Transparent Conducting Films Made from Superaligned Carbon Nanotubes, Adv. Funct. Mater., 20 (2010) 885-891.

[10] S.M. Kim, Y.W. Jo, K.K. Kim, D.L. Duong, H.-J. Shin, J.H. Han, J.-Y. Choi, J. Kong, Y.H.J.A.N. Lee, Transparent organic P-Dopant in carbon nanotubes: Bis (trifluoromethanesulfonyl) imide, ACS Nano, 4 (2010) 6998-7004.

[11] S. Bae, H. Kim, Y. Lee, X. Xu, J.S. Park, Y. Zheng, J. Balakrishnan, T. Lei, H.R. Kim, Y.I. Song, Y.J. Kim, K.S. Kim, B. Ozyilmaz, J.H. Ahn, B.H. Hong, S. Iijima, Roll-to-roll production of 30-inch graphene films for transparent electrodes, Nat. Nanotechnol., 5 (2010) 574-578.

[12] H. Kim, S.H. Bae, T.H. Han, K.G. Lim, J.H. Ahn, T.W. Lee, Organic solar cells using CVD-grown graphene electrodes, Nanotechnology, 25 (2014) 014012.

[13] L. Hu, H.S. Kim, J.-Y. Lee, P. Peumans, Y.J.A.n. Cui, Scalable coating and properties of transparent, flexible, silver nanowire electrodes, ACS Nano, 4 (2010) 2955-2963.

[14] A.R. Madaria, A. Kumar, F.N. Ishikawa, C. Zhou, Uniform, highly conductive, and patterned transparent films of a percolating silver nanowire network on rigid and flexible substrates using a dry transfer technique, Nano Res., 3 (2010) 564-573.

[15] S.J. Lee, Y.H. Kim, J.K. Kim, H. Baik, J.H. Park, J. Lee, J. Nam, J.H. Park, T.W. Lee, G.R. Yi, J.H. Cho, A roll-to-roll welding process for planarized silver nanowire electrodes, Nanoscale, 6 (2014) 11828-11834.

[16] S. Kim, S.Y. Kim, J. Kim, J.H. Kim, Highly reliable AgNW/PEDOT:PSS

hybrid films: efficient methods for enhancing transparency and lowering resistance and haziness, J. Mater. Chem. C, 2 (2014) 5636-5643.

[17] A. Dhar, T.L. Alford, Optimization of Nb2O5/Ag/Nb2O5 multilayers as transparent composite electrode on flexible substrate with high figure of merit, J. Appl. Phys., 112 (2012).

[18] Y.C. Kim, S.J. Lee, H. Jung, B.-E. Park, H. Kim, W. Lee, J.-M. Myoung, Optimization and device application potential of oxide–metal–oxide transparent electrode structure, RSC Adv., 5 (2015) 65094-65099.

[19] H. Wu, D. Kong, Z. Ruan, P.C. Hsu, S. Wang, Z. Yu, T.J. Carney, L. Hu, S. Fan, Y. Cui, A transparent electrode based on a metal nanotrough network, Nat. Nanotechnol., 8 (2013) 421-425.

[20] W.K. Kim, S. Lee, D. Hee Lee, I. Hee Park, J. Seong Bae, T. Woo Lee, J.Y. Kim, J. Hun Park, Y. Chan Cho, C. Ryong Cho, S.Y. Jeong, Cu mesh for flexible transparent conductive electrodes, Sci. Rep., 5 (2015) 10715.

[21] Y.H. Kim, C. Sachse, M.L. Machala, C. May, L. Müller-Meskamp, K. Leo, Highly Conductive PEDOT:PSS Electrode with Optimized Solvent and Thermal Post-Treatment for ITO-Free Organic Solar Cells, Adv. Funct. Mater., 21 (2011) 1076-1081.

[22] M. Vosgueritchian, D.J. Lipomi, Z. Bao, Highly Conductive and Transparent PEDOT:PSS Films with a Fluorosurfactant for Stretchable and Flexible Transparent Electrodes, Adv. Funct. Mater., 22 (2012) 421-428.

[23] N. Kim, S. Kee, S.H. Lee, B.H. Lee, Y.H. Kahng, Y.R. Jo, B.J. Kim, K. Lee, Highly conductive PEDOT:PSS nanofibrils induced by solution-processed crystallization, Adv. Mater., 26 (2014) 2268-2272, 2109.

[24] H. Sirringhaus, T. Kawase, R. Friend, T. Shimoda, M. Inbasekaran, W. Wu,

E.J.S. Woo, High-resolution inkjet printing of all-polymer transistor circuits, Science, 290 (2000) 2123-2126.

[25] S. Chung, M. Jang, S.B. Ji, H. Im, N. Seong, J. Ha, S.K. Kwon, Y.H. Kim, H. Yang, Y. Hong, Flexible high-performance all-inkjet-printed inverters: organo-compatible and stable interface engineering, Adv. Mater., 25 (2013) 4773-4777.

[26] J. Ha, S. Chung, M. Pei, K. Cho, H. Yang, Y. Hong, One-Step Interface Engineering for All-Inkjet-Printed, All-Organic Components in Transparent, Flexible Transistors and Inverters: Polymer Binding, ACS Appl. Mater. Interfaces, 9 (2017) 8819-8829.

[27] Y. Li, R. Torah, S. Beeby, J. Tudor, An all-inkjet printed flexible capacitor on a textile using a new poly (4-vinylphenol) dielectric ink for wearable applications, Sensors, 2012 IEEE, (2012) 1-4.

[28] B.S. Cook, J.R. Cooper, M.M. Tentzeris, Multi-Layer RF Capacitors on Flexible Substrates Utilizing Inkjet Printed Dielectric Polymers, IEEE Microw. Wirel. Co., 23 (2013) 353-355.

[29] H. Yan, Z. Chen, Y. Zheng, C. Newman, J.R. Quinn, F. Dotz, M. Kastler, A. Facchetti, A high-mobility electron-transporting polymer for printed transistors, Nature, 457 (2009) 679-686.

[30] H. Minemawari, T. Yamada, H. Matsui, J. Tsutsumi, S. Haas, R. Chiba, R. Kumai, T. Hasegawa, Inkjet printing of single-crystal films, Nature, 475 (2011) 364-367.

[31] D. Xie, H. Zhang, X. Shu, J.J.O.E. Xiao, Fabrication of polymer micro-lens array with pneumatically diaphragm-driven drop-on-demand inkjet technology, Opt. Express, 20 (2012) 15186-15195.

[32] J.Y. Kim, K. Pfeiffer, A. Voigt, G. Gruetzner, J. Brugger, Directly fabricated

multi-scale microlens arrays on a hydrophobic flat surface by a simple ink-jet printing technique, J. Mater. Chem., 22 (2012).

[33] W.-C. Chen, T.-J. Wu, W.-J. Wu, G.-D.J. Su, Fabrication of inkjet-printed SU-8 photoresist microlenses using hydrophilic confinement, J. Micromech. Microeng., 23 (2013).

[34] G.D. Martin, I.M. Hutchings, Fundamental of Inkjet Technology, in: I.M. Hutchings, G.D. Martin, Inkjet Technology for Digital Fabrication, John Wiley & Sons, Ltd., United Kingdom, 2013, pp. 22.

[35] Y.-L. Loo, R.L. Willett, K.W. Baldwin, J.A. Rogers, Additive, nanoscale patterning of metal films with a stamp and a surface chemistry mediated transfer process: Applications in plastic electronics, Appl. Phys. Lett., 81 (2002) 562-564.

[36] Y.-L. Loo, R.L. Willett, K.W. Baldwin, J.A. Rogers, Interfacial chemistries for nanoscale transfer printing, J. Am. Chem. Soc., 124 (2002) 7654-7655.

[37] Z. Wang, J. Yuan, J. Zhang, R. Xing, D. Yan, Y. Han, Metal Transfer Printing and Its Application in Organic Field-Effect Transistor Fabrication, Adv. Mater., 15 (2003) 1009-1012.

[38] M.A. Meitl, Y. Zhou, A. Gaur, S. Jeon, M.L. Usrey, M.S. Strano, J.A.J.N.L. Rogers, Solution casting and transfer printing single-walled carbon nanotube films, Nano Lett., 4 (2004) 1643-1647.

[39] F.N. Ishikawa, H.-k. Chang, K. Ryu, P.-c. Chen, A. Badmaev, L. Gomez De Arco, G. Shen, C.J.A.n. Zhou, Transparent electronics based on transfer printed aligned carbon nanotubes on rigid and flexible substrates, ACS Nano, 3 (2008) 73-79.

[40] Y. Lee, S. Bae, H. Jang, S. Jang, S.E. Zhu, S.H. Sim, Y.I. Song, B.H. Hong, J.H. Ahn, Wafer-scale synthesis and transfer of graphene films, Nano Lett., 10

(2010) 490-493.

[41] A.R. Madaria, A. Kumar, C. Zhou, Large scale, highly conductive and patterned transparent films of silver nanowires on arbitrary substrates and their application in touch screens, Nanotechnology, 22 (2011) 245201.

[42] A. Javey, S. Nam, R.S. Friedman, H. Yan, C.M.J.N.l. Lieber, Layer-by-layer assembly of nanowires for three-dimensional, multifunctional electronics, Nano Lett., 7 (2007) 773-777.

[43] G.S. Liu, C. Liu, H.J. Chen, W. Cao, J.S. Qiu, H.P. Shieh, B.R. Yang, Electrically robust silver nanowire patterns transferrable onto various substrates, Nanoscale, 8 (2016) 5507-5515.

[44] M.C. McAlpine, H. Ahmad, D. Wang, J.R. Heath, Highly ordered nanowire arrays on plastic substrates for ultrasensitive flexible chemical sensors, Nat. Mater., 6 (2007) 379-384.

[45] J.-h. Choi, K.-H. Kim, S.-J. Choi, H.H. Lee, Whole device printing for full colour displays with organic light emitting diodes, Nanotechnology, 17 (2006) 2246-2249.

[46] S. Liu, H.A. Becerril, M.C. LeMieux, W.M. Wang, J.H. Oh, Z. Bao, Direct Patterning of Organic-Thin-Film-Transistor Arrays via a “Dry-Taping” Approach, Adv. Mater., 21 (2009) 1266-1270.

[47] M.A. Meitl, Z.-T. Zhu, V. Kumar, K.J. Lee, X. Feng, Y.Y. Huang, I. Adesida, R.G. Nuzzo, J.A. Rogers, Transfer printing by kinetic control of adhesion to an elastomeric stamp, Nat. Mater., 5 (2005) 33-38.

[48] Y. Yang, Y. Hwang, H.A. Cho, J.H. Song, S.J. Park, J.A. Rogers, H.C. Ko, Arrays of silicon micro/nanostructures formed in suspended configurations for deterministic assembly using flat and roller-type stamps, Small, 7 (2011) 484-491.

[49] T.-H. Kim, K.-S. Cho, E.K. Lee, S.J. Lee, J. Chae, J.W. Kim, D.H. Kim, J.-Y. Kwon, G. Amaratunga, S.Y. Lee, B.L. Choi, Y. Kuk, J.M. Kim, K. Kim, Full-colour quantum dot displays fabricated by transfer printing, Nat. Photon., 5 (2011) 176-182.

[50] M.K. Choi, J. Yang, K. Kang, D.C. Kim, C. Choi, C. Park, S.J. Kim, S.I. Chae, T.H. Kim, J.H. Kim, T. Hyeon, D.H. Kim, Wearable red-green-blue quantum dot light-emitting diode array using high-resolution intaglio transfer printing, Nat. Commun., 6 (2015) 7149.

[51] A. Carlson, A.M. Bowen, Y. Huang, R.G. Nuzzo, J.A. Rogers, Transfer printing techniques for materials assembly and micro/nanodevice fabrication, Adv. Mater., 24 (2012) 5284-5318.

Chapter 2

Uniformly coated PEDOT:PSS HIL on a hydrophobic EML for solution-processed inverted PLEDs

2.1 Introduction

Organic light emitting diodes/polymer light emitting diodes (OLEDs/PLEDs) have been considered as a promising technology for advanced displays with mechanical flexibility and optical transparency [1-7]. For commercial applications and reduction of fabrication costs, the PLEDs with a high efficiency and stability should be developed using a solution process such as a spin coating or printing process [8-19]. However, formation of the multi-layer structure by the solution process, which is essential to implement highly efficient and stable devices, is relatively challenging due to limited solvent orthogonality and thus intermixing between adjacent layers [20-25]. One of the promising approaches is adoption of an inverted structure, where anodes are located at the top of the whole devices. In

general, the conventional PLEDs need vacuum-deposited low work function metals in cathodes for efficient electron injection, but most of solution-processed transparent or opaque electrodes have a high work function, which results in a low device efficiency due to a high electron injection barrier when they are applied to the cathodes [17,26]. In contrast, for the inverted structure, the electron injection can be enhanced by applying solution-processed functional layers on the cathodes. For example, air-stable zinc oxide (ZnO) has been deposited on the bottom cathodes using the spin coating as an electron transport layer to reduce the electron injection barrier [27-30]. In addition, the electron injection can be further enhanced by inserting an interlayer of polyethyleneimine (PEI) between the ZnO layer and emission layer (EML) because PEI can modify the work function of ZnO by inducing interface dipoles [31-33]. Unlike the feasibility of forming the solution-processed layers under the EML, additional coatings of functional layers on the EML by the solution process are hindered by its hydrophobic surface, making it challenging to obtain a solution-processed inverted PLED structure. Moreover, the introduction of a HIL on the EML is critical to achieving high performance in the inverted PLEDs with the ZnO/PEI layers because more efficient hole injection in the anodes facilitates more electron injection in the cathodes by hole accumulation at the PEI/EML interface [34].

To realize the high performance, most of the solution-processed inverted PLEDs have used a vacuum process for deposition of HILs such as MoO_3 and top electrodes such as Au and Al on various hydrophobic EMLs [27,30,32,33]. In fact, several papers have been reported regarding the formation of poly(3,4-ethylenedioxythiophene):poly(styrenesulfonate) (PEDOT:PSS) layers, which are widely used as the HIL in the PLEDs, on organic layers. In order to control the

wetting property of PEDOT:PSS solutions on the generally hydrophobic organic layers, they used several approaches such as surfactant addition into the PEDOT:PSS solutions [35,36], surface treatment of the organic under-layers [37,38], and dilution of the PEDOT:PSS solutions with low surface tension liquids but only for organic solar cells [38,39]. It should be noted that the surfactant addition or surface treatment can affect the electrical, optical or morphological properties of the organic layers and thus degrade the device performance due to potential surfactant residue or chemical and physical transformation, respectively. On the contrary, the dilution method changes only surface tension of the original solution without causing any degradation of the organic layers, but still improving the wetting property. However, this approach has been rarely investigated in the PLEDs because the EMLs of the PLEDs show the more hydrophobic property than the organic layers of solar cells in general [40-43].

In this **Chapter 2**, I demonstrated the inverted PLEDs with solution-processed multi-layers, especially the PEDOT:PSS HIL on the EML, sandwiched between ITO and Al electrodes by modulating the wetting property. The poor wetting property of the PEDOT:PSS solutions on the hydrophobic EML was improved by diluting the PEDOT:PSS solutions with ethanol and the optimized dilution ratio was obtained by analyzing a wetting envelope of the EML and corresponding the surface tension for the diluted solutions. The fabricated devices showed not only the high performance but also uniform light emission in one substrate. Based on my method, a systematical analysis for the wetting property enables the formation of uniform films by the solution process, which leads to high-performance and low-cost electronic devices.

2.2 Experiments

2.2.1 Fabrication of inverted PLEDs

Inverted PLEDs were fabricated on glass substrates with ITO electrodes which were used as cathodes in the inverted structures as shown in **Figure 2.1(a).** The substrates were sequentially cleaned with acetone, isopropanol, and deionized water in an ultrasonic bath. After that, the cleaned substrates were stored in an oven set to 100 ℃ for 1 h to remove any moisture on the surface and then treated by UV ozone before the deposition of upper layers. The fabrication process is illustrated in **Figure 2.1(b).** The ZnO solution was prepared with a method which was described by Y. Sun et al. [28]. Accordingly, zinc acetate dihydrate ($Zn(CH_3COO)_2 \cdot 2H_2O$, Sigma-Aldrich, 1 g) was dissolved in 2-methoxyethanol ($CH_3OCH_2CH_2OH$, Sigma-Aldrich, 10 mL) and ethanolamine ($NH_2CH_2CH_2OH$, Sigma-Aldrich, 0.28 g) was added to the solution for stabilization. The completed solution was vigorously stirred for 1 day in order to enhance hydrolysis reaction in air. The ZnO solution which was filtered with a 0.45 μm polytetrafluoroethylene filter was spin-coated at 2000 rpm for 60 sec on the ITO-coated glass substrates and then annealed at 150 ^oC for 1 h in air. On the ZnO layer, branched PEI (Sigma-Aldrich, 0.4 wt% in deionized water) was spin-coated at 5000 rpm for 50 sec and then annealed at 100 ^oC for 10 min. After that, my samples were moved to an Ar-filled glove box for the deposition of organic materials. SPG-01T (Green polymer, Merck, 1.4 wt% in toluene) was spin-coated at 3000 rpm for 60 sec and then annealed at 90 ^oC for 1 h. As-purchased PEDOT:PSS (AI4083, Heraeus, we will call this as "pristine PEDOT:PSS") was diluted with ethanol (CH_3CH_2OH, Sigma-Aldrich) with various

volume ratios. The diluted PEDOT:PSS solution was spin-coated at 2000 rpm for 60 sec and then annealed at 120 °C for 10 min. For the deposition of top anodes, my samples were loaded to a vacuum chamber that is directly connected to the glove box and Al (99.999%, CERAC) was thermally evaporated (1500 Å).

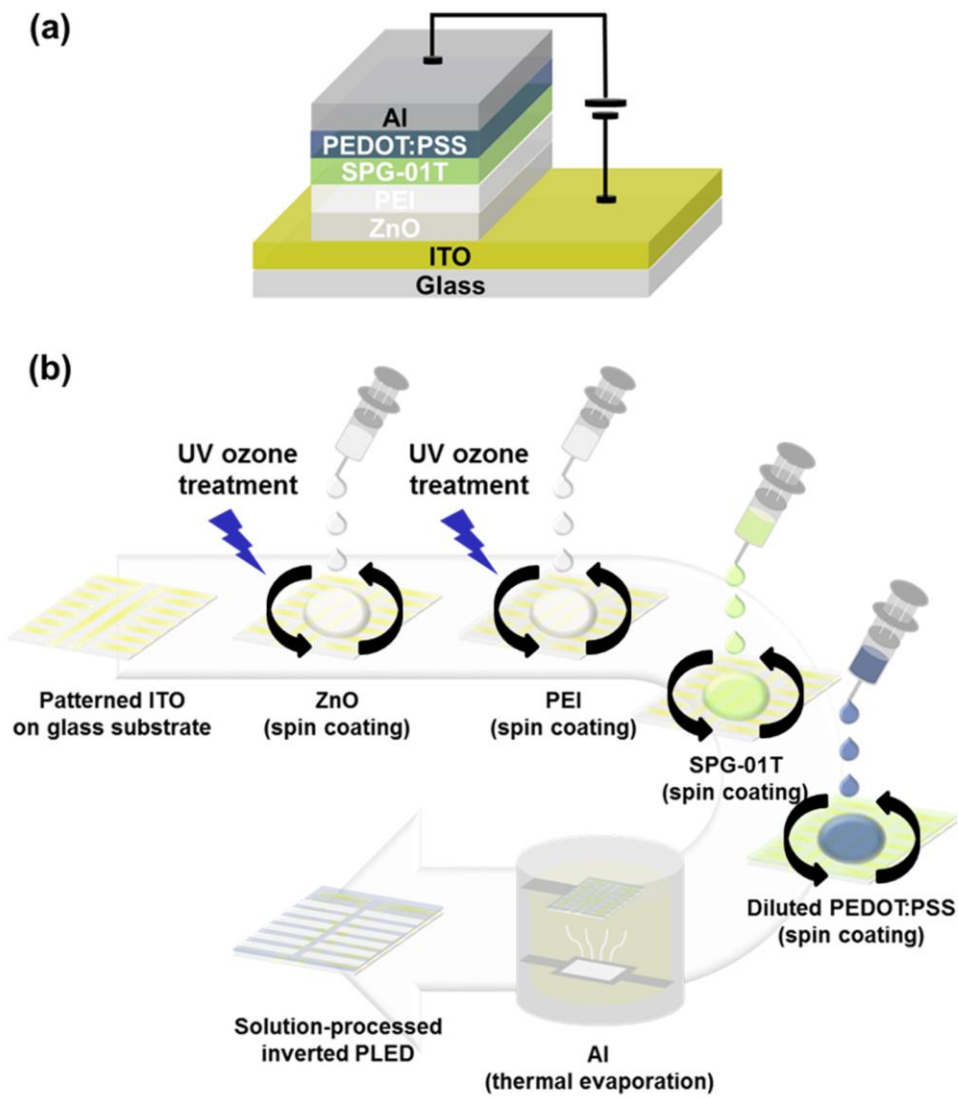

Figure 2.1 (a) Device architectures of inverted PLEDs, (b) fabrication process of inverted PLEDs.

2.2.2 Measurements

The surface tension of the diluted PEDOT:PSS solutions was measured by a surface tensiometer (KSV Model Sigma 702, KSV Instruments) and the surface energy of the solutions and EML surface was extracted from a contact angle measurement. The thickness of each layer was measured by a non-contact mode atomic force microscopy (AFM) system (XE-100, Park system) and the optical images of coated films and light emission from the devices were obtained by an optical microscope (EGTECH). The surface and shape of coated films were measured by the AFM system and 3D surface profiler (μSurf, NanoFocus), respectively. The electrical properties were measured by a digital multimeter (Keithley 2000, Keithley) and a source-measurement unit (Keithley 237, Keithley) while sweeping the bias voltage with a 0.1 V interval. The optical performance was measured by a spectrometer (CS-1000A, Konica Minolta). All measurements were performed in the air for the inverted PLEDs without encapsulation layers.

2.3 Results and Discussion

2.3.1 Ethanol-dilution method for surface energy modulation

Since a pristine PEDOT:PSS solution is hydrophilic as well known, the extremely poor wetting is expected on the hydrophobic EML materials, including SPG-01T used in this work. However, for better hole injection and thus higher device performance, the PEDOT:PSS HIL must be inserted between the EML and anodes even for the inverted PLEDs. Therefore, I have systematically investigated and further improved the wetting behavior between the PEDOT:PSS solutions and the EML surface by analyzing the wetting envelope and the polar and dispersion terms of surface tension of the PEDOT:PSS solutions. To modify the surface tension, I diluted the PEDOT:PSS solutions with ethanol at various volume ratios of 0.5:1, 1:1, 2:1, 5:1 and 10:1 as shown in **Figure 2.2(a).** It is noted that ethanol is a polar solvent which can easily dilute the aqueous PEDOT:PSS and satisfies the solvent orthogonality with the EML because the EML materials are not solved in polar solvents. In addition, since ethanol has the low surface tension of 21.40 mJ/m^2 compared to the pristine PEDOT:PSS with the surface tension of 58.31 mJ/m^2, it is expected that hydrophilicity of the pristine PEDOT:PSS can be easily modulated by changing dilution ratios and thus the wetting property of PEDOT:PSS on the EML can be further improved. **Figure 2.2(b)** indicates that a contact angle of the diluted PEDOT:PSS solutions on teflon substrates decreased when the ethanol ratio increased, which means that my dilution method is effective in enhancing the wetting property.

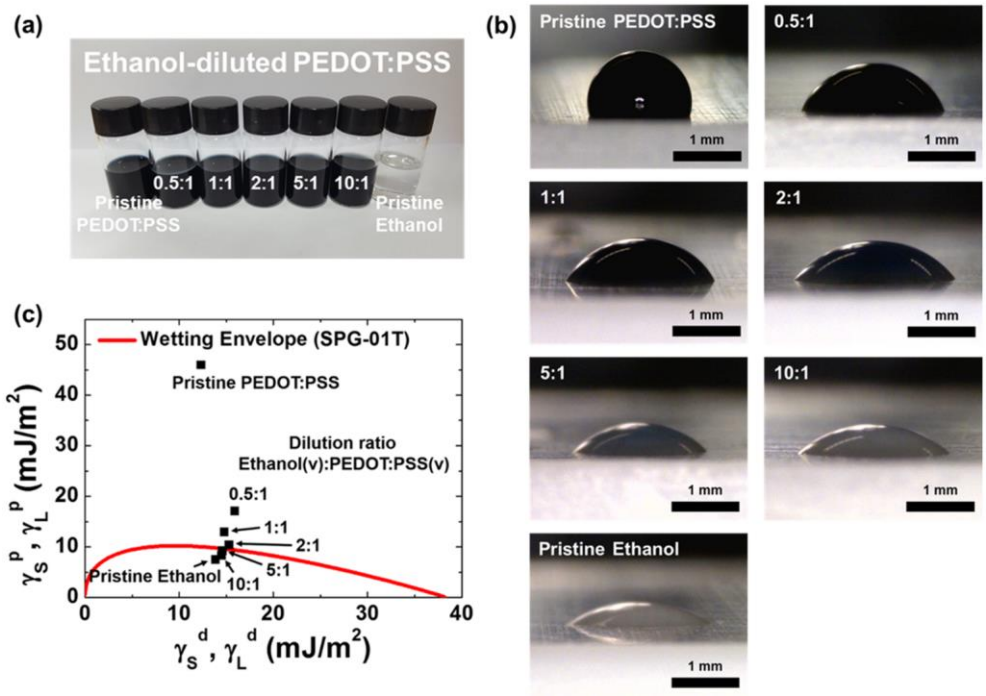

Figure 2.2 (a) A photograph of PEDOT:PSS solutions for various ratios, (b) contact angle measurements on the teflon substrates for the diluted PEDOT:PSS solutions according to the various dilution ratios, (c) a wetting envelope of SPG-01T (red line) and the polar terms of the surface tension (black square).

Dilution ratio	Contact angle on teflon (°)	Surface tension (mJ/m^2)	Dispersion term (mJ/m^2)	Polar term (mJ/m^2)
Pristine PEDOT:PSS	106.3	58.31	12.34	45.97
0.5:1	73.6	32.97	15.90	17.07
1:1	63.4	27.78	14.80	12.98
2:1	55.6	25.73	15.32	10.41
5:1	49.9	23.81	14.61	9.20
10:1	45.5	22.80	14.50	8.30
Pristine ethanol	39.7	21.36	13.85	7.51

Table 2.1 Contact angle on the teflon substrates, total surface tension and its polar and dispersion terms for the diluted PEDOT:PSS solutions according to the various dilution ratios.

Figure 2.2(c) shows the wetting envelope of the EML surface and the polar and dispersion terms of the surface tension for the envelope is usually utilized to estimate the wetting behavior of certain liquids on a solid surface [38,44-47]. First, from the measured contact angle of the EML surface, the polar and dispersion terms were extracted to be 0.04 mJ/m^2 and 38.28 mJ/m^2, respectively. And then, an equation which states the interaction between the liquid and the solid surface using the corresponding polar and dispersion terms has been derived from Young's equation and Good's equation [46,48].

$$\frac{\gamma_L(1+\cos\theta)}{2\sqrt{\gamma_L^d}} = \sqrt{\gamma_S^p}\sqrt{\frac{\gamma_L^p}{\gamma_L^d}} + \sqrt{\gamma_S^d} \quad (1)$$

where γ_L is the total surface tension of the liquid; γ_L^p is the polar term of surface tension for the liquid; γ_L^d is the dispersion term of surface tension for the liquid; γ_S^p is the polar term of surface energy for the solid; γ_S^d is the dispersion term of surface energy for the solid; and θ is the contact angle between the liquid and solid.

Using equation (1) and the measured surface energy of the EML surface, the wetting envelope function for the EML was calculated and marked as a red line in **Figure 2.2(c).** In addition, the polar and dispersion terms of the surface tension for each diluted PEDOT:PSS solution were extracted from the surface tension and the contact angle using the equation (1) as summarized in **Table 2.1** and marked as black squares in **Figure 2.2(c).** If both terms of the surface tension for a liquid are located inside the wetting envelope, the liquid has the good wetting property on the solid surface. If not, it cannot wet the solid surface and has the poor wetting property. As shown in Fig. 2(c), the black squares which represent the dilution ratio over 5:1 are located inside the envelope. Therefore, it is expected that when the dilution ratio is greater than 5:1, the diluted PEDOT:PSS solution will be uniformly coated on the EML surface.

2.3.2 Spin-coated PEDOT:PSS HIL on EML

Figure 2.3 shows the optical images of the spin-coated PEDOT:PSS films of several dilution ratios. Non-wetting phenomena are described as islands which are agglomerations of the PEDOT:PSS due to its extremely poor wetting behavior or radiation patterns which are more widespread and faded islands than the former due to the still insufficient wetting property. As shown in **Figure 2.3(a),** the pristine PEDOT:PSS was hardly coated on the EML, forming islands. As the ethanol ratio increased, the wetting property became better, but there were still islands (0.5:1 and 1:1) as shown in **Figure 2.3(b) and (c)** and radiation patterns (2:1) as shown in **Figure 2.3(d).** When the dilution ratio was greater than 5:1, islands or radiation patterns were not observed and the uniform PEDOT:PSS films were formed as shown in **Figure 2.3(e) and (f)**. However, as we investigated the magnified optical images, several voids of tens of micrometer size were still observed in case of 5:1 solution while there were no such voids in case of 10:1 solution. It is noted that the polar and dispersion terms of the 5:1 solution were located near the boundary of the wetting envelope of the EML surface and those of the 10:1 solution were located inside the envelope as shown in **Figure 2.2(c).** As a result, we can conclude that the condition when the point is located inside the envelope perfectly should be chosen to obtain the uniformly coated films by the solution process. Additionally, we measured the surface of the spin-coated PEDOT:PSS layers using AFM and 3D profiler for further investigation. As shown in **Figure 2.4(a),** the 3D profile image ($300\times300\ \mu m^2$) for 1:1 dilution condition indicates that when the dilution ratio was not optimized, the PEDOT:PSS layer was not formed into a complete film due to

the poor wetting property. However, the AFM images (5×5 μm^2) for 10:1 dilution condition show the change of surface roughness from 2.041 to 4.045 nm RMS after the spin coating on the EML as shown in **Figure 2.4(b),** which means that the 10:1 dilution condition enables complete film formation of PEDOT:PSS on the hydrophobic EML.

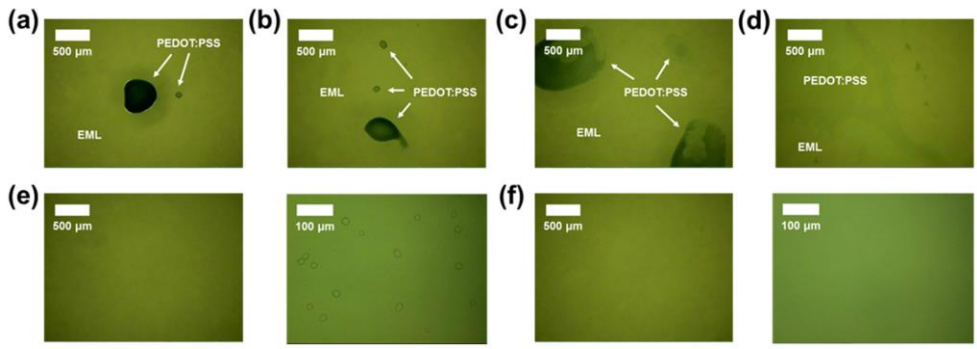

Figure 2.3 Optical images of PEDOT:PSS films on the EML for various dilution ratios (100-time magnification). (a) pristine, (b) 0.5:1, (c) 1:1, (d) 2:1, (e) 5:1, (f) 10:1. In the case of 5:1 and 10:1, higher magnification (600 times) images are also included to further investigate formation of very small voids of tens of micrometer size.

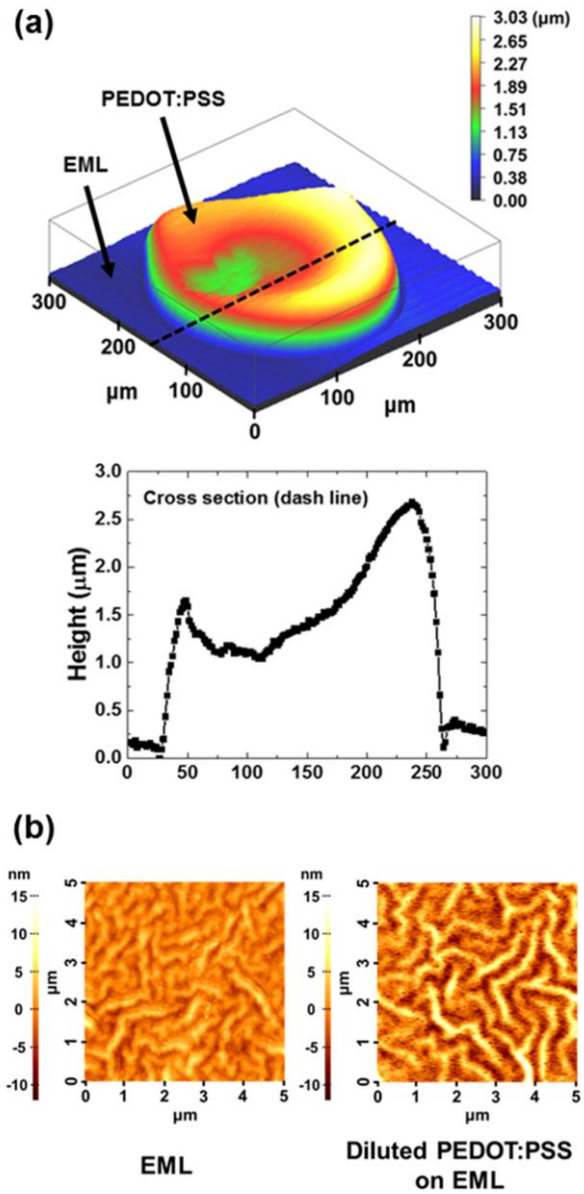

Figure 2.4 (a) A 3D profile image (top) and cross-section view at a dash line (bottom) for 1:1 dilution condition, (b) AFM images of EML (left) and diluted PEDOT:PSS on the EML (right) for 10:1 dilution condition.

2.3.3 Characteristics of inverted PLEDs

Based on my analysis, I fabricated the inverted PLEDs which have a structure of solution-processed multi-layers, especially the PEDOT:PSS HIL on the EML, sandwiched between vacuum-deposited bottom ITO (cathode) and top Al (anode) electrodes as shown in **Figure 2.1(a).** Using the 10:1 diluted PEDOT:PSS solution, we obtained a uniformly coated PEDOT:PSS HIL on the hydrophobic EML. Thicknesses of the solution-processed layers of ZnO, PEI, SPG-01T and PEDOT:PSS were 30 nm, 10 nm, 100 nm, and 20 nm, respectively. Before characterizing the devices, hole-only devices (HODs) with and without the PEDOT:PSS HIL were fabricated to investigate the effect on the hole injection. As shown in **Figure 2.5,** the HODs with the PEDOT:PSS HIL showed more than two orders of a current density compared with those without the PEDOT:PSS HIL, which means that holes are injected more effectively from the anodes to the EML due to the PEDOT:PSS HIL. Furthermore, many holes inside my inverted PLEDs can also improve the electron injection. M. Takada et al. said that the injected holes are accumulated at the PEI/EML interface and the accumulated holes induce the interfacial electric field which increases tunneling of electrons, resulting in the enhanced electron injection [34]. Therefore, an introduction of the PEDOT:PSS HIL is critical to realizing the highly efficient inverted PLEDs. **Figure 2.6** shows the emission images and the measured characteristics of the inverted PLEDs with and without the PEDOT:PSS HIL such as current density (solid symbols, mA/cm^2) and luminance (open symbols, cd/m^2) versus applied voltage (V), and current efficiency (solid symbols, cd/A) and power efficiency (open symbols, lm/W)

versus luminance (cd/m^2). As illustrated in **Figure 2.6(a) and (b)**, the inverted PLEDs with the PEDOT:PSS HIL showed a turn-on voltage of 3.3 V defined at 1 cd/m^2, a current efficiency of 9.73 cd/A and a power efficiency of 4.33 lm/W at 1000 cd/m^2, which means that my inverted PLEDs show the similar current efficiency compared to the conventional PLEDs although the operating voltage is higher due to the less effective charge injection [17]. However, when the PEDOT:PSS HIL was not used, the inverted PLEDs failed to appropriately operate in the range of the sweep voltages. As mentioned above, the PEDOT:PSS HIL in the inverted PLEDs is significant for both the hole and electron injection and thus the charge recombination can be also enhanced by the effective hole and electron injection, resulting in the high performance of the devices. Moreover, it is also important to obtain the uniform PEDOT:PSS layer because it is directly related to the uniform light emission from a pixel itself and pixel array as shown in **Figure 2.6(c).** When both wetting and non-wetting regions existed in a pixel, the light was emitted only from the wetting region (example is for 1:1 diluted PEDOT:PSS solution). As the dilution ratio increased to 10:1, the whole pixel area (1.4×1.6 mm^2) shed light uniformly. When we turned on all eight pixels in one substrate simultaneously, the devices with the uniformly coated PEDOT:PSS HIL emitted the bright light uniformly while those with the partially coated PEDOT:PSS HIL showed severely poor wetting phenomena. As a result, the PEDOT:PSS HIL enables the highly efficient inverted PLEDs with uniform characteristics in one substrate. It is also believed that all solution-processed PLEDs can be realized if the solution-processed top electrodes are deposited on the PEDOT:PSS HIL.

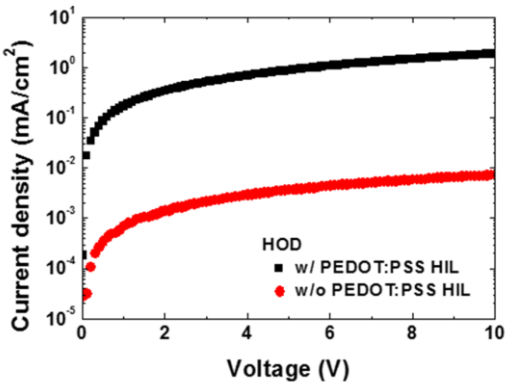

Figure 2.5 Current density versus voltage of HODs with (black square) and without a PEDOT:PSS HIL (red circle).

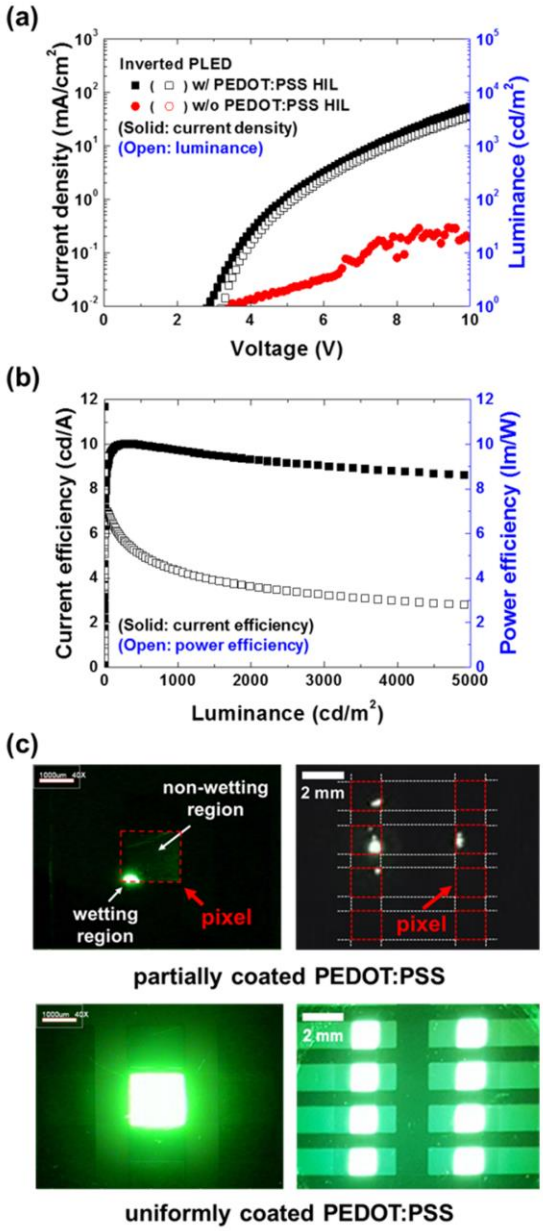

Figure 2.6 Device characteristics of inverted PLEDs. (a) current density and luminance versus voltage of inverted PLEDs with (black square) and without a PEDOT:PSS HIL (red circle), (b) current and power efficiency versus luminance-, (c) emission images of one pixel and all pixels in one substrate of inverted PLEDs with a partially (1:1 dilution condition) and uniformly (10:1 dilution condition) coated PEDOT:PSS HIL.

2.4 Summary

I demonstrated the high-performance solution-processed inverted PLEDs and PLED array by optimizing the wetting property of the PEDOT:PSS on the hydrophobic EML using the dilution method. The uniformly formed PEDOT:PSS HIL between the EML and the top anodes played an important role for the enhancement of the device performance and light emission uniformity. Although there are still rooms for further improvement, my approach showed a promising path toward all solution-processed, potentially all-printed, high-performance PLEDs. I strongly believe that both the dilution process considering the solvent orthogonality and wetting property and the printing process of the reflective cathodes and high work function polymeric anodes will further improve the device performance and provide a key enabling technology for all-printed PLED development in the near future.

Reference

[1] J. Burroughes, D. Bradley, A. Brown, R. Marks, K. Mackay, R. Friend, P. Burns, A. Holmes, Light-emitting diodes based on conjugated polymers, Nature, 347 (1990) 539-541.

[2] R. Friend, R. Gymer, A. Holmes, J. Burroughes, R. Marks, C. Taliani, D. Bradley, D. Dos Santos, J. Bredas, M. Lögdlund, Electroluminescence in conjugated polymers, Nature, 397 (1999) 121-128.

[3] G. Gustafsson, Y. Cao, G. Treacy, F. Klavetter, N. Colaneri, A. Heeger, Flexible light-emitting diodes made from soluble conducting polymers, Nature, 357 (1992) 477-479.

[4] Y. Hong, J. Kanicki, Opto-electronic properties of poly (fluorene) co-polymer red light-emitting devices on flexible plastic substrate, IEEE T. Electron Dev., 51 (2004) 1562-1569.

[5] J.-S. Park, T.-W. Kim, D. Stryakhilev, J.-S. Lee, S.-G. An, Y.-S. Pyo, D.-B. Lee, Y.G. Mo, D.-U. Jin, H.K. Chung, Flexible full color organic light-emitting diode display on polyimide plastic substrate driven by amorphous indium gallium zinc oxide thin-film transistors, Appl. Phys. Lett., 95 (2009) 013503.

[6] T.-H. Han, Y. Lee, M.-R. Choi, S.-H. Woo, S.-H. Bae, B.H. Hong, J.-H. Ahn, T.-W. Lee, Extremely efficient flexible organic light-emitting diodes with modified graphene anode, Nat. Photonics, 6 (2012) 105-110.

[7] T. Riedl, Transparent OLED Displays, in: A. Facchetti, T. Marks (Eds.), Transparent Electronics: From Synthesis to Applications, Wiley, New Jersey, 2010, 299.

[8] S. Tokito, T. Iijima, Y. Suzuri, H. Kita, T. Tsuzuki, F. Sato, Confinement of triplet energy on phosphorescent molecules for highly-efficient organic blue-light-emitting devices, Appl. Phys. Lett., 83 (2003) 569-571.

[9] K. Walzer, B. Maennig, M. Pfeiffer, K. Leo, Highly efficient organic devices based on electrically doped transport layers, Chem. Rev., 107 (2007) 1233-1271.

[10] S.J. Su, E. Gonmori, H. Sasabe, J. Kido, Highly efficient organic blue-and white-light-emitting devices having a carrier-and exciton-confining structure for reduced efficiency roll-off, Adv. Mater., 20 (2008) 4189-4194.

[11] S. Reineke, F. Lindner, G. Schwartz, N. Seidler, K. Walzer, B. Lüssem, K. Leo, White organic light-emitting diodes with fluorescent tube efficiency, Nature, 459 (2009) 234-238.

[12] R.C. Kwong, M.R. Nugent, L. Michalski, T. Ngo, K. Rajan, Y.-J. Tung, M.S. Weaver, T.X. Zhou, M. Hack, M.E. Thompson, High operational stability of electrophosphorescent devices, Appl. Phys. Lett., 81 (2002) 162-164.

[13] M. Ishii, Y. Taga, Influence of temperature and drive current on degradation mechanisms in organic light-emitting diodes, Appl. Phys. Lett., 80 (2002) 3430-3432.

[14] R. Meerheim, S. Scholz, S. Olthof, G. Schwartz, S. Reineke, K. Walzer, K. Leo, Influence of charge balance and exciton distribution on efficiency and lifetime of phosphorescent organic light-emitting devices, J. Appl. Phys., 104 (2008) 014510.

[15] H. Zheng, Y. Zheng, N. Liu, N. Ai, Q. Wang, S. Wu, J. Zhou, D. Hu, S. Yu, S. Han, All-solution processed polymer light-emitting diode displays, Nat. Commun., 4 (2013).

[16] J. Ha, S. Park, D. Kim, J. Ryu, C. Lee, B.H. Hong, Y. Hong, High-

performance polymer light emitting diodes with interface-engineered graphene anodes, Org. Electron., 14 (2013) 2324-2330.

[17] J. Ha, J. Park, J. Ha, D. Kim, S. Chung, C. Lee, Y. Hong, Selectively modulated inkjet printing of highly conductive and transparent foldable polymer electrodes for flexible polymer light-emitting diode applications, Org. Electron., 19 (2015) 147-156.

[18] M. Zhang, S. Höfle, J. Czolk, A. Mertens, A. Colsmann, All-solution processed transparent organic light emitting diodes, Nanoscale, 7 (2015) 20009-20014.

[19] H.-Y. Zhen, Y. Chen, C. Zhang, Z.-G. Zhou, K. Li, Y. Zhao, X. Mei, Q. Ling, Full-solution processed, flexible, top-emitting polymer light-emitting diodes based on the printed Ag electrodes, J. Mater. Chem. C, 5 (2017) 6400-6405.

[20] O. Hagemann, M. Bjerring, N.C. Nielsen, F.C. Krebs, All solution processed tandem polymer solar cells based on thermocleavable materials, Sol. Energ. Mat. Sol. C., 92 (2008) 1327-1335.

[21] C.W. Joo, K.S. Yook, S.O. Jeon, J.Y. Lee, Improved efficiency in solution processed green phosphorescent organic light-emitting diodes using a double layer emitting structure fabricated by a stamp transfer printing process, Org. Electron., 10 (2009) 978-981.

[22] L. Qian, Y. Zheng, J. Xue, P.H. Holloway, Stable and efficient quantum-dot light-emitting diodes based on solution-processed multilayer structures, Nat. Photonics, 5 (2011) 543-548.

[23] K.S. Yook, J.Y. Lee, Small Molecule Host Materials for Solution Processed Phosphorescent Organic Light-Emitting Diodes, Adv. Mater., 26 (2014) 4218-4233.

[24] S. Höfle, A. Schienle, C. Bernhard, M. Bruns, U. Lemmer, A. Colsmann,

Solution Processed, White Emitting Tandem Organic Light-Emitting Diodes with Inverted Device Architecture, Adv. Mater., 26 (2014) 5155-5159.

[25] S. Höfle, C. Bernhard, M. Bruns, C. Kübel, T. Scherer, U. Lemmer, A. Colsmann, Charge generation layers for solution processed tandem organic light emitting diodes with regular device architecture, ACS Appl. Mater. Interfaces, 7 (2015) 8132-8137.

[26] D. Kim, S. Jeong, H. Shin, Y. Xia, J. Moon, Heterogeneous Interfacial Properties of Ink-Jet-Printed Silver Nanoparticulate Electrode and Organic Semiconductor, Adv. Mater., 20 (2008) 3084-3089.

[27] H.J. Bolink, E. Coronado, D. Repetto, M. Sessolo, Air stable hybrid organic-inorganic light emitting diodes using ZnO as the cathode, Appl. Phys. Lett., 91 (2007) 223501.

[28] Y. Sun, J.H. Seo, C.J. Takacs, J. Seifter, A.J. Heeger, Inverted Polymer Solar Cells Integrated with a Low-Temperature-Annealed Sol-Gel-Derived ZnO Film as an Electron Transport Layer, Adv. Mater., 23 (2011) 1679-1683.

[29] J.Y. Kim, S. Noh, D. Lee, P.K. Nayak, Y. Hong, C. Lee, Solution-Processable Zinc Oxide for the Polymer Solar Cell Based on P3HT:PCBM, J. Nanosci. Nanotechno., 11 (2011) 5995-6000.

[30] M. Lu, P. de Bruyn, H.T. Nicolai, G.-J.A. Wetzelaer, P.W. Blom, Hole-enhanced electron injection from ZnO in inverted polymer light-emitting diodes, Org. Electron., 13 (2012) 1693-1699.

[31] Y. Zhou, C. Fuentes-Hernandez, J. Shim, J. Meyer, A.J. Giordano, H. Li, P. Winget, T. Papadopoulos, H. Cheun, J. Kim, A universal method to produce low–work function electrodes for organic electronics, Science, 336 (2012) 327-332.

[32] S. Höfle, A. Schienle, M. Bruns, U. Lemmer, A. Colsmann, Enhanced

Electron Injection into Inverted Polymer Light-Emitting Diodes by Combined Solution-Processed Zinc Oxide/Polyethylenimine Interlayers, Adv. Mater., 26 (2014) 2750-2754.

[33] Y.H. Kim, T.H. Han, H. Cho, S.Y. Min, C.L. Lee, T.W. Lee, Polyethylene Imine as an Ideal Interlayer for Highly Efficient Inverted Polymer Light-Emitting Diodes, Adv. Funct. Mater., 24 (2014) 3808-3814.

[34] M. Takada, T. Nagase, T. Kobayashi, H. Naito, Electron injection in inverted organic light-emitting diodes with poly (ethyleneimine) electron injection layers, Org. Electron., 50 (2017) 290-295.

[35] S.W. Heo, K.H. Baek, T.H. Lee, J.Y. Lee, D.K. Moon, Enhanced performance in inverted polymer solar cells via solution process: morphology controlling of PEDOT:PSS as anode buffer layer by adding surfactants, Org. Electron., 14 (2013) 1629-1635.

[36] A. Savva, E. Georgiou, G. Papazoglou, A.Z. Chrusou, K. Kapnisis, S.A. Choulis, Photovoltaic analysis of the effects of PEDOT:PSS-additives hole selective contacts on the efficiency and lifetime performance of inverted organic solar cells, Sol. Energ. Mat. Sol. C., 132 (2015) 507-514

[37] Q. Dong, Y. Zhou, J. Pei, Z. Liu, Y. Li, S. Yao, J. Zhang, W. Tian, All-spin-coating vacuum-free processed semi-transparent inverted polymer solar cells with PEDOT:PSS anode and PAH-D interfacial layer, Org. Electron., 11 (2010) 1327-1331.

[38] M.M. Voigt, R.C. Mackenzie, C.P. Yau, P. Atienzar, J. Dane, P.E. Keivanidis, D.D. Bradley, J. Nelson, Gravure printing for three subsequent solar cell layers of inverted structures on flexible substrates, Sol. Energ. Mat. Sol. C., 95 (2011) 731-734.

[39] R.J. Peh, Y. Lu, F. Zhao, C.-L.K. Lee, W.L. Kwan, Vacuum-free processed transparent inverted organic solar cells with spray-coated PEDOT:PSS anode, Sol. Energ. Mat. Sol. C., 95 (2011) 3579-3584.

[40] B. Park, Y.H. Huh, M. Kim, Surfactant additives for improved photovoltaic effect of polymer solar cells, J. Mater. Chem., 20 (2010) 10862-10868.

[41] W. Huang, E. Gann, L. Thomsen, A. Tadich, Y.-B. Cheng, C.R. McNeill, Metal Evaporation-Induced Degradation of Fullerene Acceptors in Polymer/Fullerene Solar Cells, ACS Appl. Mater. Interfaces, 8 (2016) 2247-2254.

[42] W.-D. Xu, W.-Y. Lai, Q. Hu, X.-Y. Teng, X.-W. Zhang, W. Huang, A hydrophilic monodisperse conjugated starburst macromolecule with multidimensional topology as electron transport/injection layer for organic electronics, Polym. Chem., 5 (2014) 2942-2950.

[43] X.-W. Zhang, Z.-F. Lei, Y.-H. Chen, K.-Y. Chen, W.-D. Xu, L. Hao, Q.-L. Fan, W.-Y. Lai, W. Huang, Efficient phosphorescent polymer light-emitting devices using a conjugated starburst macromolecule as a cathode interlayer, RSC Adv., 6 (2016) 10326-10333.

[44] D. Janssen, R. De Palma, S. Verlaak, P. Heremans, W. Dehaen, Static solvent contact angle measurements, surface free energy and wettability determination of various self-assembled monolayers on silicon dioxide, Thin Solid Films, 515 (2006) 1433-1438.

[45] D.-Y. Chung, J. Huang, D.D. Bradley, A.J. Campbell, High performance, flexible polymer light-emitting diodes (PLEDs) with gravure contact printed hole injection and light emitting layers, Org. Electron., 11 (2010) 1088-1095.

[46] C. Vicente, P. André, R. Ferreira, Simple measurement of surface free energy using a web cam, Rev. Bras. Ensino. Fis., 34 (2012) 3312.

[47] M.M. Voigt, R.C. Mackenzie, S.P. King, C.P. Yau, P. Atienzar, J. Dane, P.E. Keivanidis, I. Zadrazil, D.D. Bradley, J. Nelson, Gravure printing inverted organic solar cells: the influence of ink properties on film quality and device performance, Sol. Energ. Mat. Sol. C., 105 (2012) 77-85.

[48] C. Rulison, Two-component surface energy characterization as a predictor of wettability and dispersability, Application note 213, KRUSS GmbH, Hamburg, 2000.

Chapter 3

Transfer printing of conductive PEDOT:PSS for all solution-processed inverted PLEDs

3.1. Introduction

Organic light emitting diodes (OLEDs) have emerged as future displays such as flexible, bendable and rollable displays [1-5]. Currently, most commercial OLED products including smart phones, tablet PCs and televisions are fabricated using a vacuum process to ensure high performance and stability, while it causes high product prices by demands for high-cost vacuum equipment, expensive fine metal masks and low throughput. For low-cost and large-area mass production, a solution process such as spin coating [6-15], spray coating [11, 16] and several printing techniques [7, 8, 13, 17] has been applied to fabricating the devices with high efficiency and robustness, simultaneously.

As part of this approach, polymer light emitting diodes (PLEDs) have been extensively researched using soluble emission materials dissolved in various

organic solvents along with the solution-processed electrodes and functional layers [6-15]. Although the vacuum process has been still needed for manufacturing the solution-processed PLEDs not long ago, especially on an emission layer (EML), some groups report all solution-processed PLEDs in the recent, whereas there are still remaining rooms for further improvement in many respects. M. Zhang et al. demonstrated the transparent inverted PLEDs with a device structure of poly(3,4-ethylenedioxythiophene):poly(styrenesulfonate) (PEDOT:PSS)/zinc oxide (ZnO)/polyethyleneimine (PEI)/super yellow (SY)/tungsten oxide/PEDOT:PSS where all layers were spin coated including top and bottom PEDOT:PSS electrodes [10]. The devices were patterned by adhesive tapes and showed excellently high efficiency due to an ultrathin PEI interlayer which further promotes electron injection. Similarly, H. Zhen et al. also showed the top-emitting inverted PLEDs with the printed Ag bottom cathodes and spin-coated PEDOT:PSS top anodes whose patterning was carried out using a silk screen and polydimethylsiloxane (PDMS) stick, respectively [12]. However, these two papers used the unproductive patterning methods for the electrodes and thus demonstrated only one or a few devices on one substrate, which is unsuitable for the mass production of large-scale devices. Furthermore, Z. Shu et al. also illustrated the devices with a structure of indium tin oxide (ITO) or PEDOT:PSS/Al:ZnO:PEI/SY/PEDOT:PSS where all layers except for the EML were deposited through inkjet printing [13]. Meanwhile, when the PEDOT:PSS top anodes were inkjet printed on the plasma-treated EML, it caused extremely poor device performance due to damages of underlying layers by the surface treatments or solvents during the process. In contrast with a direct deposition of top electrodes by the solution process, dry transfer printing was employed for their deposition in the PLEDs [9, 14]. Still, it required the pre-

patterned stamp which was fabricated by photolithography to obtain the patterned top electrodes, which is not appropriate to the simple fabrication of the devices. To my knowledge, the manufacturing methods about all solution-processed PLEDs which have been introduced in previous reports are not compatible with the low-cost and large-area mass production for the highly customizable PLEDs.

In this **Chapter 3**, in order to overcome a patterning issue and avoid several damages by the surface treatments or solvents during the process, I conducted the transfer printing of PEDOT:PSS which was pre-deposited with a desired pattern size and shape using the inkjet printing. The freely and easily patternable transparent conductive electrodes (TCEs) can be transferred onto various substrates by formulating the adhesive PEDOT:PSS ink and controlling several transfer conditions. Employing the transfer printing, I also fabricated high-performance all solution-processed PLEDs (a-PLEDs) with the spin-coated functional layers and electrodes such as the inkjet-printed Ag cathodes and transferred PEDOT:PSS anodes. In this case, the dry transfer printing did not lead to any degradation in the devices. Furthermore, the devices on the plastic substrate showed excellent mechanical flexibility, maintaining their characteristics even after the bending stress. In particular, because my electrodes can be formed easily and freely using the maskless inkjet printing, the customized a-PLEDs and their arrays were demonstrated with the various-shaped pixels and fine lines, respectively, including 5×7 passive matrix PLEDs (PMPLEDs). I strongly believe that my all solution-processed flexible PLEDs pave the way for the low cost and large-area mass production of the flexible display, realizing a variety of future displays introduced in science fiction films as well.

3.2. Experiments

3.2.1 Transfer printing of PEDOT:PSS electrodes

Conducive PEDOT:PSS (HIL-1005, Orgacon) containing 2 wt% fluorosurfactant (Capstone FS-30, Chemours) was blended with a D-sorbitol aqueous solution (2.35g/g in deionized (DI) water, Sigma Aldrich) with a weight ratio of 9:1 to give an adhesive force. Using a piezoelectric inkjet printer (DMP-2831, Dimatix Corp.), the blended PEDOT:PSS was printed on the quartz substrate which was preheated in a furnace set to 800 ^{o}C for 1 h to reduce the adhesion between the PEDOT:PSS film and quartz substrate, resulting in the completed film after the drying at 110 ^{o}C for 10 min. A 450-μm-thick PDMS elastomeric stamp was prepared by pouring the PDMS mixture which was acquired by mixing a PDMS elastomer and curing agent (Sylgard 184, Dow Corning) at a weight ratio of 10:1 to a petri dish. After the thermal curing at 100 ^{o}C for 2 h, the resulting PDMS was cut in a desired size. The quartz substrate with the inkjet-printed PEDOT:PSS film and the PDMS stamp which was pretreated with an air plasma at 15 W for 6 s were attached and then pressed with a weight of 2 kg for 10 min. After a peeling off, the PDMS stamp with the PEDOT:PSS film was attached again to a target substrate which had an adhesive layer of PEDOT:PSS hole injection layer (PEDOT:PSS HIL, AI4083, Heraeus). Afterwards, the attached sample was placed on a hot plate set to 70 ^{o}C for 1 min, thereby obtaining the transferred PEDOT:PSS film after the peeling off.

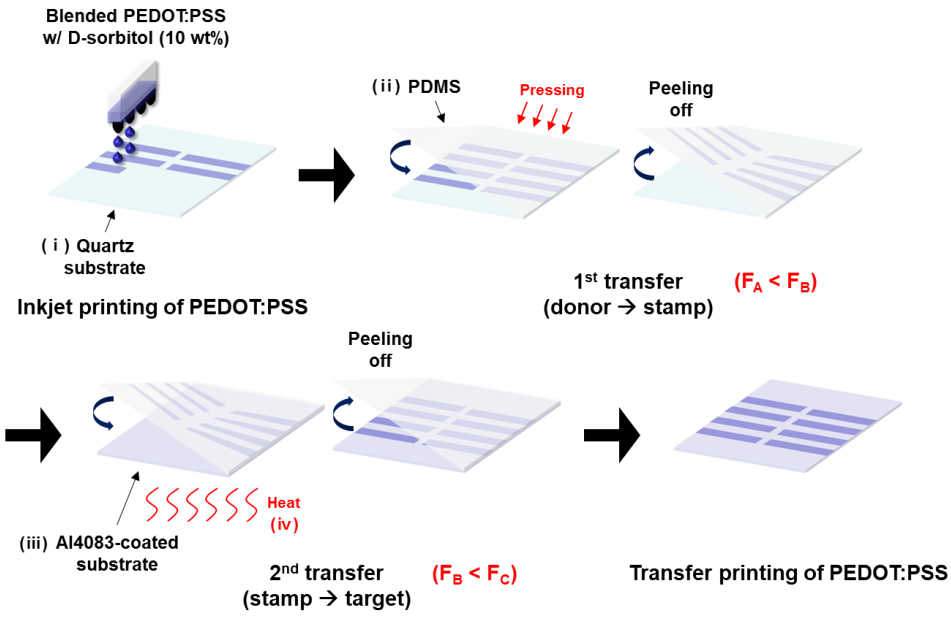

Figure 3.1 Schematic illustration of transfer printing of PEDOT:PSS.

3.2.2 Fabrication of all solution-processed PLEDs

The organometallic silver ink (JET-004T, KunShan Hisense Electronic Co., Ltd.) was deposited on the 700-μm-thick glass substrate and 120-μm-thick polyethylene-naphthalate (PEN, Q65H, Teijin Dupont Films) substrate using the inkjet printer and then the 160-nm-thick inkjet-printed Ag cathodes were achieved after annealing at 170 ^{o}C for 30 min. Afterwards, the samples were moved to an Ar-filled glove box to avoid moisture or oxygen in air atmosphere. For effective electron injection, the zinc oxide nanoparticle (ZnO NP, N-11-Slot, Nanograde) solution which was diluted with isopropyl alcohol at a weight ratio of 1:4 was spin coated at 4000 rpm for 30 s and then dried at 150 ^{o}C for 10 min, which was

repeated three times to obtain the optimized thickness of the ZnO layer. Next, the PEI solution (0.4 wt% in 2-methoxyethanol, Sigma Aldrich) was spin coated at 5000 rpm for 30 s and then cured at 100 ^{o}C for 10 min. To remove PEI residues, the samples were rinsed with ethanol for 30 s. To deposit the EML, the SY solution (0.6 wt% in toluene, PDY-132, Merck) was spin coated at 1000 rpm for 60 s and then annealed at 90 ^{o}C for 1 h. Subsequently, for effective hole injection, the diluted PEDOT:PSS HIL solutions with ethanol at a volume ratio of 1:20 and 1:10 to enhance the wetting property on the hydrophobic SY layer were spin coated at 2000 rpm for 60 s sequentially. And then, the pristine PEDOT:PSS HIL as received was further spin coated with a same recipe, forming the PEDOT:PSS HIL with the optimized thickness after drying at 120 ^{o}C for 30 min. Finally, the conductive PEDOT:PSS film on the PDMS stamp was transferred to the devices as the top anode using the abovementioned method. For comparison, we also fabricated partially solution-processed PLEDs (p-PLEDs) with the same device structure except for both electrodes which were the 150-nm-thick ITO bottom cathodes and 130-nm-thick evaporated Al top anodes on the glass substrate as the references. The schematic illustration is depicted in **Figure 3.2**.

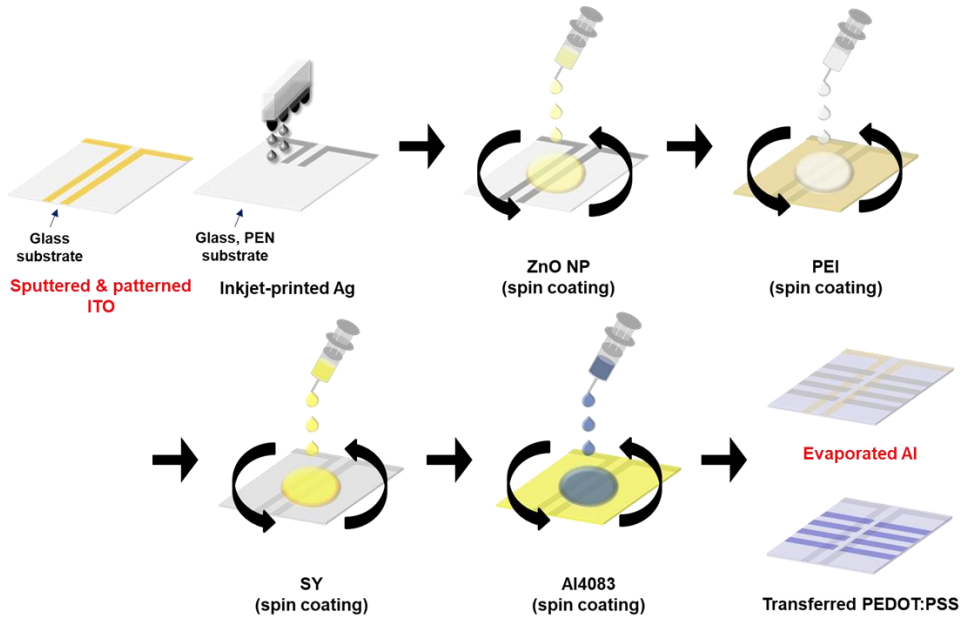

Figure 3.2 Fabrication process of PLEDs.

3.2.3 Characterizations and measurements

The adhesive force of as-purchased and blended PEDOT:PSS films was investigated using a 90° peel-off test (Universal Testing Machine, WL2100, Withlab Co., Ltd.). The contact angle (CA) measurement was conducted using a custom-made equipment. The sheet resistance and optical property of the electrodes were measured by a four point probe (FPP-5000, Changmin) and UV/Vis spectrometer (Lambda 35, PerkinElmer), respectively. For investigation of mechanical properties, the bending test was carried out using a home-made bending machine and the resistance of the electrodes was measured using a Keithley 2400 sourcemeter. The work function of the electrodes and functional

layers was examined by an ultra-violet photoelectron spectroscopy (UPS, PHI 5000 VersaProbe, ULVAC-PHI, Inc.) with He source (21.2 eV). The surface and thickness of each layer were investigated using a non-contact mode atomic force (AFM) system (XE-100, Park system) and surface profiler (DektakXT-A, Bruker). The electrical characteristics of PLEDs were measured by a digital multimeter (Keithley 2000, Keithley) and a source-measurement unit (Keithley 237, Keithley) by sweeping the bias voltage with an interval of 0.1 V. The optical performance of PLEDs was obtained by a spectrometer (CS-1000A, Konica Minolta). In order to operate the various-shaped PLEDs and arrays including the passive matrix, a DC power supply (SJ-5003D, Sejin Power Tech Co.) was connected to them, varying the applied voltage. The encapsulation was performed using a cover glass and UV-curable resin (XNR5570, Nagase ChemteX Corp.) to avoid degradation in device performance during the measurement. Before the encapsulation and measurement, the flexible devices were bended in the glove box to exclude the degradation by environmental factors.

3.3. Results and Discussion

3.3.1 Principles of transfer printing of PEDOT:PSS

In order to solve a patterning issue and minimize solvent damages during the solution process, we integrated inkjet printing and transfer printing in depositing the PEDOT:PSS film, as depicted in **Figure 3.1**. For the successful transfer printing, I formulated the blended PEDOT:PSS ink by adding a D-sorbitol aqueous solution to as-purchased PEDOT:PSS to give an adhesive force to the resulting film. D-sorbitol was widely used as an electrical glue to ensure effective mechanical and electrical bonding during a lamination process in various optoelectronic devices [18-21]. **Figure 3.3** shows a quantitative measurement of the adhesive force using a 90° peel-off test. The adhesive force of the as-purchased PEDOT:PSS film was 9.8 N/m, whereas that of the blended PEDOT:PSS film was dramatically improved to 18 N/m, which means that my blended PEDOT:PSS film allows other substrate to strongly adhere to the existing substrate containing the film. The inset images showed the successful transfer only in the case of the blended PEDOT:PSS film.

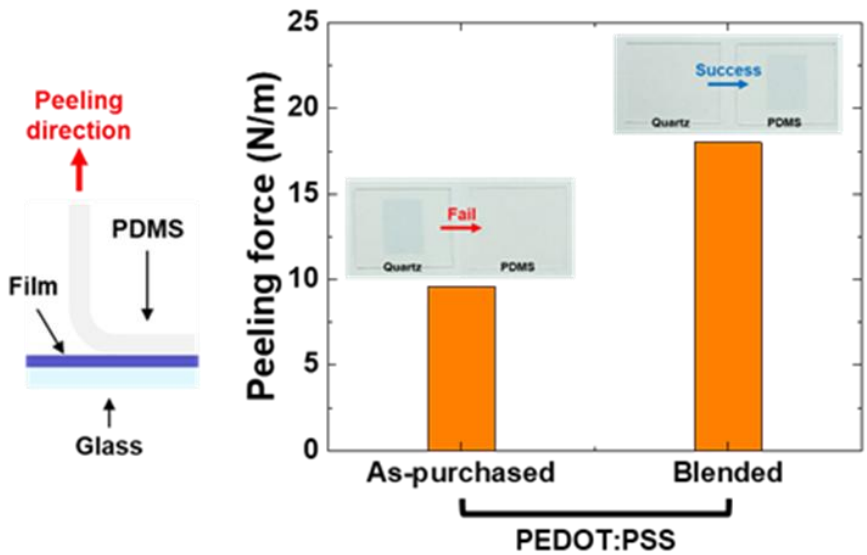

Figure 3.3 An adhesive force of as-purchased and blended PEDOT:PSS films using a 90 ^{o} peel-off test. Inset images show success or failure for two types of the PEDOT:PSS films.

In addition, I also carefully adjusted several transfer conditions to separate the attached substrates and thus transfer the PEDOT:PSS film onto the desired substrate, which is achieved by controlling the adhesion between the film and each substrate such as donor quartz, PDMS stamp and target substrates (The adhesive forces of the film with the quartz, PDMS stamp and target substrates denote F_A, F_B and F_C, respectively). As shown in **Figure 3.4**, the CA measurement was implemented to detect the variation of the adhesive force of the substrates before and after the treatment in each transfer process. The relationship with the CA and adhesive force can be inferred from the following two equations. The one states the adhesion (W_A) between two solids (S, S^*) which the adhesive force is proportional to using their surface energy [22].

$$W_A = 2\sqrt{\gamma_{S_1}^p \gamma_{S_2}^p} + 2\sqrt{\gamma_{S_1}^d \gamma_{S_2}^d} \quad (1)$$

where γ is the surface energy; and the subscripts p, d denote the polar and dispersion terms of the surface energy, respectively. The other states the interaction between the solid and liquid in terms of the CA [15].

$$\frac{\gamma_L(1+\cos\theta)}{2} = \sqrt{\gamma_S^p \gamma_L^p} + \sqrt{\gamma_S^d \gamma_L^d} \quad (2)$$

where γ is the surface energy; the subscripts S, L denote the solid and liquid, respectively; and the subscripts p, d denote the polar and dispersion terms of the surface energy, respectively; and θ is the CA between the solid and liquid.

In this work, S and S^* represent each surface such as the quartz, stamp and target substrates and the PEDOT:PSS film, respectively. As you can see Equation 1 and 2, if the CA of the liquid decreases, the total surface energy of the solid increases due to its enhanced polar and dispersion terms, thereby increasing the adhesion and thus adhesive force [22]. If not, the adhesive force of the solid decreases. Equation 3 explains the relationship with the CA and adhesive force.

$$1/CA \propto \gamma_S \ (= \gamma_S^p + \gamma_S^d) \propto W_A \propto F \quad (3)$$

Therefore, the principle of the transfer printing was analyzed by examining the CAs on both substrates in each step, accompanied by the change of the

adhesive forces.

First, for the more effective 1st transfer from the quartz substrate to the PDMS stamp, F_A should be weaker than F_B. In order to satisfy this requirement, a preheating procedure for the quartz substrate was carried out prior to the inkjet printing to reduce the adhesive force. As shown in **Figure 3.4**, the CA of the blended PEDOT:PSS solution on the quartz substrate increased from 17.8 to 30.1° after the preheating procedure, which is attributed to dehydration of OH groups on the surface of the quartz substrate [23]. In this case, the reduction of the OH groups allows the adhesion property to be declined significantly because it is generally known that the OH groups on the quartz substrate and PSS groups on the PEDOT:PSS film are H-bonded [9]. On the contrary, too excessive reduction of the OH groups hinders the precise formation of the PEDOT:PSS film via the inkjet printing due to the poor wetting property, but my preheating procedure provides the optimized condition where the well-printed film can be successfully transferred from the donor to the stamp. Furthermore, F_B can be further enhanced by pretreating the PDMS stamp with an air plasma [24-26]. As illustrated in **Figure 3.4**, the DI water CA on the PDMS changed from 97.6 to 85.6° after the plasma treatment at 15 W for 6 s, which indicates that the adhesive force of the plasma-treated PDMS stamp increased. However, too much plasma treatment is unsuitable for the 2nd transfer from the PDMS stamp to the target substrate because the excessively strong F_B prevents the detachment of the PEDOT:PSS film from the PDMS stamp. Consequently, the moderate treatments for the donor and stamp permit the successful 1st transfer while not having a negative influence on both the film formation and transfer process.

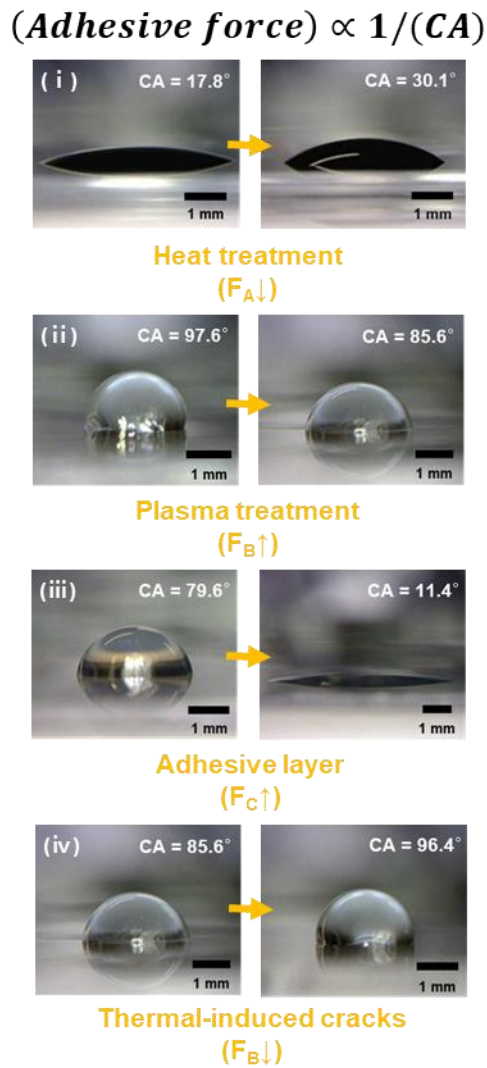

Figure 3.4 CA changes by a treatment in each transfer process. The 1st transfer (i and ii) and the 2nd transfer (iii and iv) are also marked in Figure 3.1.

After finishing the 1st transfer, the 2nd transfer was performed by making F_B weaker than F_C. When the PDMS stamp and target substrate were attached each other, the attached sample was placed on the hot plate to decrease F_B by thermal-induced cracks on the surface of the plasma-treated PDMS stamp [27]. The cracks not only reduce the contact area between the film and stamp but also promote the

hydrophobic recovery of the PDMS, facilitating the detachment of the PEDOT:PSS film from the stamp [28]. I found existence of the cracks and hydrophobic recovery through the CA change because it is announced that the CA on the surface increases when its roughness increases or the surface energy decreases [29]. **Figure 3.4** demonstrates the DI water CAs on the PDMS before and after the thermal treatment. It was found to 85.6^{o} for the non-thermal treated PDMS, whereas it was considerably increased to 96.4^{o} for the thermal-treated PDMS. Moreover, the 2nd transfer can be more easily achieved on arbitrary substrates with assistance of an less conductive PEDOT:PSS adhesive layer (i.e. PEDOT:PSS HIL) by making F_C stronger, which is probed by the CA decease on the PEN substrate from 79.6 to 11.4^{o}, as shown in **Figure 3.4**. For more in-depth understanding, **Figure 3.5** describes failure or instability of the transfer process when each condition is unsatisfied.

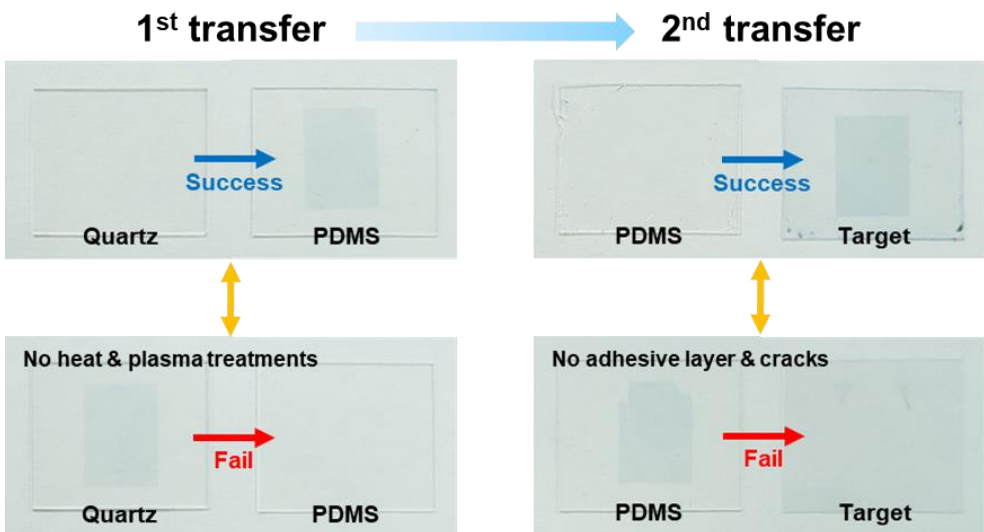

Figure 3.5 Photographs of success or fail in transfer printing of PEDOT:PSS according to transfer conditions.

Figure 3.6 presents several PEDOT:PSS films with a wide range of pattern shapes on the arbitrary target substrates such as glass, PEN and silicon substrates using the transfer printing (hereafter, I call them “transferred PEDOT:PSS films”). This approach leads to formation of the easily patternable PEDOT:PSS films with a high degree of freedom, thereby settling the patterning issue. In addition, it can avoid the solvent damages of underlying layers during the process, which means that the solvent orthogonality which should be considered carefully in the conventional solution process becomes irrelevant by the transfer process. In this paper, I focused on the transfer printing of PEDOT:PSS on the PEN substrates to explore the applicability to flexible electrodes or electronics.

Figure 3.6 Various-shaped transferred PEDOT:PSS films on the glass, PEN and silicon substrates.

3.3.2 Optoelectronic and mechanical properties

This section shows not only electrical and optical properties but also mechanical flexibility. The thickness and surface roughness of the transferred PEDOT:PSS film was 100 nm and 3.7 nm RMS, respectively, when the inkjet printing was conducted with a drop spacing of 25 μm which was fixed for the uniform film formation. As seen in **Figure 3.7**, the transferred PEDOT:PSS film on the PEN substrate exhibited a sheet resistance of 260.6 Ω/□ and a transmittance of 92.1 % at the wavelength of 550 nm. When compared with ITO on the PEN substrate, it was more transparent but less conductive, which is the typical property of the PEDOT:PSS reported in other papers [8, 30, 31]. However, when I used the blended PEDOT:PSS film for the effective transfer process, there was the slight increase of the sheet resistance compared to the as-purchased PEDOT:PSS film, as shown in **Figure 3.8**. In addition to the optoelectronic properties of the transferred PEDOT:PSS film, I also examined its mechanical stability by carrying out a bending test under a bending radius of 2 mm for 1000 cycles using a custom-made bending machine. When my PEN substrate was bended repeatedly at a bending radius smaller than 2 mm, it lost the force of restitution and plastic deformation took place. As illustrated in **Figure 3.9**, the resistance of the transferred PEDOT:PSS film was maintained almost constant after the bending test, while that of the ITO drastically increased over tens of thousands of times due to its inherent brittleness. This result was further supported by observing the change of light brightness in the light emitting diode (LED) which was placed on the PEDOT:PSS or ITO electrode before and after the 1000 bending cycles with a bending radius of

2 mm, as displayed in **Figure 3.10**. After the bending cycles, there was no outstanding change of the light brightness in the LED connected to the PEDOT:PSS at the same applied voltage, while the LED connected to the ITO did not emit any light due to its extremely increased resistance. Therefore, my transferred PEDOT:PSS electrodes can be utilized as flexible TCEs like as-printed PEDOT:PSS electrodes [8].

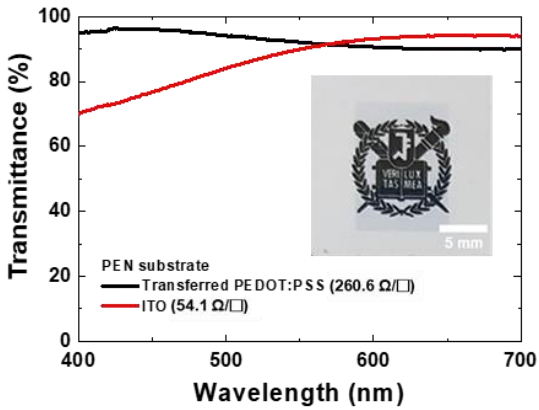

Figure 3.7 A sheet resistance and a transmittance in the visible wavelength range of transferred PEDOT:PSS and ITO films on PEN substrates.

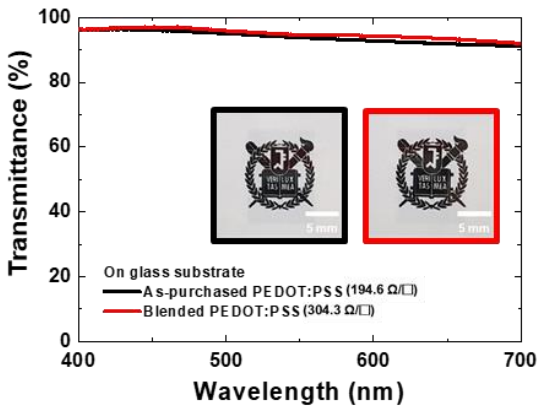

Figure 3.8 A sheet resistance and a transmittance in the visible wavelength range of as-purchased and blended PEDOT:PSS films on glass substrates (as-printed).

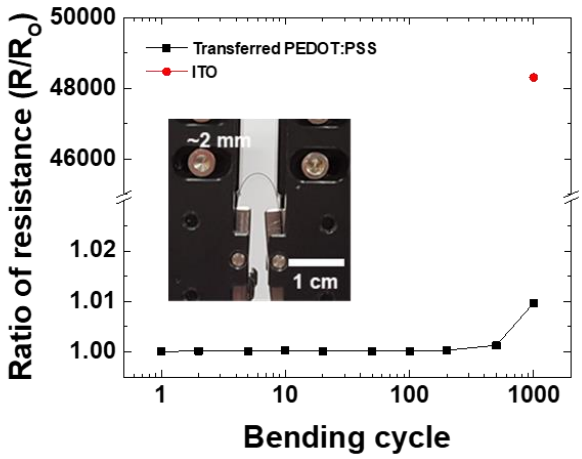

Figure 3.9 A bending test at a bending radius of 2 mm for 1000 cycles of transferred PEDOT:PSS and ITO films on PEN substrates.

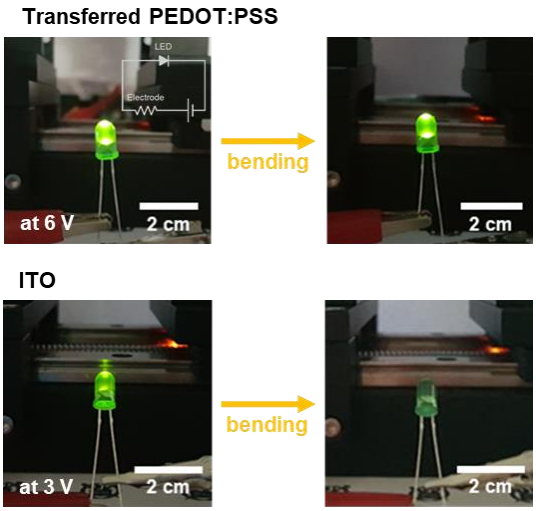

Figure 3.10 Light brightness change of a LED which is connected with transferred PEDOT:PSS and ITO films on PEN substrates at a bending radius of 2 mm over 1000 cycles.

3.3.3 Characteristics of rigid p-PLEDs and a-PLEDs

Based on these results, the transferred PEDOT:PSS electrodes were applied to top anodes of inverted PLEDs for realization of a-PLEDs. For comparison, p-PLEDs were also fabricated with the same device structure except for both electrodes which were the ITO bottom cathodes and evaporated Al top anodes. However, both devices have different thicknesses of the PEDOT:PSS HIL and ZnO/PEI layer (i.e. 30 nm PEDOT:PSS HIL, 10/3 nm ZnO/PEI layer in the p-PLED; 90 nm PEDOT:PSS HIL, 25/6 nm ZnO/PEI layer in the a-PLED) for the optimized device characteristics. Therefore, as shown in **Figure 3.11**, three types of the devices were prepared such as the p-PLEDs on the glass substrate and a-PLEDs on the glass and PEN substrates while the thickness of SY was fixed to 80 nm in all devices. In the a-PLEDs, the functional layers including ZnO, PEI, SY and PEDOT:PSS HIL were spin coated on the inkjet-printed Ag bottom cathodes sequentially and then the transferred PEDOT:PSS electrodes were deposited on the devices without the top anodes. The detailed fabrication process and its schematic illustration are described in Experimental section and **Figure 3.2**, respectively. In order to achieve high device performance, hole and electron injections were improved by inserting the PEDOT:PSS HIL and ZnO/PEI layer, respectively. Especially, a poor wetting property of the PEDOT:PSS HIL on the hydrophobic SY was improved by diluting it with ethanol, as explained in my previous publication [15]. In addition, the ZnO layer was implemented not only to enhance the electron injection but also to prevent exciton quenching at the adjacent electrodes [32]. I also used an ultrathin PEI interlayer on the ZnO layer because it further promotes

the electron injection due to the reduced work function by the interface dipole [32-34]. Energy band diagram in **Figure 3.12** explains well-defined energy levels, which is determined by a UPS measurement and reference from a previous report [14]. Therefore, they facilitate both hole and electron injections and thus realizing the high device efficiency.

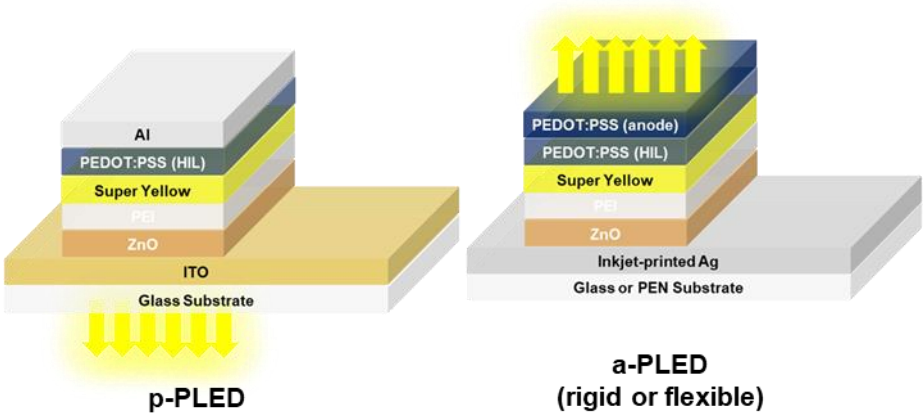

Figure 3.11 Device architectures of p-PLEDs and a-PLEDs.

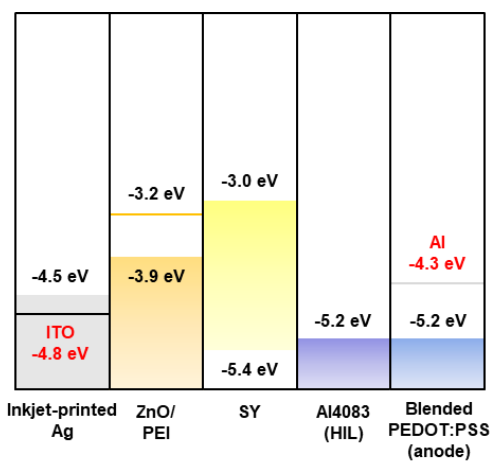

Figure 3.12 Energy band diagram of p-PLEDs and a-PLEDs.

Figure 3.13 shows the device characteristics of the p-PLEDs and a-PLEDs on the glass and PEN substrates such as current density (solid symbols, mA/cm^2) and luminance (open symbols, cd/m^2) versus applied voltage (V), and current efficiency (solid symbols, cd/A) and power efficiency (open symbols, lm/W) versus luminance (cd/m^2). In the glass substrate, my a-PLEDs showed a turn-on voltage of 2.2 V defined at 1 cd/m^2, which is similar with the p-PLEDs. In addition, the p-PLEDs exhibited a current efficiency of 10.6 cd/A and a power efficiency of 8.0 lm/W at 1000 cd/m^2, while the a-PLEDs exhibited a current efficiency of 10.4 cd/A and a power efficiency of 7.2 lm/W at 1000 cd/m^2. Although my a-PLEDs were fabricated via all solution processing, especially in forming both electrodes, the comparable characteristics of two devices are attributed to the proper energy alignment between the EML and each electrode, as seen in **Figure 3. 12**. Because the charge injection can be affected by not only the injection barrier but also the interface property [35-38], the similar charge recombination appears in the p-PLEDS and a-PLEDs, thereby exhibiting the corresponding current efficiency. However, the high resistance of the PEDOT:PSS anodes distorts the operational voltage, especially in the high voltage region, which is confirmed by the smaller power efficiency in the a-PLEDs. As the current level increases over 1 mA, a voltage drop becomes dominant, which means that the higher applied voltage is needed to maintain the same luminance. Therefore, I expect the more improved device performance if the more conductive top anodes were developed.

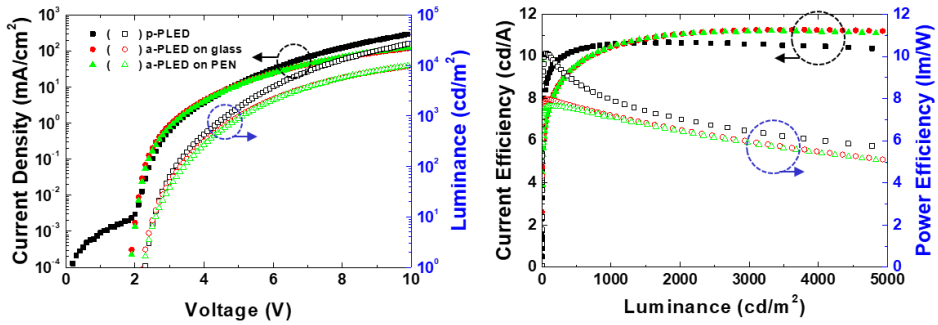

Figure 3.13 IVL- (left), efficiencies (right) of p-PLEDs on the glass substrate (black square), a-PLEDs on the glass substrate (red circle) and a-PLEDs on the PEN substrate (green triangle).

In terms of the current efficiency, following two reasons suppress further enhancement of the device performance of the a-PLEDs. First, the coffee-ring effect during the inkjet printing occurs a non-uniform surface profile of the Ag electrode unlike the wet-etched ITO, as shown in **Figure 3.14**. Although both electrodes have a similar surface roughness, it not only deteriorates the electron injection property but also causes severe exciton quenching at the protruding region in the cathodes where the relatively thinner ZnO/PEI layer can be formed. As seen in **Figure 3.15**, actually, more gradual increase of the luminance as the function of the current was observed in the case of the a-PLEDs with the thin ZnO/PEI layer, which comes from the exciton quenching at the prominent area of the Ag cathodes. Therefore, in order to prevent or relieve the exciton quenching, the thickness of the ZnO/PEI layer became thicker. Second, the difference of optical performances of the reflective electrodes in each device influences total light extraction. The bottom-emission p-PLEDs and top-emission a-PLEDs utilize the evaporated Al and inkjet-printed Ag as the reflective electrodes, respectively. However, the inkjet-printed Ag showed a relative reflectance of 88.6 % by the

evaporated Al at the wavelength of 550 nm, which means the decrease of reflected light from the reflective electrodes in the case of the a-PLEDs. Moreover, although the evaporated Al does not transmit any light, the inkjet-printed Ag has very little transmittance, which also reduces the amounts of the reflected light toward the emission direction. The electrical and optical properties of both reflective electrodes were summarized in **Table 3.1**. It is expected that the more efficient a-PLEDs will be manufactured if the high-quality Ag electrodes are created via the inkjet printing.

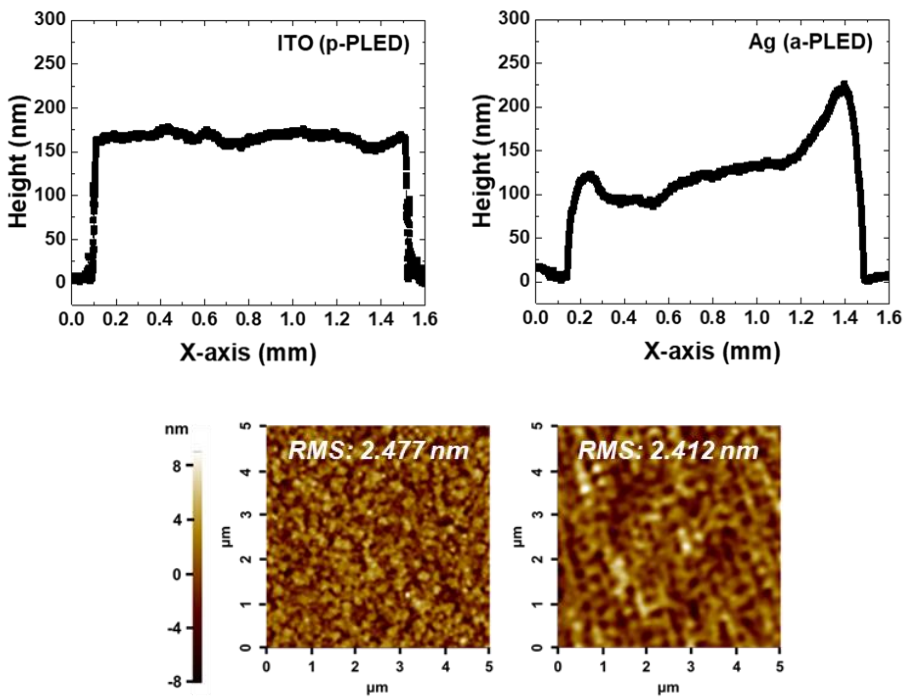

Figure 3.14 A surface profile (top) and morphology (bottom) of bottom electrodes of PLEDs. Sputtered and wet-etched ITO (p-PLED, left), Inkjet-printed Ag (a-PLED, right).

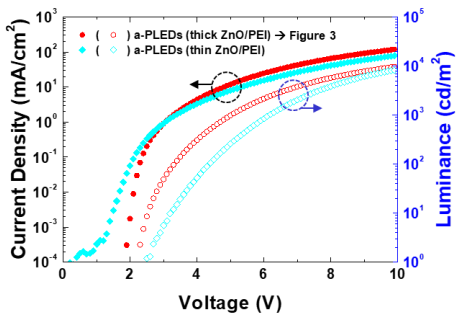

Figure 3.15 IVL of a-PLEDs with thick and thin ZnO/PEI layers.

	Sheet resistance (Ω/□)	Relative reflectance at 550 nm (%)	Transmittance at 550 nm (%)	Thickness (nm)
Evaporated Al	0.27	100.0	0.0	135.5
Inkjet-printed Ag	0.57	88.6	1.2	162.2

Table 3.1 Electrical and optical properties and thickness of reflective electrodes in each device.

3.3.4 Characteristics of flexible a-PLEDs

Employing this manufacturing method, the a-PLEDs on the PEN substrate were also fabricated, showing the comparable device performance to those on the glass substrate. In addition, I further investigated the mechanical flexibility of the devices for the application to the flexible display. **Figure 3.16** shows the device characteristics of the a-PLEDs on the PEN substrate whether a bending stress is applied or not. After the devices were bended using a syringe with a diameter of 7 mm for 100 cycles, no significant degradation in the device characteristics was observed in I-V-L and efficiency curves. In terms of the current efficiency at 1000 cd/m^2, they remained about 91.3 % compared to the no-bended devices. It is ascribed to the excellent mechanical properties of all layers, including the transferred PEDOT:PSS anodes, which means that my devices can be applied to the flexible display which has the high mechnical robustness under various deformation conditions. The device characteristics of all devices are summarized in **Table 3.2**.

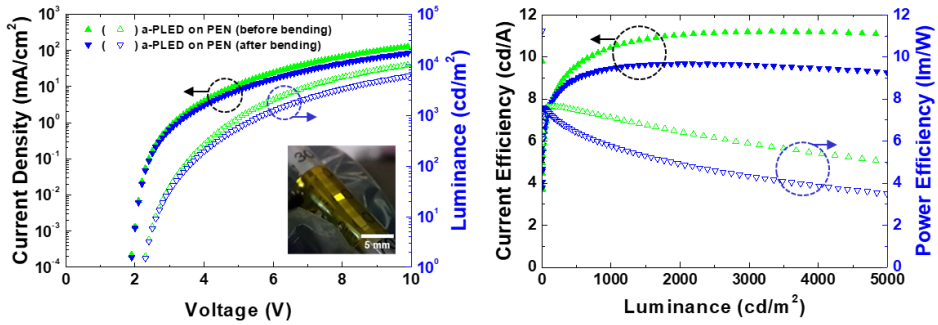

Figure 3.16 IVL- (left), efficiencies (right) of a-PLEDs on the PEN substrate before (green triangle) and after 100 bending cycles (blue inverted triangle).

Device	Turn-on voltage	Voltage at 1 mA	Efficiencies around 1000 cd/m²		
	(V)	(V)	cd/A	lm/W	Luminance (cd/m²)
p-PLED on glass	2.3	6.4	10.6	8.0	944.6
a-PLED on glass	2.2	7.1	10.4	7.2	981.2
a-PLED on PEN	2.2	7.0	10.4	7.1	987.5
a-PLED (bending)	2.2	8.0	9.5	5.8	1005.6

Table 3.2 The characteristics of PLEDs.

3.3.5 Highly customizable a-PLEDs including PMPLEDs

Taking advantage of the maskless patterning in depositing both electrodes via the inkjet printing, which means that it is easy to define the pixel, I also demonstrated the curtomized a-PLEDs with various-shaped pixels and their arrays with fine lines on the glass and PEN substrates. In this work, without any effort in manufacturing the shadow masks every time according to the desired pattern, my a-PLEDs are highly customizable by simply changing the electrode pattern during the inkjet printing of the Ag and PEDOT:PSS electrodes. **Figure 3.17(a)** exhibits several emission images of the a-PLEDs, displaying ‘EXIT’ illustration which is realized by the patterned PEDOT:PSS top anodes and certain words which indicate what substrates the patterned Ag bottom cathodes are fabricated on. In addition, the a-PLED arrays with different pixel lines in the range of several hundreds of micrometers in width were fabricated to explore the applicability of high-resolution display. As shown in **Figure 3.17(b)**, the a-PLED arrays on the glass substrate had the pixel widths of 200, 500, 1000 μm for both the Ag bottom cathodes and PEDOT:PSS top anodes. In particular, the 10×10 a-PLED array with a 500 μm pixel width on the PEN substrate emitted the light normally even under the bending state. I expect that the line width can be more reduced if the more fine pattring method for the Ag and PEDOT:PSS electrodes is developed such as electrohydrodynamic printing [39]. Employing this scheme, we also constructed the 5×7 PMPLEDs on the glass substrate which were connected with a micro controller unit. As displayed in **Figure 3.17(c)**, a variety of characters such as ‘S’, ‘N’, ‘U’, ‘A’, ‘X’, ‘E’ and ‘L’ were clearly observed without any distortion or

crosstalk between the pixels. To my knowledge, for the first time, the PMPLEDs were successfully manufactured via all solution processing. As a result, my a-PLEDs and their arrays show the huge potential for the low-cost and large-area mass production of the future display if the large-area manufacturing and transfer methods are developed.

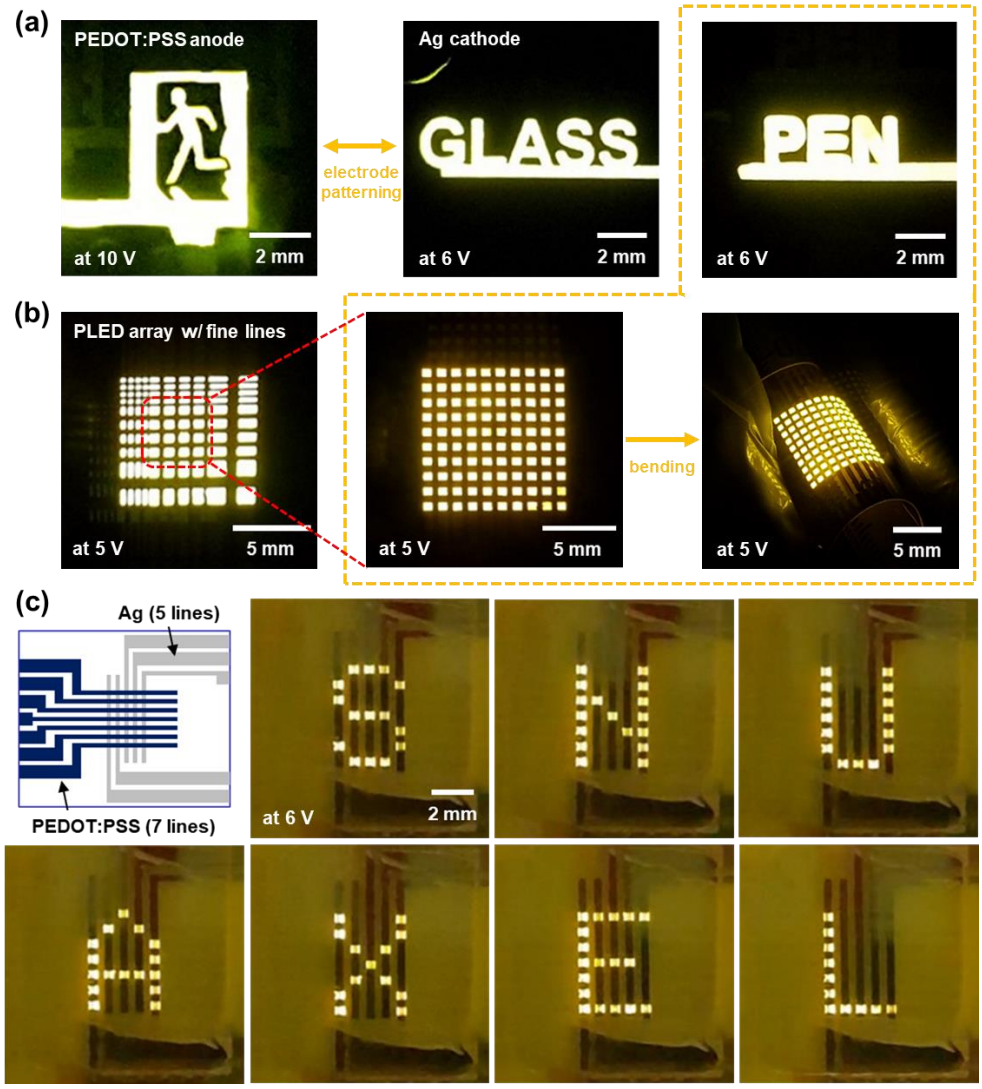

Figure 3.17 Applications of a-PLEDs on glass and PEN substrates (a) Various-shaped pixels of a-PLEDs, (b) a-PLED arrays on glass and PEN substrates with fine lines, (c) A circuit diagram and capture images of all solution-processed PMPLED displaying various types of characters.

3.4. Summary

I integrated the inkjet printing and transfer printing in creating the PEDOT:PSS films as the TCEs and employed them to fabricate the a-PLEDs as the top anodes on the rigid and plastic substrates. In order to conduct the transfer printing successfully, I formulated the blended PEDOT:PSS ink with the adhesive force and adjusted the adhesion between the PEDOT:PSS film and substrates by controlling several transfer conditions. In addition, because my transfer printing of PEDOT:PSS enables the easy patterning and minimal solvent damages, the high-performance rigid and flexible a-PLEDs and their arrays were fabricated, varying the pixel shapes and widths via the highly customizable Ag and PEDOT:PSS electrodes. In particular, the PMPLEDs were also demonstrated, showing the potential for realizing the commercial display products using all solution processing. I strongly believe that if the large-area transfer process is developed and inkjet printing instead of the spin coating is used to form the functional layers, the scalability for the cost-effective mass production in manufacturing the PLEDs will be achieved, leading to the expansion of display areas such as interactive, advertisement and ubiquitous displays which can be embedded anywhere and used anytime.

Reference

[1] L. Zhou, A. Wanga, S.-C. Wu, J. Sun, S. Park, T.N. Jackson, All-organic active matrix flexible display, Appl. Phys. Lett., 88 (2006).

[2] D.U. Jin, J.S. Lee, T.W. Kim, S.G. An, D. Straykhilev, Y.S. Pyo, H.S. Kim, D.B. Lee, Y.G. Mo, H.D. Kim, 65.2: Distinguished Paper: World-Largest (6.5”) Flexible Full Color Top Emission AMOLED Display on Plastic Film and Its Bending Properties, SID Symp. Dig. Tech. Pap., 40 (2009) 983-985.

[3] M. Noda, N. Kobayashi, M. Katsuhara, A. Yumoto, S.i. Ushikura, R.i. Yasuda, N. Hirai, G. Yukawa, I. Yagi, K. Nomoto, 47.3: A Rollable AM-OLED Display Driven by OTFTs, SID Symp. Dig. Tech. Pap., 41 (2010) 710-713.

[4] S. Kim, H.J. Kwon, S. Lee, H. Shim, Y. Chun, W. Choi, J. Kwack, D. Han, M. Song, S. Kim, S. Mohammadi, I. Kee, S.Y. Lee, Low-power flexible organic light-emitting diode display device, Adv. Mater., 23 (2011) 3511-3516.

[5] K. Nomoto, M. Noda, N. Kobayashi, M. Katsuhara, A. Yumoto, S.i. Ushikura, R.i. Yasuda, N. Hirai, G. Yukawa, I. Yagi, 36.1: Invited paper: Rollable OLED display driven by organic TFTs, SID Symp. Dig. Tech. Pap., 42 (2011) 488-491.

[6] J. Ha, S. Park, D. Kim, J. Ryu, C. Lee, B.H. Hong, Y. Hong, High-performance polymer light emitting diodes with interface-engineered graphene anodes, Org. Electron., 14 (2013) 2324-2330.

[7] H. Zheng, Y. Zheng, N. Liu, N. Ai, Q. Wang, S. Wu, J. Zhou, D. Hu, S. Yu, S. Han, W. Xu, C. Luo, Y. Meng, Z. Jiang, Y. Chen, D. Li, F. Huang, J. Wang, J. Peng, Y. Cao, All-solution processed polymer light-emitting diode displays, Nat. Commun., 4 (2013) 1971.

[8] J. Ha, J. Park, J. Ha, D. Kim, S. Chung, C. Lee, Y. Hong, Selectively modulated inkjet printing of highly conductive and transparent foldable polymer electrodes for flexible polymer light-emitting diode applications, Org. Electron., 19 (2015) 147-156.

[9] N. Kim, H. Kang, J.H. Lee, S. Kee, S.H. Lee, K. Lee, Highly conductive all-plastic electrodes fabricated using a novel chemically controlled transfer-printing method, Adv. Mater., 27 (2015) 2317-2323.

[10] M. Zhang, S. Hofle, J. Czolk, A. Mertens, A. Colsmann, All-solution processed transparent organic light emitting diodes, Nanoscale, 7 (2015) 20009-20014.

[11] K. Gilissen, J. Stryckers, P. Verstappen, J. Drijkoningen, G.H.L. Heintges, L. Lutsen, J. Manca, W. Maes, W. Deferme, Ultrasonic spray coating as deposition technique for the light-emitting layer in polymer LEDs, Org. Electron., 20 (2015) 31-35.

[12] H. Zhen, Y. Chen, C. Zhang, Z. Zhou, K. Li, Y. Zhao, X. Mei, Q. Ling, Full-solution processed, flexible, top-emitting polymer light-emitting diodes based on printed Ag electrodes, J. Mater. Chem. C, 5 (2017) 6400-6405.

[13] Z. Shu, E. Beckert, R. Eberhardt, A. Tünnermann, ITO-free, inkjet-printed transparent organic light-emitting diodes with a single inkjet-printed Al:ZnO:PEI interlayer for sensing applications, J. Mater. Chem. C, 5 (2017) 11590-11597.

[14] S. Kee, N. Kim, B. Park, B.S. Kim, S. Hong, J.H. Lee, S. Jeong, A. Kim, S.Y. Jang, K. Lee, Highly Deformable and See-Through Polymer Light-Emitting Diodes with All-Conducting-Polymer Electrodes, Adv. Mater., 30 (2018) 1703437.

[15] J. Park, J. Ha, N. Seong, S. Lee, C. Lee, H. Yang, Y. Hong, Highly efficient solution-processed inverted polymer light emitting diodes with uniformly coated

poly(3,4-ethylenedioxythiophene):poly(styrene-sulfonate) layers on a hydrophobic emission layer using a dilution method, Thin Solid Films, 660 (2018) 782-788.

[16] S. Liu, X. Zhang, M. Yin, H. Feng, J. Zhang, L. Zhang, W. Xie, Coffee-Ring-Free Ultrasonic Spray Coating Single-Emission Layers for White Organic Light-Emitting Devices and Their Energy-Transfer Mechanism, ACS Appl. Energy Mater., 1 (2017) 103-112.

[17] M. Fleuster, M. Klein, P. Roosmalen, A. Wit, H. Schwab, 44.2: Mass Manufacturing of Full Color Passive-Matrix and Active-Matrix PLED Displays, SID Symp. Dig. Tech. Pap., 35 (2004) 1276-1279.

[18] J. Ouyang, Y. Yang, Conducting Polymer as Transparent Electric Glue, Adv. Mater., 18 (2006) 2141-2144.

[19] J. Huang, G. Li, Y. Yang, A Semi-transparent Plastic Solar Cell Fabricated by a Lamination Process, Adv. Mater., 20 (2008) 415-419.

[20] C. Shimada, S. Shiratori, Viscous conductive glue layer in semitransparent polymer-based solar cells fabricated by a lamination process, ACS Appl. Mater. Interfaces, 5 (2013) 11087-11092.

[21] C.-Y. Lin, N.-W. Hu, H.-W. Chang, C.-Y. Lu, C.-Y. Chen, C.-C. Wu, Efficient transparent small-molecule organic light-emitting devices adopting laminated transparent top electrodes, Org. Electron., 28 (2016) 25-30.

[22] G.-S. Liu, C. Liu, H.-J. Chen, W. Cao, J.-S. Qiu, H.-P.D. Shieh, B.-R. Yang, Electrically robust silver nanowire patterns transferrable onto various substrates, Nanoscale, 8 (2016) 5507-5515.

[23] T. Suzuki, T. Sekine, K. Yamamoto, K. Fukutani, Change in the surface OH group on soda lime silicate glass and silica glass after heat treatment in nitrogen atmosphere, J. Non-Cryst. Solids, 464 (2017) 89-91.

[24] S. Bhattacharya, A. Datta, J.M. Berg, S. Gangopadhyay, Studies on surface wettability of poly (dimethyl) siloxane (PDMS) and glass under oxygen-plasma treatment and correlation with bond strength, J. Microelectromech. S., 14 (2005) 590-597.

[25] S.M. Hong, S.H. Kim, J.H. Kim, H.I. Hwang, Hydrophilic surface modification of PDMS using atmospheric RF plasma, J. Phys. Conf. Ser., 34 (2006) 656.

[26] M. Zhang, J. Wu, L. Wang, K. Xiao, W. Wen, A simple method for fabricating multi-layer PDMS structures for 3D microfluidic chips, Lab Chip, 10 (2010) 1199-1203.

[27] W.W. Tooley, S. Feghhi, S.J. Han, J. Wang, N.J. Sniadecki, Thermal fracture of oxidized polydimethylsiloxane during soft lithography of nanopost arrays, J. Micromech. Microeng., 21 (2011) 054013.

[28] H. Hillborg, U. Gedde, Hydrophobicity recovery of polydimethylsiloxane after exposure to corona discharges, Polymer, 39 (1998) 1991-1998.

[29] S. Yu, Y. Sun, Y. Ni, X. Zhang, H. Zhou, Controlled formation of surface patterns in metal films deposited on elasticity-gradient PDMS substrates, ACS Appl. Mater. Interfaces, 8 (2016) 5706-5714.

[30] C.-K. Cho, W.-J. Hwang, K. Eun, S.-H. Choa, S.-I. Na, H.-K. Kim, Mechanical flexibility of transparent PEDOT:PSS electrodes prepared by gravure printing for flexible organic solar cells, Sol. Energy Mater. Sol. Cells, 95 (2011) 3269-3275.

[31] M. Vosgueritchian, D.J. Lipomi, Z. Bao, Highly Conductive and Transparent PEDOT:PSS Films with a Fluorosurfactant for Stretchable and Flexible Transparent Electrodes, Adv. Funct. Mater., 22 (2012) 421-428.

[32] S. Hofle, A. Schienle, M. Bruns, U. Lemmer, A. Colsmann, Enhanced electron injection into inverted polymer light-emitting diodes by combined solution-processed zinc oxide/polyethylenimine interlayers, Adv. Mater., 26 (2014) 2750-2754, 2618.

[33] Y. Zhou, C. Fuentes-Hernandez, J. Shim, J. Meyer, A.J. Giordano, H. Li, P. Winget, T. Papadopoulos, H. Cheun, J. Kim, M. Fenoll, A. Dindar, W. Haske, E. Najafabadi, T.M. Khan, H. Sojoudi, S. Barlow, S. Graham, J.L. Bredas, S.R. Marder, A. Kahn, B. Kippelen, A universal method to produce low-work function electrodes for organic electronics, Science, 336 (2012) 327-332.

[34] M. Takada, T. Nagase, T. Kobayashi, H. Naito, Electron injection in inverted organic light-emitting diodes with poly(ethyleneimine) electron injection layers, Org. Electron., 50 (2017) 290-295.

[35] N.G. Park, M.Y. Kwak, B.O. Kim, O.K. Kwon, Y.K. Kim, B. You, T.W. Kim, Y.S. Kim, Effects of indium-tin-oxide surface treatment on organic light-emitting diodes, Jpn. J. Appl. Phys., 41 (2002) 1523.

[36] Q. Huang, G. Evmenenko, P. Dutta, T.J. Marks, Molecularly “engineered” anode adsorbates for probing OLED interfacial structure− charge injection/luminance relationships: Large, structure-dependent effects, J. Am. Chem. Soc., 125 (2003) 14704-14705.

[37] S. Jung, N. Park, M. Kwak, B. Kim, K. Choi, Y. Cho, Y. Kim, Y. Kim, Surface treatment effects of indium–tin oxide in organic light-emitting diodes, Opt. Mater., 21 (2003) 235-241.

[38] J.C. Scott, Metal–organic interface and charge injection in organic electronic devices, J. Vac. Sci. Technol. A, 21 (2003) 521-531.

[39] M.S. Onses, E. Sutanto, P.M. Ferreira, A.G. Alleyne, J.A. Rogers, Mechanisms,

Capabilities, and Applications of High-Resolution Electrohydrodynamic Jet Printing, Small, 11 (2015) 4237-4266.

Chapter 4

A facile patterning of silver nanowire networks for low-voltage driven flexible electronics

4.1. Introduction

The development of flexible transparent conductive electrodes (TCEs) has been considered as a key issue for realization of flexible electronics in the areas of optoelectronics [1-6], touch panels [7-9], wearable devices and robotics [10, 11] which can be applied and embedded to ubiquitous environments. Currently, indium tin oxide (ITO) is a commonly used TCE in the rigid electronics but its inherent brittleness hinders the application to the flexible electronics because multiple micro-cracks by an external force make deterioration of a conductivity and surface roughness [12, 13]. Therefore, there have been many reports about the flexible TCEs such as carbon nanotubes [14, 15], graphene [16, 17], oxide-metal-oxide [18, 19], metal grids [20, 21], metal nanowires [22-25] and conductive polymers [13, 26-28]. Among them, the metal nanowires, especially silver nanowires (AgNWs),

are one of promising candidates to replace the ITO due to compatibility with a solution process and comparable optoelectronic properties with the ITO while exhibiting superior mechanical flexibility. In addition, various methods or treatments for the AgNWs have enabled an enhancement of electrical or optical properties such as synthesis of long nanowires [8, 9, 29, 30], welding at the junctions [25, 31-34] and alignment control [35-37].

For the practical application of the AgNWs to commercial products, a patterning method of the AgNWs should be also developed because the formation of electrodes which can be deposited with a desired pattern size and shape at a precise location is critical for the high-resolution flexible electronics to be operated normally and accurately at the same time. Although many groups have studied the patterning methods of the AgNWs such as photolithography [24, 38-40], laser ablation [41-43] and spray or drop coating using a shadow mask [44-47], these methods have limited the low-cost and large-area mass production, which comes from the high equipment cost, process complexity and low design freedom of patterning. Furthermore, the acid wet etching during the photolithography or high laser power during the laser ablation can damage the plastic substrates, which is incompatible with the flexible electronics. On the contrast, several printing techniques such as inkjet printing [48, 49] and electrohydrodynamic printing [50, 51], which are known as a facile patterning method, have been employed to conduct the AgNW patterning. However, in order to prevent nozzle clogging during the printing, the shortened or sonicated AgNWs are restrictively used in the TCEs because an extremely high resistance appears to be transparent in the visible wavelength range.

Unlike direct deposition methods mentioned above, the pre-deposited AgNW

networks can be transferred onto various substrates as one of indirect deposition methods [22. 52-55]. Meanwhile, the reported transfer methods still need the pre-structured stamps using the photolithography or additional patterning processes to acquire the patterned AgNW electrodes. Recently, J. Ahn et al. detailed the creation of the patterned AgNW networks via the transfer from the AgNWs/hydrophobic film onto the tonor-printed copy paper [54]. However, the AgNW networks were deposited by floating and then scooping them up on the hydrophobic substrates in a water bath because the high-quality AgNW formation on the hydrophobic surface is difficult using the conventional coating methods. The complex and low-throughput coating method is not compatible with the low-cost and large-scale fabrication. Although there was another similar approach using silver nanoparticles and nanowires [55], a high-content suspension was used in preparing the sample due to the poor wetting property of the hydrophobic surface, which means that this electrode is not also suitable for the transparent electrodes due to its opaqueness.

In this **Chapter 4**, in order to resolve abovementioned issues in previous papers, I demonstrated the highly conductive and transparent AgNW networks which can be patterned easily and freely by combining the inkjet printing and transfer process. First, I conducted the inkjet printing of poly (3, 4-ethylenedioxythiophene):poly (styrenesulfonate) (PEDOT:PSS) which was blended with a D-sorbitol aqueous solution as an adhesive (hereafter, we call it “blended PEDOT:PSS”), thereby obtaining a simply patterned transfer medium. Secondly, I carried out a spin coating of AgNW dispersion solutions on a plasma-treated polydimethylsiloxane (PDMS) stamp to acquire the highly conductive and transparent AgNW networks. Finally, the PEDOT:PSS transfer medium and AgNW-coated PDMS stamp were attached and the heating and cooling processes

was followed. After peeling off the PDMS stamp from the attached one, the AgNW networks were selectively transferred only onto the region of the inkjet-printed PEDOT:PSS transfer medium, resulting in the highly customizable AgNW electrodes. Employing the facile patterning method, my AgNW-transferred PEDOT:PSS electrodes were formed on the various substrates such as glass, plastic and silicon substrates according to the purpose of use, showing not only excellent optoelectronic properties but also fine lines with hundreds of micrometer in width. In addition, their electrical and optical properties were highly tunable by controlling AgNW coating conditions and the previous issues of the AgNWs such as a high surface roughness and weak adhesion with the substrate were overcome by the partially embedded AgNWs in the PEDOT:PSS matrix. Especially, in the plastic substrate, superior mechanical flexibility as well as outstanding optoelectronic properties was observed for the electrodes unlike the brittle ITO. Finally, I applied my AgNW-transferred PEDOT:PSS electrodes to various flexible electronics such as such as light-emitting diode (LED) arrays as bus electrodes and all solution-processed polymer light emitting diodes (PLEDs) as bus and pixel electrodes. I strongly believe that my TCEs enable the flexible electronics which require the high-performance TCEs to remain their characteristics under the mechanical deformation and consume less power while ensuing the low-cost and large-area mass production, simultaneously.

4.2. Experiments

4.2.1 Preparation of AgNW networks on a PDMS stamp

Before deposition of the AgNWs, the PDMS stamp was prepared by mixing a PDMS elastomer base and curing agent (Sylgard 184, Dow Corning) at a weight ratio of 10:1 and then pouring it onto a petri dish, followed by the planarization for the 1200-μm-thick PDMS stamp. After thermal curing at 100 ^{o}C of 2 h, the completed PDMS stamp was cut in a desired size. The AgNW solution (diameter = 32 nm, length = 25 μm, Nanopyxis) as a dispersion solution in isopropyl alcohol (IPA) with a concentration of 1 wt% was further diluted with IPA at a volume ratio of 1:3 to obtain the uniform AgNW networks. Afterwards, the prepared PDMS stamp was treated with an air plasma at 15 W for 15 s to enhance the wetting property because the non-treated PDMS stamp showed an extremely hydrophobic property. The resulting AgNW solution was spin coated on the plasma-treated PDMS stamp at 2000 rpm for 60 s, which was repeated six times for the optimization of electrical and optical properties for the AgNW networks. After drying at room temperature for 1 h to remove solvents and minimize the effect by thermal-induced PDMS expansion simultaneously, the completed AgNW networks were immersed with a salt solution for 1 min where sodium chloride (NaCl) was dissolved in deionized (DI) water with a concentration of 1 wt% and then washed in the deionized (DI) water for 9 min in order to further increase the conductivity of the AgNW networks without any loss of transmittance.

4.2.2 Preparation of inkjet-printed PEDOT:PSS

D-Sorbitol (Sigma Aldrich) was used in this work to acquire an adhesive force of PEDOT:PSS films. The conductive PEDOT:PSS (HIL-1005, Orgacon) containing 2 wt% fluorosurfactant (Capstone FS-30, Chemours) was mixed with a D-Sorbitol aqueous solution at a weight ratio of 9:1. The D-sorbitol solution was prepared by dissolving the powder in the DI water with a concentration of 2.35 g/g. After stirring for 1 h, the blended PEDOT:PSS ink was completed, increasing the adhesive force without significant conductivity loss. After that, the pre-patterned PEDOT:PSS film was obtained using a piezoelectric inkjet printer (DMP-2831, Dimatix Corp.) on the various substrates in accordance with the purpose of use. Each substrate was prepared according to the following procedures. In glass substrates, the substrates were cleaned with acetone, isopropyl alcohol and deionized (DI) water, sequentially, in an ultrasonic bath and then stored in an oven set to 100 ^{o}C for 1 h to remove any moisture on the surface. Before the inkjet printing, there was no need for a surface treatment for the glass substrates. Meanwhile, in polyethylene-naphthalate (PEN, Q65H, Teijin Dupont Films) substrates, without any cleaning process, it was treated with an UV-ozone cleaner for 5 min to enhance the wetting property. After the inkjet printing with the desired pattern, the samples were annealed at 120 ^{o}C for 1 h, leading to the customized PEDOT:PSS transfer medium.

4.2.3 Selective transfer of AgNWs onto a transfer medium

The transfer medium with the pre-patterned PEDOT:PSS film and the AgNW-coated PDMS stamp were attached while applying the mild pressure using a roller for conformal contact. Subsequently, the attached sample was placed on the hot plate set to 100 ^{o}C for 10 min to enable the effective AgNW transfer from the PDMS stamp onto the transfer medium. After cooling at room temperature for 5 min, the PDMS stamp was peeled off and the AgNW networks were selectively transferred only onto the region of the PEDOT:PSS transfer medium, resulting in the simply patterned AgNW electrodes.

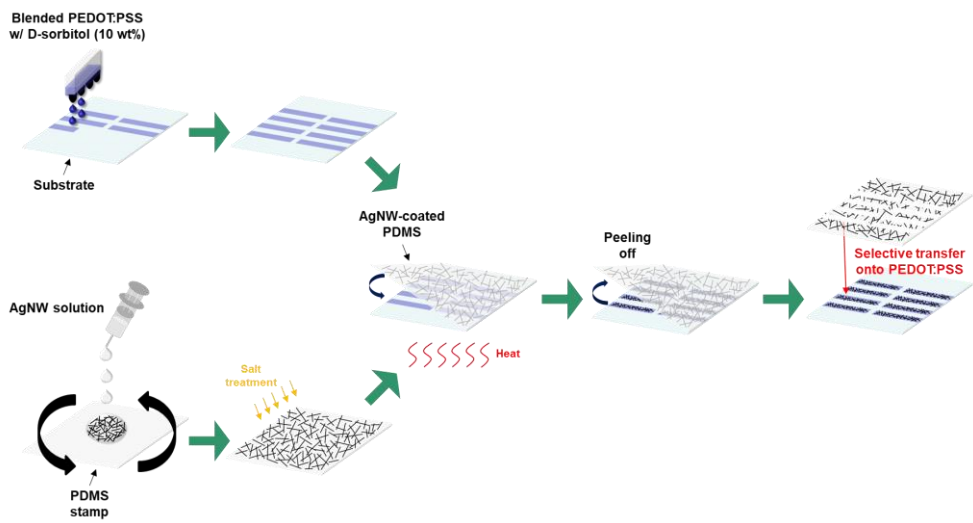

Figure 4.1 Schematic illustration of fabrication process of AgNW-transferred PEDOT:PSS films.

4.2.4 Characterizations and measurements

A 90^{o} peel-off test and contact angle measurement were conducted using a universal testing machine (WL2100, With Lab Co., Ltd.) and custom-made equipment, respectively, to explore a transfer principle in each procedure. The sheet resistance of the electrodes was measured by a four-point probe (FPP-5000, Changmin) and their optical property was obtained using a UV/VIS spectrometer (Lambda 35, Perkin Elmer). The images were taken with an optical microscope (DSX-HRSU, OLYMPUS Corp.) and a field emission scanning electron microscope (FE-SEM, Hitachi S-48000). The surface roughness and thickness were examined by a non-contact mode atomic force (AFM) system (XE-100, Park system). For investigation of the mechanical property for my electrodes, the bending test was carried out using a custom-made bending machine and their resistance was measured by a Keithley 2400 sourcemeter during the bending stress.

4.2.5 Applications to flexible electronics

First, red light-emitting diodes (LEDs, SML-P11UT, ROHM Semiconductor) were placed on the AgNW-transferred PEDOT:PSS electrodes using a pick-and-place machine (TM220A, Hangzhou Dengxin Technology Co., Ltd.) to achieve 5x5 LED arrays. For conformal bonding between the LED and electrode, silver epoxy (ABLEBOND 84-1LMISR4, Henkel) was dispensed using an automatic dispenser (SHOTmini 200Sx, Musashi Engineering). Second, all solution-processed PLEDs under low-operation voltage were fabricated by conducting the additional AgNW transfer onto the devices with the only PEDOT:PSS top anodes, which is described in Chapter 3. Due to the weak adhesion between the PEDOT:PSS anodes and devices, we prepared the AgNW networks on the PDMS stamp which was pre-treated with the reduced plasma time from 15 to 10 s. The completed devices were encapsulated using a cover glass and UV-curable resin (XNR5570, Nagase ChemteX Corp.). The electrical and optical characteristics of PLEDs were measured by a digital multimeter (Keithley 2000, Keithley) and a source-meter unit (Keithely 237, Keithley) by sweeping the bias voltage with an interval of 0.1 V and a spectrometer (CS-1000A, Konica Minolta), respectively.

4.3. Results and Discussion

4.3.1 Principles of AgNW-transferred PEDOT:PSS

I conducted a facile patterning of AgNW networks by integrating the inkjet printing of the PEDOT:PSS transfer medium and selective transfer of the AgNW networks only onto the region of the transfer medium, as depicted in **Figure 4.1**. First, I prepared the inkjet-printed PEDOT:PSS film as the transfer medium. In order to give an adhesive force to the PEDOT:PSS film, I formulated the blended PEDOT:PSS ink by mixing as-purchased PEDOT:PSS with a D-sorbitol aqueous solution which is extensively used in a lamination process to ensure mechanical and electrical bonding between the film and interface [56-59]. In this work, the increased adhesive force of the PEDOT:PSS film enables the conformal attachment with the AgNW networks when they are attached. We quantitatively compared the adhesive force of the as-purchased and blended PEDOT:PSS films using a 90^{o} peel-off test, as shown in **Figure 4.2**. Clearly, the adhesive force of the blended PEDOT:PSS film was 18 N/m, while that of the as-purchased PEDOT:PSS film was 9.8 N/m. The (i) and (ii) images in **Figure 4.4** also illustrate the successful transfer of the AgNW networks onto the blended PEDOT:PSS film unlike the as-purchased one, which means that my blended PEDOT:PSS film and AgNW networks are merged to one film, facilitating the transfer process via the adhesion formation.

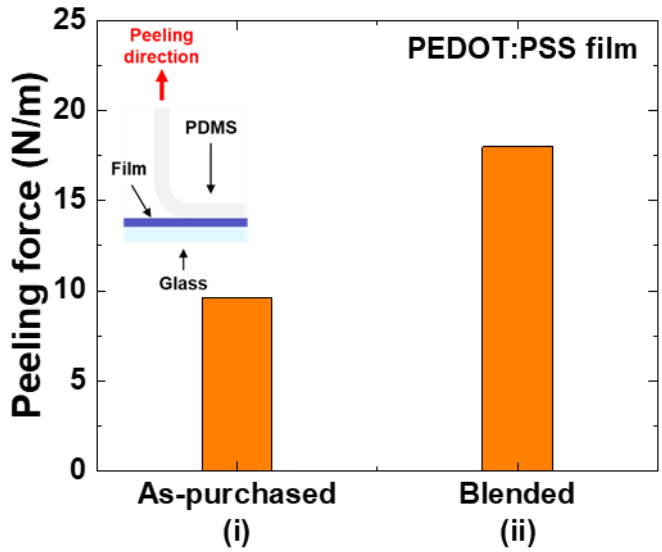

Figure 4.2 A adhesive force of as-purchased and blended PEDOT:PSS films using a 90 ^{o} peel-off test.

Second, the AgNW networks were formed on the PDMS stamp using a spin coating to obtain superior optoelectronic properties originated from their intrinsic characteristics. To acquire the uniform AgNW networks and the optimized optoelectronic characteristics for the use of TCEs, I performed a spin coating of the IPA-diluted AgNW solution six times on the plasma-treated PDMS stamp because a high concentration of the AgNW solution and inherent hydrophobicity of the non-treated PDMS hinder the uniform coating of the AgNW networks. In addition, their conductivity was further enhanced by the salt treatment due to reduction of Ag ions and more preferential re-deposition at the AgNW junctions [25, 34]. Finally, I attached the substrate containing the transfer medium and the AgNW-coated PDMS stamp and carefully adjusted several transfer conditions, especially transfer temperature, to separate the AgNWs networks from the stamp and thus transfer

them onto the PEDOT:PSS film. It is announced that when thermal is applied to the PDMS with the silica-like structure caused by the plasma treatment, cracks appear on the surface of the PDMS [60]. In this case, they reduce the contact area between the film and interface, thereby decreasing the adhesion and separating it from the PDMS easily. The existence of cracks was confirmed by the DI water contact angle (CA) measurement because the CA increases with the surface roughness [61]. **Figure 4.3** exhibits the DI water CAs on the PDMS substrates before and after the heat treatment. The CA increased from 80.7 to 89.8^{o} after the heat treatment, which means that the adhesive force of the AgNWs with the PDMS stamp becomes weak. For the attached sample, because the AgNWs and PEDOT:PSS film were merged to one film as discussed above, the adhesive force of the AgNWs can be considered identical to that of the AgNW/PEDOT:PSS film. At the same time, it is smaller than that of the AgNW/PEDOT:PSS film with the substrate and there is no change in the substrate without the PEDOT:PSS film, which results in the selective transfer of the AgNW networks from the PDMS to the PEDOT:PSS transfer medium, as seen in the (ii) and (iii) images in **Figure 4.4**. Therefore, I can conclude that the adhesive transfer medium and heat treatment for the attached sample are key enabling techniques for achieving the selective transfer of the AgNW networks onto the region of the PEDOT:PSS transfer medium.

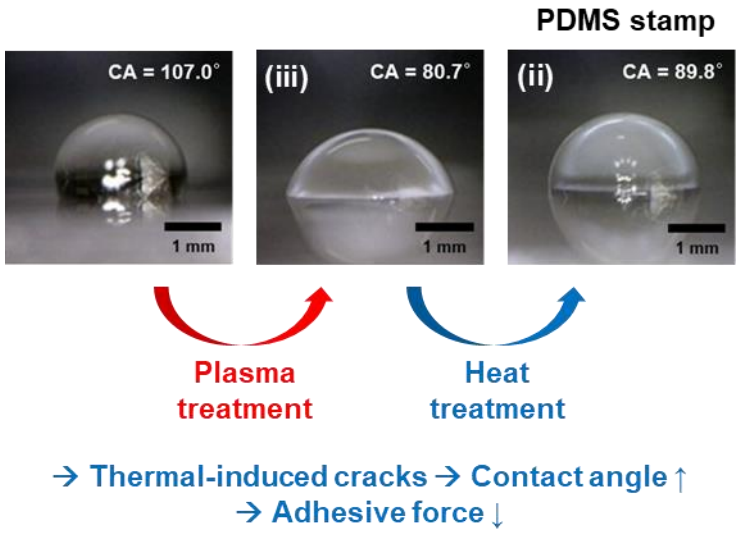

Figure 4.3 CA changes after plasma and heat treatments for uniform formation of AgNW networks and effective AgNW transfer, respectively.

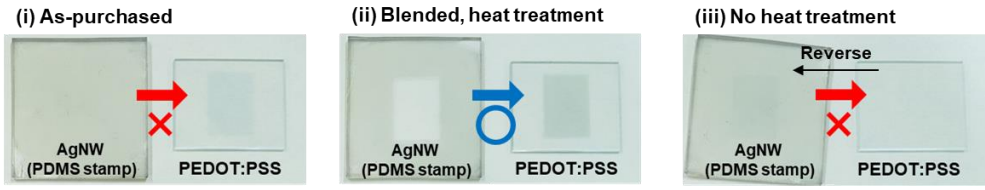

Figure 4.4 Photographs of success or fail of AgNW transfer onto a PEDOT:PSS transfer medium according to transfer conditions. (i) ~ (iii) are also marked in Figure 4.2 and 4.3.

Figure 4.5 presents several AgNW-transferred PEDOT:PSS films with character, digit and mark patterns on glass, PEN and PDMS substrates, respectively. Interestingly, the AgNW-transferred PEDOT:PSS film can be produced with the pattern corresponding to that of the inkjet-printed PEDOT:PSS transfer medium precisely without any residue on the detached AgNW region. Furthermore, the resulting film can be applied to diverse areas such as flexible or stretchable

electrodes if it is created on plastic or elastomeric substrates. In this paper, I explored the potential for the flexible electrodes and their application to flexible electronics.

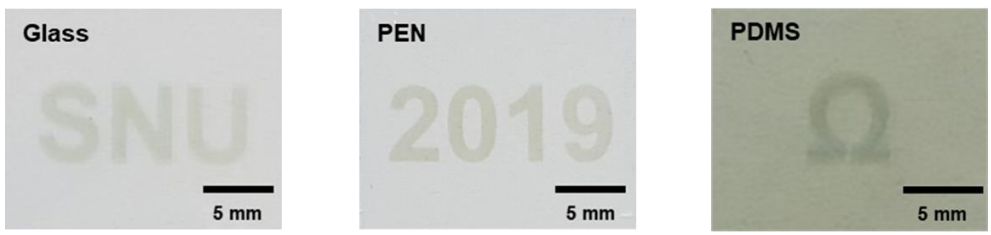

Figure 4.5 Various-shaped AgNW-transferred PEDOT:PSS films on glass, PEN, PDMS substrates.

4.3.2 Optoelectronic properties

Based on the easily patternable AgNW-transferred PEDOT:PSS films, I investigated their electrical and optical properties. As illustrated in **Figure 4.6**, in the glass substrate, my AgNW-transferred PEDOT:PSS electrode showed a sheet resistance of 8.2 Ω/□ (hereafter, we call it "R_{sh}") and a transmittance of 87.4 % at the wavelength of 550 nm (hereafter, we call it "T"), while the only PEDOT:PSS electrode showed R_{sh} of 391.9 Ω/□ and T of 97.1 %. The significantly decreased sheet resistance is attributed to the attachment of the highly conductive AgNW networks on the PEDOT:PSS film, which leads to the less transparent but more conductive TCEs. Actually, my electrode exhibited comparable performance with the only AgNW electrode, which means that the transfer process does not deteriorate the optoelectronic properties of the AgNW networks. In order to explore the applicability to the flexible TCEs, the AgNW-transferred PEDOT:PSS electrode on the PEN substrate was fabricated and its characteristics were evaluated. The PEN electrode presented R_{sh} of 10.4 Ω/□ and T of 90.7 % which are comparable to those of the glass electrode, which indicates that its optoelectronic properties are independent on the substrate types. Moreover, its performance was superior to that of ITO on the PEN substrate (i.e. R_{sh} = 54.1 Ω/□ at T = 89.9 %) because the PEN ITO is less conductive and transparent than the glass ITO in general [13]. In addition, when figure of merit (FOM) which is one of the parameters to estimate the TCEs was compared in the PEN substrate [62], the AgNW-transferred PEDOT:PSS electrode presented a higher value than the ITO, as displayed in **Figure 4.6**. Therefore, I can conclude that my AgNW-transferred PEDOT:PSS

electrode on the plastic substrate is the most promising alternative to the ITO in terms of the optoelectronic properties. The optoelectronic properties and fabrication or patterning methods of the AgNWs in previous works are summarized in **Table 4.1**, showing that my electrode can be fabricated and patterned via the simple process with comparable or superior characteristics.

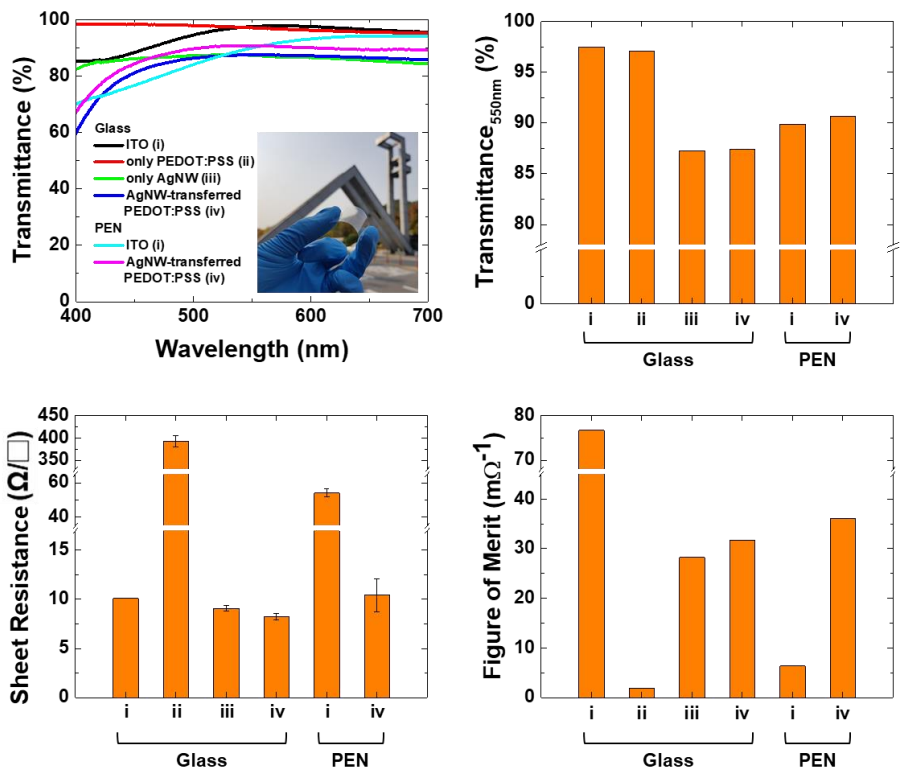

Figure 4.6 A transmittance in visible wavelength range and 550 nm wavelength, a sheet resistance and a figure of merit of ITO, only PEDOT:PSS, only AgNW and AgNW-transferred PEDOT:PSS films on glass and PEN substrates.

Reference	Substrate	Sheet resistance (Ω/□)	Transmittance (% at 550 nm)	Fabrication method	Pattering method
This work	Glass, PEN[a]	10.4	90.7	Spin coating (Transfer printing)	Inkjet-printed transfer medium
[22]	PET[b]	10.0	85.0	Vacuum filtration (Transfer printing)	Patterned PDMS stamp
[24]	Glass, PET	22.0	90.8	Spin coating	Photolithography
[25]	PET, PEN	5.0	92.0	Mayer rod coating Spray coating	Shadow mask
[40]	TPU[c]	20.0	87.8	Spin coating	Photolithography
[41]	Glass	12.0	84.4	Vacuum filtration Mayer rod coating	Laser ablation
[43]	Glass	15.0-25.0	85.0	Spin coating	Laser ablation
[45]	Glass, PET	20.0	> 80.0	Spray coating	Shadow mask
[48]	PET	19.0	< 50	Inkjet printing	Inkjet printing
[51]	Glass, PET, PDMS[d] and so no	< 4.0	opaque	EHD[e] printing	EHD printing
[54]	Paper	0.6~2.3	opaque	Spray coating (Transfer printing)	Tonor-printed transfer medium

[a] polyethylene naphthalate, [b] polyethylene terephthalate, [c] thermoplastic urethane, [d] polydimethylsiloxane, [e] electrohydrodynamic

Table 4.1 Optoelectronic properties and fabrication and patterning methods of AgNW networks in this work and previous reports**.**

4.3.3 Partially embedded AgNWs in the PEDOT:PSS matrix

This section shows a surface morphology of the only AgNW and AgNW-transferred PEDOT:PSS films on the glass substrate. In the SEM images in **Figure 4.7** including the cross-section and top views, the AgNW networks were embedded in the PEDOT:PSS matrix, providing the surface planarization of the AgNWs. It is further supported by the fact that the thickness of the AgNW-transferred PEDOT:PSS film was 250 nm which is much larger than that of the only PEDOT:PSS and AgNW film. In contrast, the only AgNW film were relatively more prominent as reported in other papers [23-25]. Based on these results, a surface roughness of each film was also examined by the AFM measurement. The surface roughness of the only AgNW film was found to 30.9 ± 3.7 nm root-mean-square (RMS), while that of the AgNW-transferred PEDOT:PSS film was dramatically decreased to 16.3 ± 1.6 nm RMS. It indicates that the AgNW networks were partially embedded in the PEDOT:PSS matrix. In addition, I can expect the enhanced adhesion between the AgNWs and substrate by the embedded AgNWs. **Figure 4.8** exhibits the change of resistance after the adhesion test by the 3M scotch taping test. The only AgNW film lost its conductivity after no more than a few cycles, whereas the AgNW-transferred PEDOT:PSS film presented the slightly increased resistance even after the taping test for 100 cycles. Therefore, these results verify that the selective transfer of the AgNWs onto the PEDOT:PSS film overcomes drawbacks of the conventional AgNW networks such as the high surface roughness and weak adhesion with the substrate, facilitating the pattering method. Meanwhile, the smoother AgNW networks with stronger adhesion with

the substrate should be obtained for the use of bottom electrodes in optoelectronic devices.

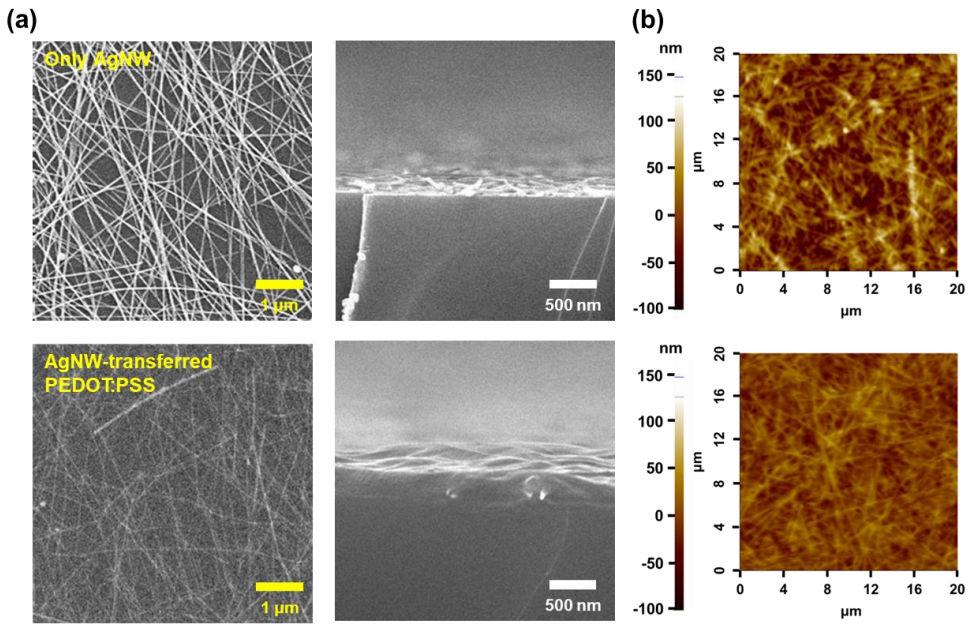

Figure 4.7 (a) SEM images-, (b) AFM images of only AgNW and AgNW-transferred PEDOT:PSS films.

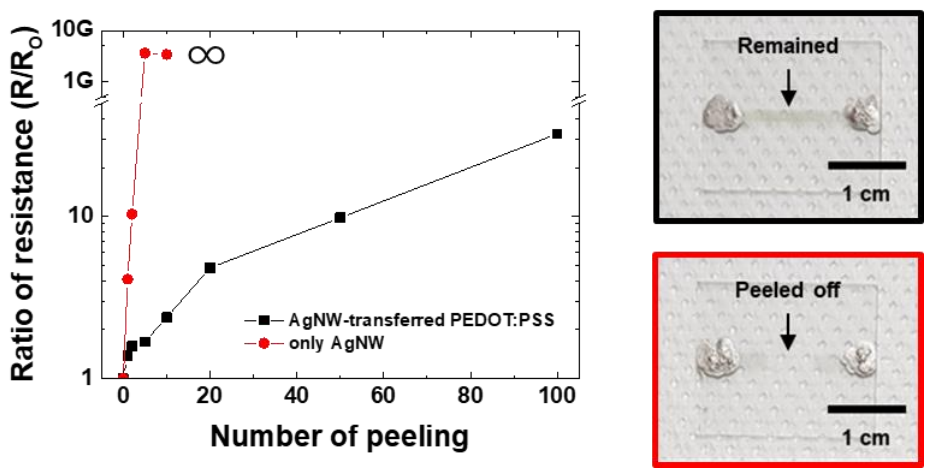

Figure 4.8 An adhesion test using a scotch tape for only AgNW and AgNW-transferred PEDOT:PSS films.

4.3.4 Tunable optoelectronic properties

Furthermore, a wide range of electrodes with different optoelectronic properties were fabricated via control of coating conditions in forming the AgNW networks. The AgNW networks with various characteristics were obtained by controlling number of coatings such as 3, 6 and 9 times and preparing several kinds of the AgNW solutions with IPA-dilution ratios of 1:9, 1:3, 1:1 and no dilution. **Figure 4.9** shows photographs and change of the electrode properties according to the AgNW coating conditions. The R_{sh} was changed from 1.9 to 38.6 Ω/□, while corresponding T was from 34.0 to 93.5 %. Because it is generally announced that the thicker conductive film makes itself more conductive but less transparent for the same material, the performance of the AgNW-transferred PEDOT:PSS electrodes can be tuned delicately, depending on the purpose.

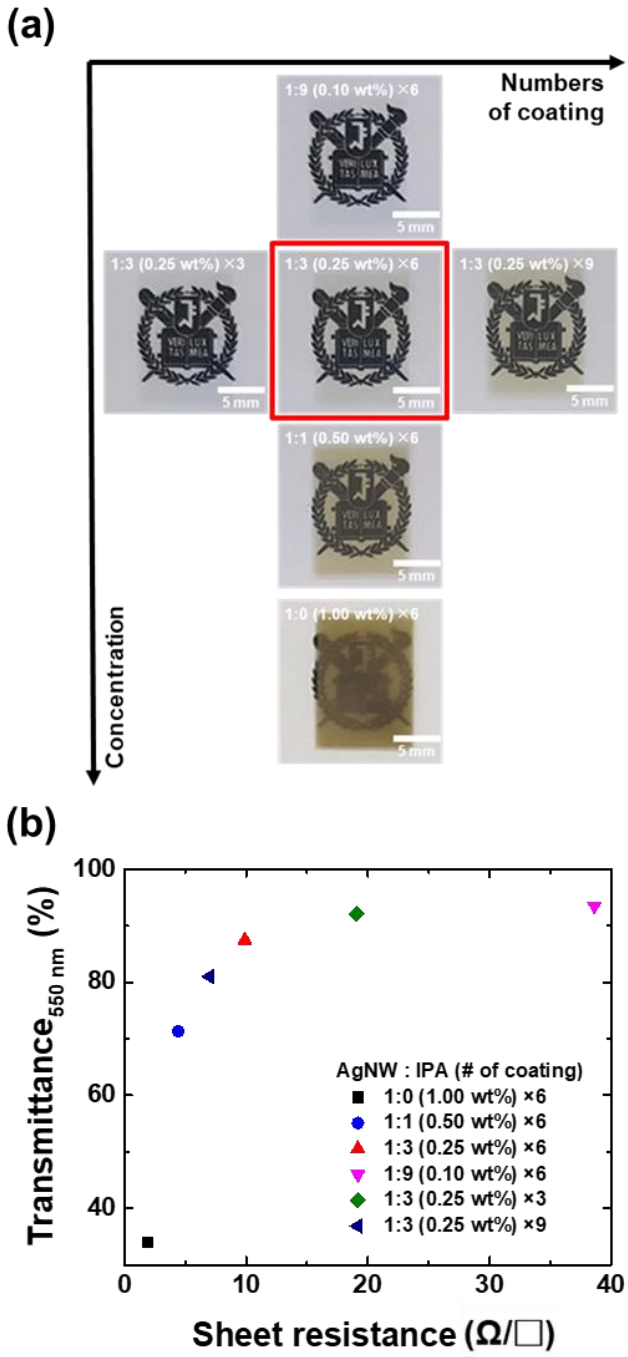

Figure 4.9 (a) Photographs-, (b) A sheet resistance and transmittance at 550 nm wavelength of a wide range of AgNW-transferred PEDOT:PSS films with different optoelectronic properties.

4.3.5 Fine patterning

In addition to abovementioned characteristics, taking advantages of the highly customizable AgNW networks via their selective transfer onto the inkjet-printed PEDOT:PSS transfer medium, I demonstrated the fine patterning of the AgNW networks. **Figure 4.10(a)** and **(b)** shows the AgNW-transferred PEDOT:PSS lines with hundreds of micrometers in width such as 100, 200, 500 μm on the glass and PEN substrates which coincide with the inkjet-printed PEDOT:PSS transfer media. As shown in **Figure 4.10(c)**, the light-emitting diode (LED) which is connected with the electrical bias via the electrode was implemented to verify the high conductivity of my electrode even at the narrow-width electrode. In the case of the AgNW-transferred PEODT:PSS electrode, the considerable resistance reduction allowed more bright light emission at the same voltage owing to the decreased voltage drop at the electrode compared to the only PEDOT:PSS electrode, which means that the device with the AgNW-transferred PEDOT:PSS electrodes consume less power compared to that with the less conductive electrodes. My electrode not only shows outstanding optoelectronic properties but also provides the simple patterning method by integrating the inkjet printing and transfer printing, which is suitable for the low-cost and large-area mass production.

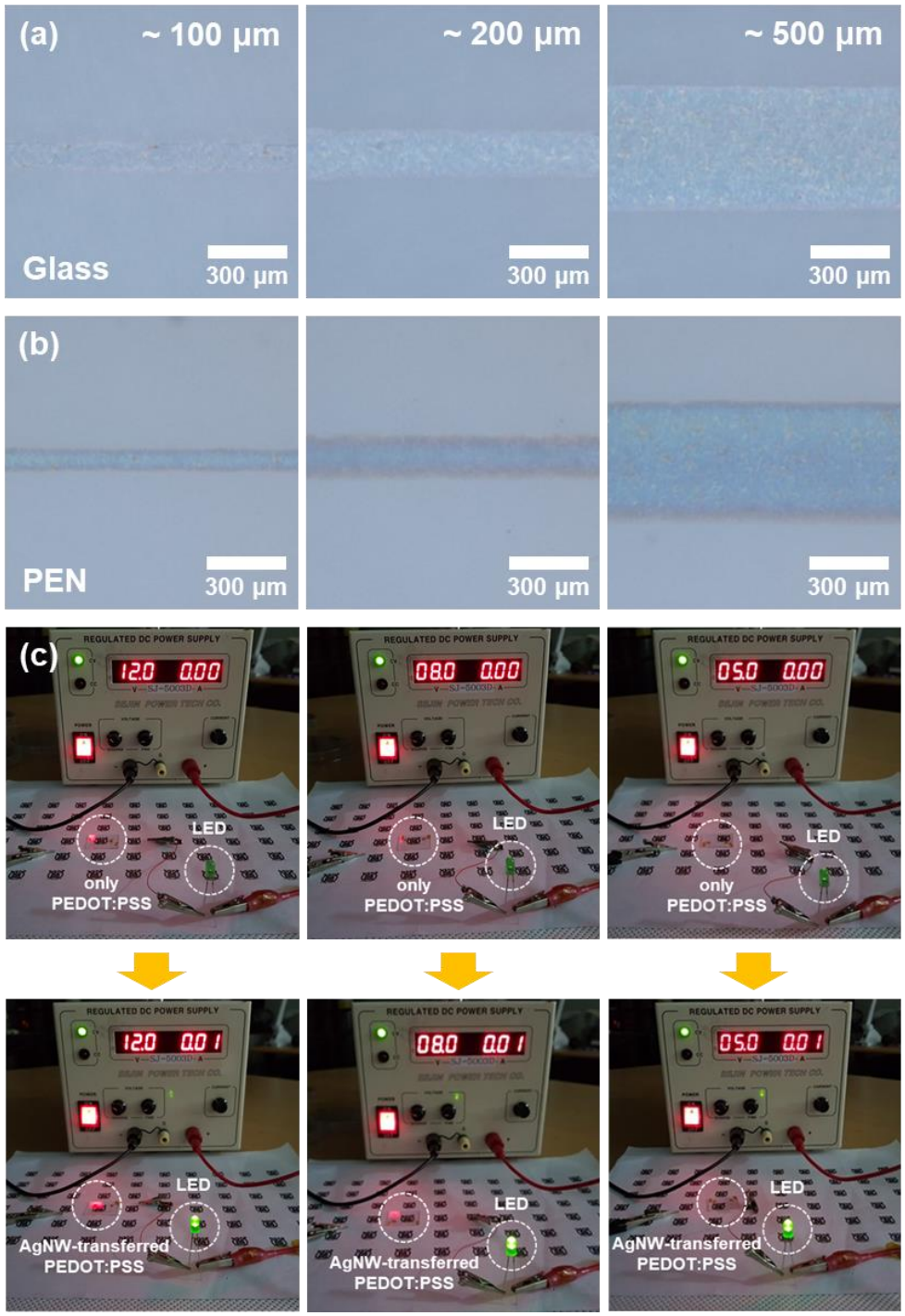

Figure 4.10 AgNW-transferred PEDOT:PSS fine lines with 100, 200 and 500 μm. (a) on glass, (b) on PEN. (c) Light brightness of a LED which is placed on only PEDOT:PSS and AgNW-transferred PEDOT:PSS with fine lines (LED size: 6 mm × 10 mm).

4.3.6 Mechanical flexibility

To further explore the applicability of the flexible electrodes, mechanical flexibility was investigated using a bending test under various bending radii of 2, 4, 6, 8 and 10 mm. As shown in **Figure 4.11**, my AgNW-transferred PEDOT:PSS electrode on the PEN substrate maintained its resistance after 1000 bending cycles at all bending radii, exhibiting little resistance change of 1.09 even at the radius of 2 mm which is the most severe condition among what we carried out. However, the ITO on the PEN substrate presented dramatic increase of the resistance after the bending test due to its inherent brittleness and thus fracture creation by the mechanical stress. In addition, as seen in **Figure 4.12**, when the LED was connected with my electrode and then the bending was performed, the brightness of LED light remained at the same voltage before and after the 1000 bending cycles at the radius of 2 mm, whereas any light emission was not observed in the case of the ITO. Therefore, my AgNW-transferred PEDOT:PSS electrode which shows the great mechanical stability can be applied to the flexible electronics. Furthermore, employing my facile patterning method, the high-performance TCEs can be patterned with a high degree of freedom, which makes them highly customizable and broadly applicable for the flexible electronics in a low fabrication cost.

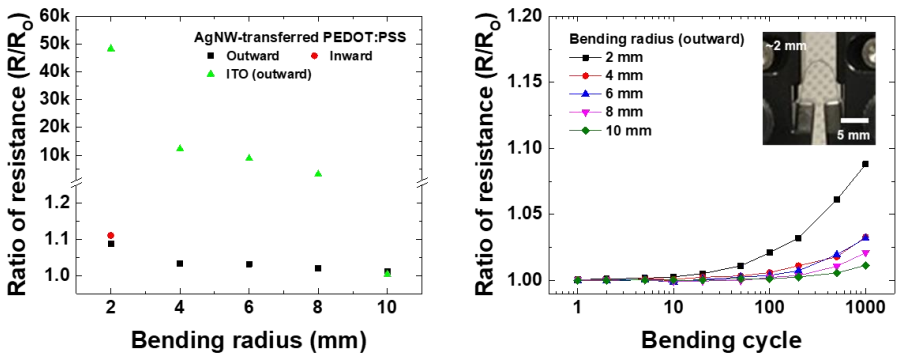

Figure 4.11 A bending test of AgNW-transferred PEDOT:PSS and ITO on PEN substrates. (a) Resistance change at various bending radii for 1000 cycles, (b) A cycling test at various bending radii during 1000 cycles.

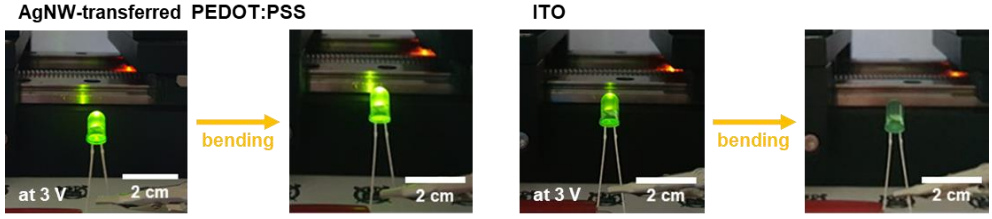

Figure 4.12 Light brightness change of a LED which is connected with AgNW-transferred PEDOT:PSS and ITO films on PEN substrates at a bending radius of 2 mm over 1000 cycles.

4.3.7 Applications to flexible electronics

Based on these results, I applied the AgNW-transferred PEDOT:PSS electrodes to several flexible electronic applications such as the 5x5 LED arrays and all solution-processed PLEDs, as displayed in Fig. 7. In the applications, my simple patterning method of the AgNWs facilitated the circuit design with a high degree of freedom unlike the conventional methods because, in my mask-free method, I only need to input the patterning design during the PEDOT:PSS printing and conduct the AgNW transfer onto the pre-patterned PEDOT:PSS transfer medium. **Figure 4.13** shows the 5x5 LED arrays which are placed on the PEN substrate with the AgNW-transferred PEDOT:PSS electrode circuits. When the voltage bias of 15 V was applied to the arrays, all LEDs in the arrays emitted light brightly and operated normally, exhibiting a clear background image unlike the previous report in my group using the opaque electrode [63]. In addition, when the LED arrays were operated even under the bending state using a syringe with a radius of 3.5 mm, there was no distortion or instability in the LED operation due to the remarkable mechanical flexibility of my electrode. **Figure 4.14** presents all solution-processed PLEDs on the glass and PEN substrates with the AgNW-transferred PEDOT:PSS top anodes. Along with the simple modification in manufacturing the PLEDs, they were completed by conducting the additional AgNW transfer onto all solution-processed PLEDs with the only PEDOT:PSS top anodes. As shown in **Figure 4.14(b) and (c)**, the devices with the AgNW-transferred PEDOT:PSS top anodes were operated under lower operation voltage at the same current level compared to those with the only PEDOT:PSS top anodes. As

a result, the low voltage-driven PLEDs were achieved via the additional AgNW transfer onto the top anodes, maintaining their optical performance. In addition, the devices on the PEN substrate operated normally under the bending state, showing the light emission without any degradation. Consequently, several demonstrations using my high-performance flexible TCEs show the potential for realizing the cost-effective and large-area flexible electronics with low power consumption.

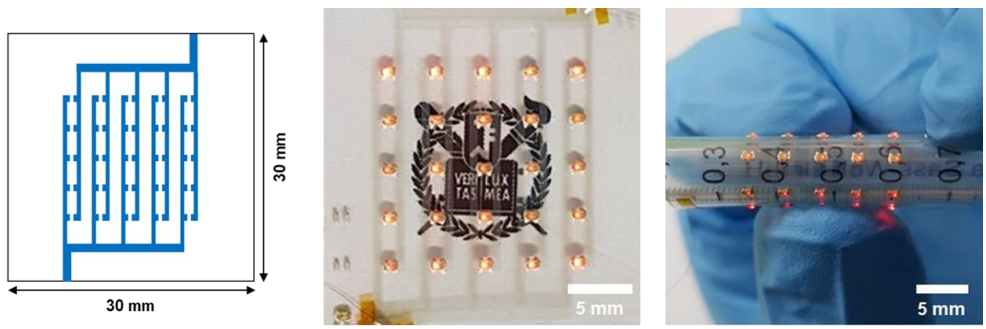

Figure 4.13 5×5 LED arrays on the AgNW-transferred PEDOT:PSS electrode circuits. A circuit diagram (left), a flat state (middle), and a bending state (right).

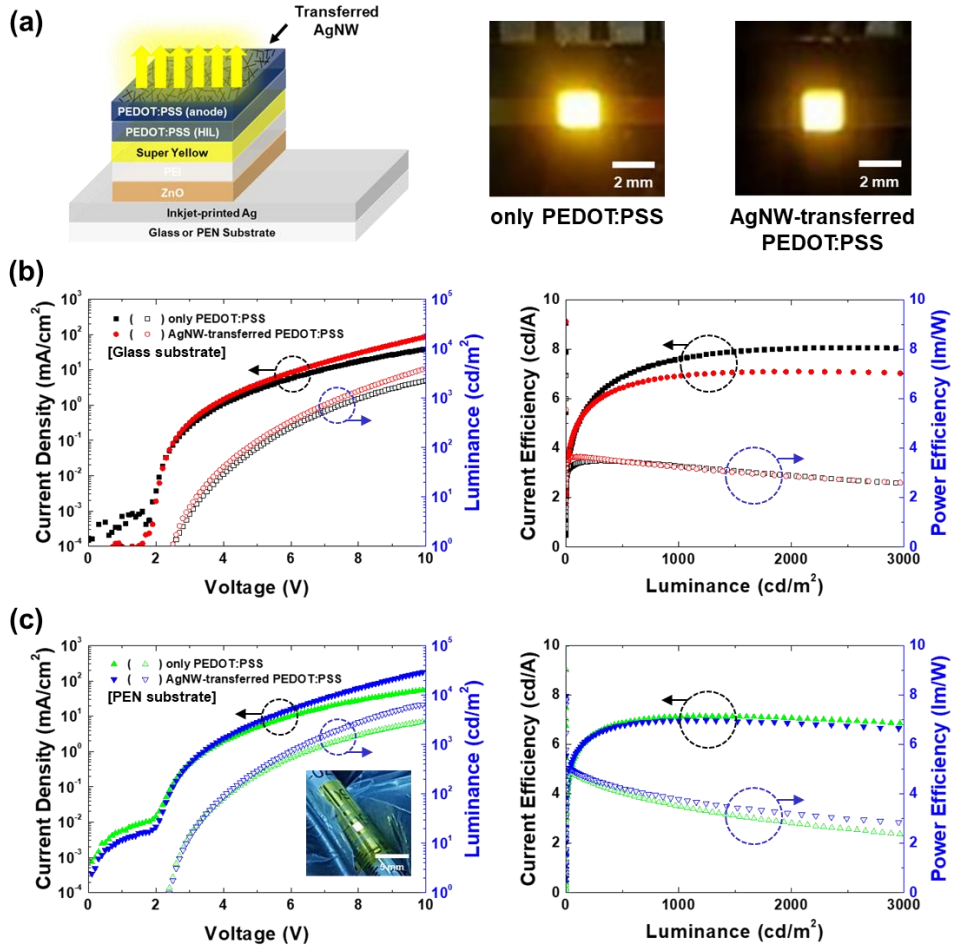

Figure 4.14 (a) A device architecture (left) and emission images of PLEDs (right), (b) IVL- (left), efficiencies (right) of a-PLEDs on the glass substrate with only PEDOT:PSS top anodes (black square) and with AgNW-transferred PEDOT:PSS top anodes (red circle), (c) IVL- (left), efficiencies (right) of a-PLEDs on the PEN substrate with only PEDOT:PSS top anodes (green triangle) and with AgNW-transferred PEDOT:PSS top anodes (blue inverted triangle).

4.4. Summary

I demonstrated the facile patterning method of the AgNW networks by conducting the inkjet printing of the PEDOT:PSS transfer medium and selective transfer of the AgNW networks onto it. The AgNW-transferred PEDOT:PSS TCE on the PEN substrate showed not only the superior optoelectronic properties but also the more outstanding mechanical stability compared to the ITO. A variety of electrodes with different optoelectronic properties were also fabricated by adjusting the coating conditions of the AgNWs. In addition, because it can be patterned easily with a high design freedom, it exhibited the fine-line electrodes with hundreds of micrometers in width while consuming less power due to their high conductivity and thus reduced voltage drop. Furthermore, the previous issues of the AgNWs such as the high surface roughness and weak adhesion with the substrate were overcome by the partially embedded AgNWs in the PEDOT:PSS matrix, allowing the smoother surface and stronger adhesion with the substrate. Finally, employing my electrodes, I demonstrated several applications such as the 5x5 LED arrays and all solution-processed PLEDs under the low-operation voltage. The formation of the high-performance flexible TCEs and their facile patterning pave the way for realization of the highly customizable flexible electronics in the cost-effective and large-area fabrication. For the future, the application areas using my electrodes will be further expanded including bottom electrodes of the optoelectronic devices and stretchable electronics through the development of the embedding structure.

Reference

[1] A. Sugimoto, H. Ochi, S. Fujimura, A. Yoshida, T. Miyadera, M. Tsuchida, Flexible OLED displays using plastic substrates, J. Sel. Topics Quantum Electron., 10 (2004) 107-114.

[2] S. Kim, H.J. Kwon, S. Lee, H. Shim, Y. Chun, W. Choi, J. Kwack, D. Han, M. Song, S. Kim, S. Mohammadi, I. Kee, S.Y. Lee, Low-power flexible organic light-emitting diode display device, Adv. Mater., 23 (2011) 3511-3516.

[3] S. Lee, J.-S. Yeo, Y. Ji, C. Cho, D.-Y. Kim, S.-I. Na, B.H. Lee, T. Lee, Flexible organic solar cells composed of P3HT: PCBM using chemically doped graphene electrodes, Nanotechnology, 23 (2012) 344013.

[4] W.J. da Silva, H.P. Kim, A.R. bin Mohd Yusoff, J. Jang, Transparent flexible organic solar cells with 6.87% efficiency manufactured by an all-solution process, Nanoscale, 5 (2013) 9324-9329.

[5] D.U. Jin, J.S. Lee, T.W. Kim, S.G. An, D. Straykhilev, Y.S. Pyo, H.S. Kim, D.B. Lee, Y.G. Mo, H.D. Kim, 65.2: Distinguished Paper: World-Largest (6.5”) Flexible Full Color Top Emission AMOLED Display on Plastic Film and Its Bending Properties, SID Symp. Dig. Tech. Pap., 40 (2009) 983-985.

[6] S. Chung, M. Jang, S.B. Ji, H. Im, N. Seong, J. Ha, S.K. Kwon, Y.H. Kim, H. Yang, Y. Hong, Flexible high-performance all-inkjet-printed inverters: organo-compatible and stable interface engineering, Adv. Mater., 25 (2013) 4773-4777.

[7] J. Wang, M. Liang, Y. Fang, T. Qiu, J. Zhang, L. Zhi, Rod-coating: towards large-area fabrication of uniform reduced graphene oxide films for flexible touch screens, Adv. Mater., 24 (2012) 2874-2878.

[8] J. Lee, P. Lee, H. Lee, D. Lee, S.S. Lee, S.H. Ko, Very long Ag nanowire synthesis and its application in a highly transparent, conductive and flexible metal electrode touch panel, Nanoscale, 4 (2012) 6408-6414.

[9] J. Lee, P. Lee, H.B. Lee, S. Hong, I. Lee, J. Yeo, S.S. Lee, T.-S. Kim, D. Lee, S.H. Ko, Room-Temperature Nanosoldering of a Very Long Metal Nanowire Network by Conducting-Polymer-Assisted Joining for a Flexible Touch-Panel Application, Adv. Funct. Mater., 23 (2013) 4171-4176.

[10] C. Pang, C. Lee, K.-Y. Suh, Recent advances in flexible sensors for wearable and implantable devices, J. Appl. Polym. Sci., 130 (2013) 1429-1441.

[11] T.Q. Trung, N.E. Lee, Flexible and Stretchable Physical Sensor Integrated Platforms for Wearable Human-Activity Monitoringand Personal Healthcare, Adv. Mater., 28 (2016) 4338-4372.

[12] S.-I. Na, S.-S. Kim, J. Jo, D.-Y. Kim, Efficient and Flexible ITO-Free Organic Solar Cells Using Highly Conductive Polymer Anodes, Adv. Mater., 20 (2008) 4061-4067.

[13] J. Ha, J. Park, J. Ha, D. Kim, S. Chung, C. Lee, Y. Hong, Selectively modulated inkjet printing of highly conductive and transparent foldable polymer electrodes for flexible polymer light-emitting diode applications, Org. Electron., 19 (2015) 147-156.

[14] C. Feng, K. Liu, J.-S. Wu, L. Liu, J.-S. Cheng, Y. Zhang, Y. Sun, Q. Li, S. Fan, K. Jiang, Flexible, Stretchable, Transparent Conducting Films Made from Superaligned Carbon Nanotubes, Adv. Funct. Mater., 20 (2010) 885-891.

[15] S.M. Kim, Y.W. Jo, K.K. Kim, D.L. Duong, H.-J. Shin, J.H. Han, J.-Y. Choi, J. Kong, Y.H.J.A.N. Lee, Transparent organic P-Dopant in carbon nanotubes: Bis (trifluoromethanesulfonyl) imide, ACS Nano, 4 (2010) 6998-7004.

[16] S. Bae, H. Kim, Y. Lee, X. Xu, J.S. Park, Y. Zheng, J. Balakrishnan, T. Lei, H.R. Kim, Y.I. Song, Y.J. Kim, K.S. Kim, B. Ozyilmaz, J.H. Ahn, B.H. Hong, S. Iijima, Roll-to-roll production of 30-inch graphene films for transparent electrodes, Nat. Nanotechnol., 5 (2010) 574-578.

[17] H. Kim, S.H. Bae, T.H. Han, K.G. Lim, J.H. Ahn, T.W. Lee, Organic solar cells using CVD-grown graphene electrodes, Nanotechnology, 25 (2014) 014012.

[18] A. Dhar, T.L. Alford, Optimization of Nb2O5/Ag/Nb2O5 multilayers as transparent composite electrode on flexible substrate with high figure of merit, J. Appl. Phys., 112 (2012).

[19] Y.C. Kim, S.J. Lee, H. Jung, B.-E. Park, H. Kim, W. Lee, J.-M. Myoung, Optimization and device application potential of oxide–metal–oxide transparent electrode structure, RSC Adv., 5 (2015) 65094-65099.

[20] H. Wu, D. Kong, Z. Ruan, P.C. Hsu, S. Wang, Z. Yu, T.J. Carney, L. Hu, S. Fan, Y. Cui, A transparent electrode based on a metal nanotrough network, Nat. Nanotechnol., 8 (2013) 421-425.

[21] W.K. Kim, S. Lee, D. Hee Lee, I. Hee Park, J. Seong Bae, T. Woo Lee, J.Y. Kim, J. Hun Park, Y. Chan Cho, C. Ryong Cho, S.Y. Jeong, Cu mesh for flexible transparent conductive electrodes, Sci. Rep., 5 (2015) 10715.

[22] A.R. Madaria, A. Kumar, F.N. Ishikawa, C. Zhou, Uniform, highly conductive, and patterned transparent films of a percolating silver nanowire network on rigid and flexible substrates using a dry transfer technique, Nano Res., 3 (2010) 564-573.

[23] L. Hu, H.S. Kim, J.-Y. Lee, P. Peumans, Y.J.A.n. Cui, Scalable coating and properties of transparent, flexible, silver nanowire electrodes, ACS Nano, 4 (2010) 2955-2963.

[24] S. Kim, S.Y. Kim, J. Kim, J.H. Kim, Highly reliable AgNW/PEDOT:PSS

hybrid films: efficient methods for enhancing transparency and lowering resistance and haziness, J. Mater. Chem. C, 2 (2014) 5636-5643.

[25] S.J. Lee, Y.H. Kim, J.K. Kim, H. Baik, J.H. Park, J. Lee, J. Nam, J.H. Park, T.W. Lee, G.R. Yi, J.H. Cho, A roll-to-roll welding process for planarized silver nanowire electrodes, Nanoscale, 6 (2014) 11828-11834.

[26] Y.H. Kim, C. Sachse, M.L. Machala, C. May, L. Müller-Meskamp, K. Leo, Highly Conductive PEDOT:PSS Electrode with Optimized Solvent and Thermal Post-Treatment for ITO-Free Organic Solar Cells, Adv. Funct. Mater., 21 (2011) 1076-1081.

[27] M. Vosgueritchian, D.J. Lipomi, Z. Bao, Highly Conductive and Transparent PEDOT:PSS Films with a Fluorosurfactant for Stretchable and Flexible Transparent Electrodes, Adv. Funct. Mater., 22 (2012) 421-428.

[28] N. Kim, S. Kee, S.H. Lee, B.H. Lee, Y.H. Kahng, Y.R. Jo, B.J. Kim, K. Lee, Highly conductive PEDOT:PSS nanofibrils induced by solution-processed crystallization, Adv. Mater., 26 (2014) 2268-2272, 2109.

[29] J. Jiu, T. Araki, J. Wang, M. Nogi, T. Sugahara, S. Nagao, H. Koga, K. Suganuma, E. Nakazawa, M. Hara, H. Uchida, K. Shinozaki, Facile synthesis of very-long silver nanowires for transparent electrodes, J. Mater. Chem. A, 2 (2014) 6326-6330.

[30] B. Bari, J. Lee, T. Jang, P. Won, S.H. Ko, K. Alamgir, M. Arshad, L.J. Guo, Simple hydrothermal synthesis of very-long and thin silver nanowires and their application in high quality transparent electrodes, J. Mater. Chem. A, 4 (2016) 11365-11371.

[31] J. Lee, I. Lee, T.S. Kim, J.Y. Lee, Efficient welding of silver nanowire networks without post-processing, Small, 9 (2013) 2887-2894.

[32] D.P. Langley, M. Lagrange, G. Giusti, C. Jimenez, Y. Brechet, N.D. Nguyen, D. Bellet, Metallic nanowire networks: effects of thermal annealing on electrical resistance, Nanoscale, 6 (2014) 13535-13543.

[33] T. Tokuno, M. Nogi, M. Karakawa, J. Jiu, T.T. Nge, Y. Aso, K. Suganuma, Fabrication of silver nanowire transparent electrodes at room temperature, Nano Res., 4 (2011) 1215-1222.

[34] H. Kang, Y. Kim, S. Cheon, G.R. Yi, J.H. Cho, Halide Welding for Silver Nanowire Network Electrode, ACS Appl. Mater. Interfaces, 9 (2017) 30779-30785.

[35] S. Kang, T. Kim, S. Cho, Y. Lee, A. Choe, B. Walker, S.J. Ko, J.Y. Kim, H. Ko, Capillary Printing of Highly Aligned Silver Nanowire Transparent Electrodes for High-Performance Optoelectronic Devices, Nano Lett., 15 (2015) 7933-7942.

[36] B. Park, I.G. Bae, Y.H. Huh, Aligned silver nanowire-based transparent electrodes for engineering polarisation-selective optoelectronics, Sci. Rep., 6 (2016) 19485.

[37] J.E. Lim, S.M. Lee, S.S. Kim, T.W. Kim, H.W. Koo, H.K. Kim, Brush-paintable and highly stretchable Ag nanowire and PEDOT:PSS hybrid electrodes, Sci. Rep., 7 (2017) 14685.

[38] D.H. Kim, K.C. Yu, Y. Kim, J.W. Kim, Highly stretchable and mechanically stable transparent electrode based on composite of silver nanowires and polyurethane-urea, ACS Appl. Mater. Interfaces, 7 (2015) 15214-15222.

[39] Y. Kim, C.-H. Song, M.-G. Kwak, B.-K. Ju, J.-W. Kim, Flexible touch sensor with finely patterned Ag nanowires buried at the surface of a colorless polyimide film, RSC Adv., 5 (2015) 42500-42505.

[40] S. Jun, B.-K. Ju, J.-W. Kim, Ultra-Facile Fabrication of Stretchable and Transparent Capacitive Sensor Employing Photo-Assisted Patterning of Silver

Nanowire Networks, Advanced Materials Technologies, 1 (2016).

[41] S. Hong, J. Yeo, J. Lee, H. Lee, P. Lee, S.S. Lee, S.H. Ko, Selective Laser Direct Patterning of Silver Nanowire Percolation Network Transparent Conductor for Capacitive Touch Panel, J. Nanosci. Nanotechnol., 15 (2015) 2317-2323.

[42] J.-W. Yoon, W.S. Chang, S.H. Cho, Laser direct patterning of AgNW/CNT hybrid thin films, Opt. Laser Eng., 73 (2015) 40-45.

[43] H. Oh, M. Lee, Laser-induced electrical property patterning of Ag nanowire transparent electrode, Mater. Lett., 176 (2016) 110-113.

[44] T. Akter, W.S. Kim, Reversibly stretchable transparent conductive coatings of spray-deposited silver nanowires, ACS Appl. Mater. Interfaces, 4 (2012) 1855-1859.

[45] S.-E. Park, S. Kim, D.-Y. Lee, E. Kim, J. Hwang, Fabrication of silver nanowire transparent electrodes using electrohydrodynamic spray deposition for flexible organic solar cells, J. Mater. Chem. A, 1 (2013).

[46] J. Krantz, K. Forberich, P. Kubis, F. Machui, J. Min, T. Stubhan, C.J. Brabec, Printing high performance reflective electrodes for organic solar cells, Org. Electron., 17 (2015) 334-339.

[47] G.S. Liu, C. Liu, H.J. Chen, W. Cao, J.S. Qiu, H.P. Shieh, B.R. Yang, Electrically robust silver nanowire patterns transferrable onto various substrates, Nanoscale, 8 (2016) 5507-5515.

[48] D.J. Finn, M. Lotya, J.N. Coleman, Inkjet printing of silver nanowire networks, ACS Appl. Mater. Interfaces, 7 (2015) 9254-9261.

[49] H. Lu, J. Lin, N. Wu, S. Nie, Q. Luo, C.-Q. Ma, Z. Cui, Inkjet printed silver nanowire network as top electrode for semi-transparent organic photovoltaic devices, Appl. Phys. Lett., 106 (2015).

[50] H. Lee, B. Seong, J. Kim, Y. Jang, D. Byun, Direct alignment and patterning of silver nanowires by electrohydrodynamic jet printing, Small, 10 (2014) 3918-3922.

[51] Z. Cui, Y. Han, Q. Huang, J. Dong, Y. Zhu, Electrohydrodynamic printing of silver nanowires for flexible and stretchable electronics, Nanoscale, 10 (2018) 6806-6811.

[52] M.S. Miller, J.C. O'Kane, A. Niec, R.S. Carmichael, T.B. Carmichael, Silver nanowire/optical adhesive coatings as transparent electrodes for flexible electronics, ACS Appl. Mater. Interfaces, 5 (2013) 10165-10172.

[53] J. Ahn, J.W. Seo, J.Y. Kim, J. Lee, C. Cho, J. Kang, S.Y. Choi, J.Y. Lee, Self-Supplied Nano-Fusing and Transferring Metal Nanostructures via Surface Oxide Reduction, ACS Appl. Mater. Interfaces, 8 (2016) 1112-1119.

[54] J. Ahn, J.W. Seo, T.I. Lee, D. Kwon, I. Park, T.S. Kim, J.Y. Lee, Extremely Robust and Patternable Electrodes for Copy-Paper-Based Electronics, ACS Appl. Mater. Interfaces, 8 (2016) 19031-19037.

[55] S. Kim, T.G. Yun, C. Kang, M.-J. Son, J.-G. Kang, I.-H. Kim, H.-J. Lee, C.-H. An, B. Hwang, Facile fabrication of paper-based silver nanostructure electrodes for flexible printed energy storage system, Mater. Des., 151 (2018) 1-7.

[56] J. Ouyang, Y. Yang, Conducting Polymer as Transparent Electric Glue, Adv. Mater., 18 (2006) 2141-2144.

[57] J. Huang, G. Li, Y. Yang, A Semi-transparent Plastic Solar Cell Fabricated by a Lamination Process, Adv. Mater., 20 (2008) 415-419.

[58] C. Shimada, S. Shiratori, Viscous conductive glue layer in semitransparent polymer-based solar cells fabricated by a lamination process, ACS Appl. Mater. Interfaces, 5 (2013) 11087-11092.

[59] C.-Y. Lin, N.-W. Hu, H.-W. Chang, C.-Y. Lu, C.-Y. Chen, C.-C. Wu, Efficient transparent small-molecule organic light-emitting devices adopting laminated transparent top electrodes, Org. Electron., 28 (2016) 25-30.

[60] W.W. Tooley, S. Feghhi, S.J. Han, J. Wang, N.J. Sniadecki, Thermal fracture of oxidized polydimethylsiloxane during soft lithography of nanopost arrays, J. Micromech. Microeng., 21 (2011) 054013.

[61] S. Yu, Y. Sun, Y. Ni, X. Zhang, H. Zhou, Controlled formation of surface patterns in metal films deposited on elasticity-gradient PDMS substrates, ACS Appl. Mater. Interfaces, 8 (2016) 5706-5714.

[62] G. Haacke, New figure of merit for transparent conductors, J. Appl. Phys., 47 (1976) 4086-4089.

[63] J. Byun, B. Lee, E. Oh, H. Kim, S. Kim, S. Lee, Y. Hong, Fully printable, strain-engineered electronic wrap for customizable soft electronics, Sci. Rep., 7 (2017) 45328.

Chapter 5 Conclusion

In this thesis, I report all solution-processed flexible polymer light emitting diodes (PLEDs) by introducing all solution processing including a wetting property engineering and transfer printing on the hydrophobic emission layer (EML). By integrating the inkjet printing and transfer printing as a key technique in this thesis, I demonstrated easily patternable transparent conductive electrodes (TCEs) such as the transferred poly(3,4-ethylenedioxythiophene): poly(styrenesulfonate) (PEDOT:PSS) top anodes of the PLEDs and silver nanowire (AgNW)-transferred PEDOT:PSS electrodes with excellent optoelectronic properties. Consequently, two approaches were combined to realize the low voltage-driven PLEDs which satisfy the simplicity of fabrication.

First, I improved the wetting property of the PEDOT:PSS hole injection layer (HIL) on the hydrophobic EML by an ethanol-dilution method. By diluting the pristine PEDOT:PSS HIL with ethanol with several volume ratios, I found the optimized the dilution condition, thereby obtaining the uniformly coated PEDOT:PSS HIL on the hydrophobic EML. Based on these results, I successfully fabricated highly efficient solution-processed inverted PLEDs sandwiched between the sputtered indium tin oxide (ITO) bottom cathodes and evaporated Al top anodes. In addition, the uniformly coated PEDOT:PSS HIL plays a key role in the devices for the uniform light emission on one substrate.

Second, I integrated the inkjet printing and transfer printing of conductive PEDOT:PSS to realize all solution-processed PLEDs on the rigid and flexible substrates. For the successful transfer printing of PEDOT:PSS, I formulated the adhesive PEDOT:PSS ink and adjusted several transfer conditions by controlling the adhesion between the PEDOT:PSS film and each interface. Based on these results, the transferred PEDOT:PSS electrodes were applied to the top anodes of all solution-processed PLEDs with solution-processed functional layers on the inkjet-printed Ag bottom cathodes. The devices on glass and polyethylene-naphthalate (PEN) substrates showed high performance and mechanical robustness in the case of those on the PEN substrate. In addition, because both Ag and PEDOT:PSS electrodes can be patterned with a high degree of freedom via the mask-free inkjet printing, highly customizable PLEDs via all solution processing were achieved with the various-shaped pixels and fine lines. In particular, all solution-processed passive matrix PLEDs (PMPLEDs) were successfully manufactured without any distortion or crosstalk between the pixels. To my knowledge, the PMPLEDs via all solution processing were demonstrated for the first time.

Third, I conducted a facile patterning of AgNW networks by integrating the inkjet printing of the PEDOT:PSS transfer medium and selective transfer of the AgNWs only on the region of the transfer medium. The AgNW-transferred PEDOT:PSS films showed excellent optoelectronic properties which is originated from the AgNW networks and were easily patternable with a high degree of freedom via the inkjet-printed PEDOT:PSS transfer medium. Therefore, my AgNW-transferred PEDOT:PSS films were highly customizable, exhibiting the fine lines with hundreds of micrometers in width without any effort in manufacturing the designed shadow masks every time. In addition, their

optoelectronic properties were highly tunable by controlling the AgNW coating conditions and previous issues of the AgNWs such as a high surface roughness and weak adhesion with the substrates were overcome by the partially embedded AgNWs in the PEDOT:PSS matrix. To explore the applicability of flexible electrodes, my electrodes were bended with various bending radii and their resistance was maintained almost constant even at a bending radius of 2 mm for 1000 cycles. Consequently, my AgNW-transferred PEDOT:PSS electrodes on the PEN substrate showed not only superior optoelectronic properties but also excellent mechanical flexibility compared to ITO on the PEN substrate. Based on these results, I applied the high-performance TCEs to the flexible electronics such as 5×5 light emitting diode (LED) arrays and all solution-processed PLEDs for low-voltage operation. I combined two approaches introduced in Chapter 3 and 4 for the realization of low-voltage driven all solution-processed PLEDs. Consequently, the PLEDs with the AgNW-transferred PEDOT:PSS top anodes exhibited a lower operating voltage than those with the only PEDOT:PSS anodes while maintaining the optical performance.

From this Ph.D. dissertation, I strongly believe that my contribution paves the way for the realization of the cost-effective and large-area mass production of the future display via all solution-processed PLEDs under low-operation voltage. If the large-area fabrication techniques containing the inkjet printing and transfer printing are developed, the scalability of low-cost mass production in manufacturing highly customizable and low-power PLEDs will be achieved, leading to the embodiment of the interactive and ubiquitous future display which is utilized anytime and embedded anywhere.

Appendix

Portions of the work discussed in this dissertation are also presented in the following already published and to-be-published papers:

1. **J. Park**, J. Ha, N. Seong, S. Lee, C. Lee, H. Yang, and Y. Hong*, “Highly efficient solution-processed inverted polymer light emitting diodes with uniformly coated poly(3,4-ethylenedioxythiophene):poly(styrene-sulfonate) layers on a hydrophobic emission layer using a dilution method”, Thin Solid Films, 660, 782 (2018)
2. **J. Park** et al., “Highly Customizable All Solution-processed Polymer Light Emitting Diodes via Integration with Inkjet Printing and Transfer Printing of Conductive Polymer” (manuscript in preparation)
3. **J. Park** et al., “A facile patterning method of AgNW networks” (manuscript will be in preparation)

Publications and Conferences

[1] International Journals

1. **J. Park**, J. Ha, N. Seong, S. Lee, C. Lee, H. Yang, and Y. Hong*, “Highly efficient solution-processed inverted polymer light emitting diodes with uniformly coated poly(3,4-ethylenedioxythiophene):poly(styrene-sulfonate) layers on a hydrophobic emission layer using a dilution method”, Thin Solid Films, 660, 782 (2018)
2. **J. Park** et al., “Highly Customizable All Solution-processed Polymer Light Emitting Diodes via Integration with Inkjet Printing and Transfer Printing of Conductive Polymer” (manuscript in preparation)
3. **J. Park** et al., “A facile patterning method of AgNW networks” (manuscript will be in preparation)

i. J. Ha, **J. Park**, J. Ha, D. Kim, S. Chung, C. Lee, Y. Hong*, “Selectively Modulated Inkjet Printing of Highly Conductive and Transparent Foldable Polymer Electrodes for Flexible Polymer Light-Emitting Diode Applications”, Organic Electronics, 19, 147 (2015)

ii. H. Im, H. Song, **J. Park**, Y. Hong, J. Ha, S.-B. Ji, J. Jeong, and Y. Hong*, “Accurate Defect Density-of-State Extraction Based on Back Channel Surface Potential Measurement for Solution-Processed Metal-Oxide Thin

Film Transistors", IEEE Transactions on Electron Devices, 64, 1683 (2017)

iii. T.-Y. Kim†, J. Ha†, K. Cho, J. Pak, J. Seo, **J. Park**, J.-K. Kim, S. Chung*, Y. Hong*, and T. Lee*, "Transparent Large-Area MoS2 Phototransistors with Inkjet-Printed Components on Flexible Platforms", ACS Nano, 11, 10273 (2017)

iv. S. Lee, S. Lee, H. Yoon, C.-K. Lee, C. Yoo, **J. Park**, J. Byun, G. Kim, B. Lee, B. Lee, and Y. Hong*, "Printed cylindrical lens pair for application to the seam concealment in tiled display", Optics Express, 26, 824 (2018)

[2] Oral Presentation

1. **J. Park**, J. Ha and Y. Hong*, "Electrical Analysis of Solution-processed PLEDs with Impedance Spectroscopy in the Vicinity of the Turn-on Voltage", The 13th International Meeting on Information Display (IMID 2013), Daegu, Korea, August (2013)
2. **J. Park**, J. Ha, N. Seong, C. Lee, and Y. Hong*, "Solution-processed inverted polymer light-emitting diode", SPIE Photonics West 2016, San Francisco, February (2016)
3. **J. Park**, G. Kim, H. Yoon, S. Jeong, S. Lee, C. Lee and Y. Hong*, "Solution-Processed Inverted Polymer Light Emitting Diodes with Transferred PEDOT:PSS Top Anodes", SPIE Photonics West 2019, San Francisco, February (2019) (accepted)

[3] Poser Presentation

1. **J. Park**, J. Ha, K. Kim, C. Lee, and Y. Hong*, “Inverted polymer light-emitting diodes with solution-processed multilayers using diluted PEDOT:PSS”, European Materials Research Society (E-MRS), Lille, France, May (2014)
2. **J. Park**, J. Ha, H. Yoon, G. Kim, N. Seong, C. hee Lee, and Y. Hong*, “Enhanced Operational Lifetime of Polymer Light Emitting Diodes with Inverted Structures”, The 8th International Workshop on Flexible & Printable Electronics (IWFPE 2016), Jeonju, Korea, November (2016)
3. **J. Park**, J. Ha, N. Seong, C. Lee, and Y. Hong*, "Introduction of solution-processed PEDOT:PSS as a hole-injection layer for highly efficiency inverted polymer light-emitting diodes", The 4th International Conference on Advanced Electromaterials (ICAE 2017), Jeju island, Korea, November (2017)

한글 초록

본 논문에서는 미래 디스플레이 구현을 위한 저비용 및 대면적의 대량 생산 가능성을 보여 주는 저전압에서 구동 가능한 전 용액 공정 기반의 플렉시블 폴리머 발광다이오드를 제작하였다. 최근 많은 연구 그룹에서 스핀 코팅, 잉크젯 프린팅, 트랜스퍼 프린팅과 같은 다양한 공정 방법으로 전 용액 공정 기반의 폴리머 발광다이오드를 보고하고 있지만, 맞춤 제작과 저전력 소비 면에서 제품으로의 상업화를 위해선 많은 개선 사항들이 존재하고 있다.

첫 번째로, 소수성인 발광층 위에 용액 공정으로 추가 층을 형성하는 것은 웨팅 특성의 불일치로 어려움을 겪고 있다. 다양한 광학 소자에서 PEDOT:PSS 정공 주입층의 웨팅 특성을 향상시키기 위해, 계면 활성제 추가, 유기 하부 층에 대한 표면 처리, 낮은 표면 장력을 가지는 용액과 희석 방법 등이 보고 되고 있는데, 이러한 방법들 중에서 희석 방법이 유기 층이나 전체 소자에 어떠한 손상을 일으키지 않으면서 용액의 표면 장력만 바꾼다는 점에서 이점을 가진다. 에탄올과의 최적화된 희석 농도를 통해, PEDOT:PSS 정공 주입층이 소수성인 발광층 위에 균일하게 코팅 되었다. 이 방법을 이용해 스퍼터링 된 ITO와 증착 된 알루미늄 전극 사이에 소수성 발광층 위 PEDOT:PSS 정공 주입층을 포함하는 용액 공정 기반 다층 구조의 역방향 폴리머 발광다이오드를

제작하였다. 위 소자에서 균일하게 형성된 PEDOT:PSS 정공 주입층은 소자의 특성 향상 및 한 기판 내에서의 균일한 발광 특성에 있어서 중요한 역할을 한다.

두 번째로, 전 용액 공정 기반의 폴리머 발광다이오드를 제작하기 위해 기존에 사용된 진공 증착 방식의 전극을 용액 공정 방식의 전극으로 교체할 필요가 있다. 이러한 소자에 대한 많은 연구들이 보고되고 있지만, 양 전극을 형성하는데 있어 복잡하고 고비용의 제작 방식은 저비용 및 대면적 디스플레이 상품 개발에 있어 적합하지 않다. 간편한 픽셀 형성을 위해 폴리머 발광다이오드의 전극은 쉽고 자유롭게 패터닝이 되어야 하지만, 기존의 연구들은 하나의 소자 데모를 위한 목적으로만 비생산적인 전극 패터닝 기술을 사용하였다. Solvent orthogonality 또한 충족이 되어야 용액 공정 시 발생할 수 있는 하부 층의 손상을 막음으로써, 소자 특성의 저하를 방지할 수 있다. 위의 두 문제를 해결하기 위해 잉크젯 프린팅과 트랜스퍼 프린팅 방식의 조합을 통한 전도성 PEDOT:PSS 층을 형성하여 전극에 대한 간편한 패터닝을 달성하고 용액에 의한 소자의 손상을 최소화 하였다. 트랜스퍼 된 PEDOT:PSS 층을 얻기 위해, D-sorbitol 용액을 PEDOT:PSS 용액에 첨가해 접착력이 있는 층을 형성하였고, PEDOT:PSS 층과 donor quartz, PDMS 스탬프, target 기판 각각과의 접착력을 조절하였다. 이 방법을 이용하여 트랜스퍼 된 PEDOT:PSS 전극을 잉크젯 프린팅 된 실버 음극 위 스핀코팅으로 형성된 기능층을 가지는 전 용액 공정 기반 역방향 폴리머 발광다이오드의 상부 양극으로 적용하였다. 단단한 그리고 유연한

소자는 고성능을 보여줄 뿐만 아니라 구부러짐 상태에서도 정상적으로 동작하였다. 또한 잉크젯 프린팅을 통한 실버와 PEDOT:PSS 전극의 마스크가 필요 없는 패터닝 기술을 이용하여 다양한 픽셀 모양과 얇은 라인을 가지는 주문 제작된 발광다이오드와 어레이를 제작하였다. 특히 전 용액 공정 기반의 500 마이크로미터 픽셀 너비를 가지는 5×7 패시브 매트릭스 폴리머 발광다이오드가 처음으로 데모 되었으며, 픽셀 간 crosstalk 없이 다양한 글자를 표시하였다.

세 번째로, 전극의 낮은 전도성은 소자가 동작하는 동안 큰 전압 강하에 따른 높은 소비 전력을 요구하게 한다. 앞서 제작한 소자 또한 트랜스퍼 된 PEDOT:PSS 전극의 높은 면저항으로 인해 낮은 전력 효율을 보여주고 있다. 따라서 복잡한 공정 방식이 아닌 간단한 방법으로 전 용액 공정 발광다이오드를 포함하는 저전압 구동이 가능한 플렉시블 전자 소자로의 응용을 위한 고성능의 플렉시블 전극을 개발할 필요가 있었다. 이에 본 저자는 PEDOT:PSS 트랜스퍼 매개체에 대한 잉크젯 프린팅과 실버 나노와이어의 트랜스퍼 매개체 위로만의 선택적 트랜스퍼 기술을 융합하여 고성능 플렉시블 전극에 대한 간단한 패터닝 방법을 개발하였다. 첫 번째로 실버 나노와이어의 트랜스퍼를 위해 D-sorbitol 용액을 첨가한 혼합된 PEDOT:PSS 잉크를 제조하여 PEDOT:PSS 박막과 실버 나노와이어 막이 강하게 접착하도록 하였다. 이 잉크를 이용하여 다양한 기판 상에 원하는 모양으로 PEDOT:PSS 박막을 잉크젯 프린팅하여 맞춤 제작의 PEDOT:PSS 트랜스퍼 매개체를 제작하였다. 두 번째로 스핀 코팅을 이용해 플라즈마 처리된 PDMS 스탬프 위에 매우

전도성이 높고 투명한 실버 나노와이어 막을 제작하였다. 마지막으로 PEDOT:PSS 박막이 형성된 기판과 실버 나노와이어가 코팅된 PDMS 스탬프가 하나로 접착된 샘플에 대하여 열 처리를 진행하여 실버 나노와이어의 선택적 트랜스퍼를 가능하게 하였고, 결과적으로 자유도가 높게 맞춤 제작이 가능한 실버 나노와이어가 트랜스퍼 된 PEDOT:PSS 전극을 제작하였다. 이 원리를 이용해 이 전극은 사용될 목적에 따라 다양한 기판 상에 제작되었으며, 우수한 전기광학적 특성을 가지고 있을 뿐만 아니라 수백 마이크로의 너비를 가지는 얇은 라인을 간단한 방법으로 형성할 수 있었다. 또한 실버 나노와이어 코팅 조건 조절을 통해 전극의 전기광학적 특성을 자유롭게 바꿀 수 있었고, 높은 표면 거칠기 및 하부 기판과의 약한 접착력과 같은 기존에 보고된 실버 나노와이어 막의 문제점들이 PEDOT:PSS 매트릭스 안에 부분적으로 임베딩된 실버 나노와이어의 구조에 의해 개선되었다. 플라스틱 기판 위 전극은 기존의 투명 전극으로 많이 사용되는 ITO에 비해 전기광학적 특성이 우수할 뿐만 아니라 기계적 특성 또한 우수하였다. 이러한 플렉시블 전극을 이용하여 LED 어레이 및 전 용액 공정의 폴리머 발광다이오드와 같은 맞춤 제작의 플렉시블 전자 소자로의 응용을 데모하였다. 특히 저전압에서 구동 가능한 폴리머 발광다이오드는 광학적 특성을 유지하면서 낮은 동작 전압을 보여 주었다.

주요어 : 폴리머 발광다이오드, 용액 공정, 잉크젯 & 트랜스퍼 프린팅, PEDOT:PSS, 실버 나노와이어, 플렉시블 (유연성)
학번 : 2012-20772